University of Tripoli
Faculty of engineering
Materials and Metallurgical Engineering Department

Correlation of Retained Austenite Amount in Oil Quenched Carbon Steel with Electrical Resistivity

Submitted by:

Eng. Mahmoud Mohamed Belhaj

Supervised by:

Dr. Nuri Zreiba (Professor)
Dr. Mohamed Milad.

Thesis was submitted in Partial Fulfillment of the requirements for the master's degree in Materials and Metallurgical Eng. Department

Fall 2023

Acknowledgements

I would like to take this opportunity to express my respect and appreciation to everyone who has helped me during my study. First my deep thanks to my supervisor Dr Nuri Zreiba who gave me the idea for this project and supported me with advice and research papers that facilitated the completion of this work. Also appreciate the support of my second supervisor Dr. Mohamed Milad. Many thanks to Dr Mohamed salem who supported me with steel samples needed to carry out this work. I extend my deepest thanks to Dr Mohamed Spita and Eng. Yousef souliman from the Libyan Center Solar Energy Research and Studies who provided me with a Jundle device for electrical resistivity measurements. I also thank Mr Sulaiman S.belhol from Libyan Petroleum Institute who supervised the test of X- ray diffraction. Special thanks to faculty members in the Materials and Metallurgical Engineering Department especially the head of the department Dr Mokhtar Abuzrieba who facilitated all procedures for addressing research centers. Finally I would like to thank my family, my uncle Salah Nwiegy who supervised the chemical composition analysis of the specimen in The Iron and Steel Factory Missurata, and special thanks for my parents for their continued support and encouragement until I finished this work.

Abstract

Retained austenite amount (R.A) has an important effect on the mechanical stability of steel. In this project, three methods for %R.A measurements, namely metallography, X-ray diffraction and electrical resistivity have been studied.
Two types of medium carbon steel have been used for the study. The first type is a medium carbon steel referred to as S1 contains 0.371%C. The second type is a medium carbon steel referred to as S2 contains 0.262%C. The two types of steels have been used to study retained austenite amount by quenching them in three different quenching media. The quenching media chosen are water, corn oil and used oil for car engine.
Due to low carbon content of steels used (less than 0.6%), measurement of retained austenite using metallographic techniques was difficult. It is well known that at lower carbon contents, the morphology of martensite is predominantly nonlenticular, and detection of the austenite by metallography in such a matrix was impossible.
Measurement of retained austenite by X-ray diffraction has shown that %R.A increases with carbon and/or manganese content and increases with the cooling rate of quenching. For fixed quenching media, it was found that S1 steel which contains higher carbon and manganese content gives higher %R.A than S2 steel. For one type of steel, it was found that water quench gives the highest %R.A. Quenching of S1 steel in water gave 14.44% of R.A which is higher than that of used oil for car engine and corn oil. The latter two gave 11.9 % and 9.34 % of R.A respectively. Quenching of S2 steel in water gave 4.4 % of R.A which is higher than that of used oil for car engine and corn oil which gave 2.11 % and 2.53 % of R.A respectively.
Measurement of retained austenite by electrical resistivity which is the main focus of this project is based on Matthiessen rule which states that the total resistivity depends on the resistivities of impurities, defects, and 2nd phase. It was found that the electrical resistivity (E.R) is affected strongly by alloying elements content. E.R increased from the literature value of 9.58 μΩ.cm for pure iron to the measured value of 14.96 μΩ.cm for S2 steel and to 21.68 μΩ.cm for S1 steel. It was also found that E.R is affected strongly by the quenching process and the cooling rate. E.R of S1 and S2 steels before any treatment (as received) are 21.68 and 14.96 μΩ.cm respectively. These values increased to 31.98 and 24.86 μΩ.cm for corn oil quench respectively. It also increased to 41.36 and 30.35μΩ.cm for water quench respectively. It was found that %R.A is responsible for an increase in the electrical resistivity of quenched steel. The %R.A value of 2.11% was recorded for used oil for car engine quenched S2 steel which has an E.R of 25.75 μΩ.cm. This 2.11% value was the smallest value obtained. The largest value was recorded for water quenched S1 steel (of 14.44%) which has E.R of 41.36 μΩ.cm.
As a final comparison between the three methods for measuring retained austenite, the metallography method was unsuccessful due to low carbon content of steels used. In case of XRD and E.R methods, they follow the same trend. Furthermore, both methods gave highest %R.A value for water quenched S1 steel and lowest %R.A value for corn oil quenched S2 steel. This can imply that E.R method could be applicable for retained austenite measurement in steels.

Table of Contents

Page number

List of Figures

Page number

List of Tables

Page number

Chapter 1
Introduction

The microstructure produced in quenched carbon steel can consist of a martensite phase with some amount of retained austenite (R.A). R.A results when steel is incompletely transformed to martensite at room temperature. R.A plays a crucial effect in mechanical properties of steels and therefore its volume fraction, morphology, and distribution need to be analyzed. The presence of R.A in tooling components manufactured from quenched and tempered martensitic steels can often lead to performance problems and cause premature failure of the components. R.A is soft and ductile as compared to tempered martensite, and the transformation of R.A to martensite during service leads to a volume expansion (up to 4%) that may decrease tooling tolerances and/or cause the formation of residual tensile stresses in the component [1,2,3,4]. The transformation may also increase the hardness/brittleness of the material which can lead to performance problems or failure of the component. Failures of tooling components are especially undesirable from a manufacturing perspective because of the costs associated with tooling replacement and the loss of production capabilities. Thus, the detection and estimation of R.A. in respect of its amount, size, and distribution, besides thermal stability, have been considered to be a key factor in the design and manufacturing of these high strength steels [5,6].

Several techniques were developed to calculate the amount of retained austenite in heat treated steels, including x-ray diffraction (XRD), optical microscopy combined with image analysis, scanning electron microscopy (SEM) and magnetization measurements [7,8].

Among all these techniques, X-ray diffraction is the most frequently used because the facilities are widely available and it is also able to measure the crystallographic texture and the stress state in the material [1, 9].

The usefulness of the metallographic procedure is limited for retained austenite measurement when %R.A is lower than 15%. [10].

Electrical resistivity measurement is also likely to give a prediction about the R.A content. The electrical resistivity is strongly affected by the concentration of the imperfections within the material structure (which depend on temperature and composition). Any atom located away from its equilibrium position may cause an interaction with the electrons resulting in electron scattering. This effect leads to a decrease in the mean free path, a reduction of electron mobility, and an increase in the electrical resistivity. In the same context, the random distribution of interstitial or substitutional atoms decreases the mean free path of electrons resulting in an increase of electrical resistivity [11]. As the resistivity of ferrite, martensite and austenite are different, the compositions and volume fractions of these phases are different as a result of different heat treatment, which leads to different steel resistivities or conductivities. So this nondestructive testing method could relate the electrical properties of quenched steel to its metallographic results [12]. Such method is expected to support the unreliable metallographic method and the costly x-ray diffraction method.

This research investigates the quenching heat treatment of plain carbon steel by using different types of quenching media. These different media are expected to produce steels with different microstructures in terms of different content of retained austenite phase, which can dramatically affect the properties of steel. This research will also study the change in electrical resistivity of the quenched steel and how much it is affected by the content of retained austenite phase, where the electrical resistivity of the steel is strongly function of the carbon content and its distribution within the steel. Finally, R.A content will also be measured by electrical resistivity which will be correlated to the %R.A measured by X-ray diffraction and metallography techniques if it is possible. The main objective of this study is to realize the effectiveness of employing the electrical resistivity phenomena to anticipate the amount of retained austenite in the tested steel. So this study will prove the validity of using electrical resistivity measurement to make a prediction of the amount of retained austenite within the steel.

The remainder of this thesis is divided into the following chapters:

- Chapter 2 provides a literature review that introduces background information and the previous work,
- Chapter 3 details the experimental procedure including materials, processing steps and characterization techniques,
- Chapter 4 presents the results of the experiments and discusses the results and their significance with respect to existing literature.
- Chapter 5 summarizes the findings of this thesis and provides suggestions for future work in this field.

Chapter 2
Literature Review

2.1. Carbon Steel

Before consideration of steel or other iron-base alloys, it is helpful to explain what steel is. The common dictionary definition is "a hard, tough metal composed of iron, alloyed with various small percentage of carbon and often variously with other metals called alloying elements". The most common alloying elements allowed in plain-carbon steel are manganese (1.65% max) and silicon (0.60% max) [13]. Fundamentally, all steels are mixtures, or more properly, alloys of iron and carbon. Plain carbon steels are widely used for many industrial applications and manufacturing on account of their low cost and easy fabrication [14]. However, even the so-called plain-carbon steels have small, but specified, amounts of manganese and silicon plus small and generally unavoidable amounts of phosphorus and sulfur. According to their carbon content, the plain carbon steel can be categorized as low-carbon (<0.3% C), medium-carbon (0.3–0.7% C) and high-carbon (0.7–1.7% C) steels [15, 16]. The carbon content of plain-carbon steels may be as high as 2.0%, but such an alloy is rarely found except in some tool steels. Carbon content of commercial steels usually ranges from 0.05 to about 1.0%. Thus, at room temperature, conventional steels consist of a mixture of cementite and ferrite (essentially iron). Each of these is known as a phase (defined as a physically homogeneous and distinct portion of a material system). When steel is heated above 727 ºC, cementite dissolves in the matrix, and a new phase is formed, which is called austenite. Note that phases of steel should not be confused with structures. There are only three phases involved in any steel; ferrite, carbide (cementite), and austenite, whereas there are several structures or mixtures of structures. Carbon is almost insoluble in the alpha or ferrite phase. However, it is quite soluble in gamma iron. Carbon actually dissolves; that is, the individual atoms of carbon lose themselves in the interstices among the iron atoms. Certain interstices within the FCC structure (austenite) are considerably more accommodating to carbon than are those of ferrite.

Ferrite is essentially a solid solution of iron containing carbon or one or more alloying elements such as silicon, chromium, manganese, and nickel. According to the iron-carbon phase diagram (Figure 2.1), a very little carbon (0.022% C) can dissolve in ferrite (α Fe), even at the eutectoid temperature of 727 °C. If the carbon content exceeds the solubility limit of 0.022%, the carbon forms another phase called cementite. A mixture of Ferrite and Cementite forms a constituent called Pearlite. A fully pearlitic microstructure is formed at the eutectoid composition of 0.77% C. Pearlite is formed by cooling the steel through the eutectoid temperature (the temperature of 727 °C in Figure 2.1 by the following reaction:

$$\text{Austenite} \xrightarrow{\text{slow cooling}} \text{Pearlite (Cementite + Ferrite)}$$

The cementite and ferrite in pearlite form as parallel plates called lamella. Hence, pearlite is essentially a composite microstructure consisting of a very hard carbide phase, cementite, and a very soft and ductile ferrite phase. Like pearlite, bainite is a composite of ferrite and cementite. But unlike pearlite, the ferrite in Bainite has an acicular morphology and the carbides are discrete particles. Because of these morphological differences, bainite has much different property characteristics than pearlite. In general, bainitic steels have high strength coupled with good toughness,

whereas pearlitic steels have high strength with poor toughness. The austenite gamma phase does not exist at room temperature in plain-carbon and low-alloy steels, other than as small amounts of retained austenite that did not transform during rapid cooling. The crystal structure of austenite is face-centered cubic (FCC) as compared to ferrite, which has a (BCC) lattice.

Rapid cooling from austenite phase produces a new structure called martensite. martensite is essentially a supersaturated solid solution of carbon in iron. The amount of carbon in martensite far exceeds that found in solid solution in ferrite. Because of this, the normal body centered cubic (BCC) lattice is distorted in order to accommodate the carbon atoms. The distorted lattice becomes body-centered tetragonal (BCT). In plain-carbon and low-alloy steels, this supersaturating is generally produced through very rapid cooling from the austenite phase region (quenching in water, iced-water, brine, iced brine, oil or aqueous polymer solutions) to avoid forming ferrite, pearlite, and bainite. Some highly alloyed steels can form martensite upon air cooling. Depending on carbon content, martensite in its quenched state can be very hard and brittle, and because of this brittleness, martensitic steels are usually tempered to restore some ductility and increase toughness [17].

In steels, two distinct morphologies of martensite can form. One of them is called lath martensite and the other is called plate martensite.

The lath shape martensite also known as non-lenticular martensite has the shape of a strip where individual laths are too fine to be resolved under optical microscope and any retained austenite is too fine to be resolved. This type of martensite forms in steel containing less than 0.5% C. The well-known classical type of martensite is the plate martensite commonly called lenticular martensite. At high magnification the lenticular martensite plates are composed of stacks of very fine twins. This type forms in steels which have higher carbon content (more than 0.6%C) plus other alloying elements [17].

2.2. Heat Treatment Process

The microstructure of a material (or an alloy) and its properties can be altered by heating it at a definite temperature and time and then allowing it to cool at suitable rate. This heat treatment process can be performed on all types of materials including ceramics and composites. During this process, the material undergoes phase, microstructural and crystallographic changes [13]. The purpose of steel heat treatment is mainly to improve its mechanical properties (usually ductility, hardness, yield strength, tensile and impact resistance). The electrical conductivity, corrosion, and thermal properties may also be altered during the process of heat treatment [18,19].

In order to obtain the typical of multi-phase steel microstructure, a three-step heat treatment is required. This standard heat treatment is tailored specifically to enrich the austenite phase with carbon so that austenite can be stabilized down to room temperature. The heat treatment path consists of heating the material to a certain temperature followed by a hold and a cooling to room temperature. The heat treatment path and the chemical composition should be designed to promote the formation of carbon-saturated austenite, which can be retained in the microstructure when the steel is quenched to room temperature [20,21].

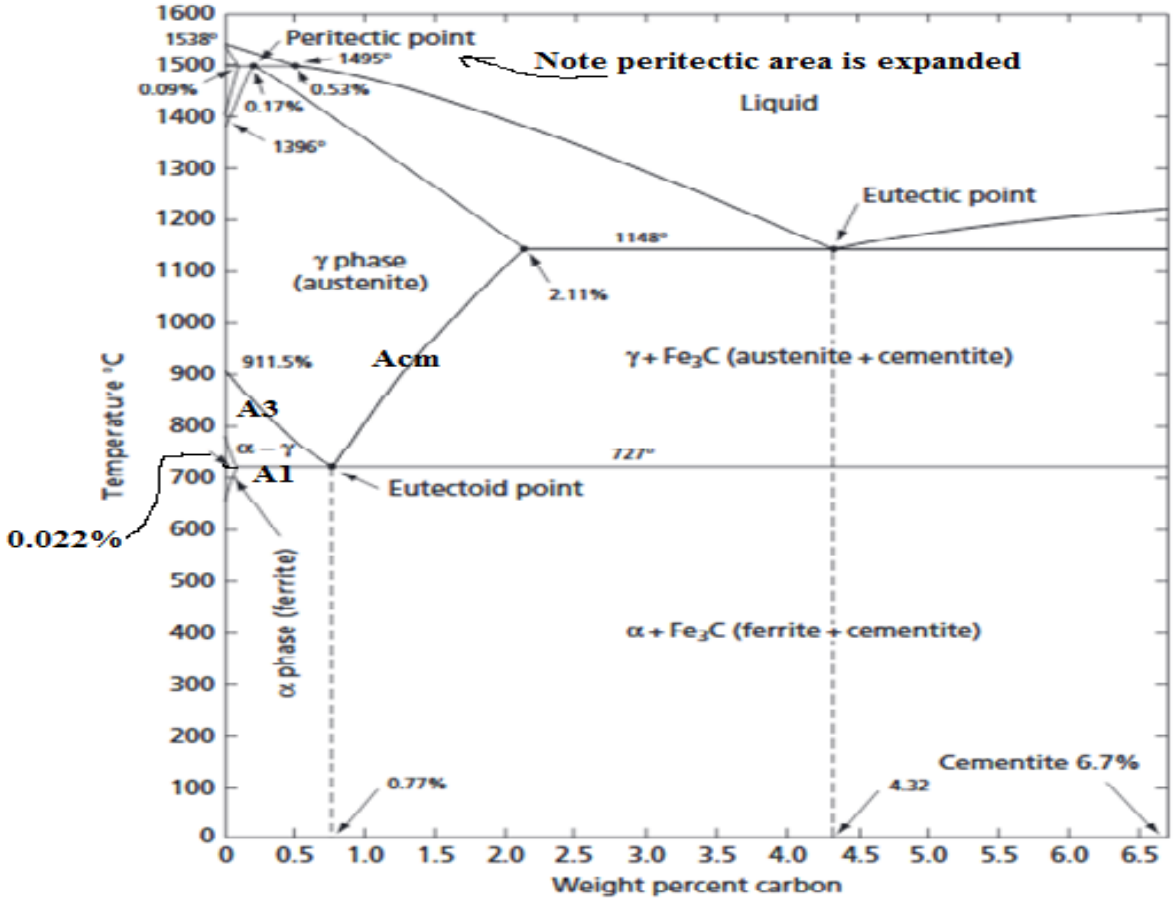

Figure 2.1 Iron carbon phase daigram [22].

2.2.1. Hardening (quenching) of Steel

Hardening is a type of heat treatment process carried out in order to increase hardness of steel by heating it above critical point and then allowing it to cool down by immersing in quenching medium such as water or oil. Quenching process is performed in order to produce a desired microstructure in the sample. In general, the quenching is a relatively complex process and can be considered as a heat transfer problem. The selection of optimum parameters of the quenching process is very important to ensure the achievement of the desired properties of the machine component [22]. There are three main steps in quenching process, heating "annealing" the specimen to certain temperature, holding it at a temperature (if required) for a sufficient period for completion of austenite formation, followed by rapid cooling to room temperature. Each of these steps strongly affects the microstructure and the properties of the material [23].

The annealing temperature for the first step of the heat treatment is chosen such that it lies within the intercritical region of the Fe-C phase diagram as shown in Figure 2.1. The area denoted as austenite is actually an area within which iron can retain much dissolved carbon. In fact, most heat treating operations (notably annealing, normalizing, and heating for hardening) begin with heating the alloy into the austenitic range to dissolve the carbide in the iron. The nucleation of austenite in ferrite-pearlite structures occurs first at carbides. Once austenite has nucleated in pearlite, its subsequent growth is presumably controlled by the rate of carbon diffusion in the austenite [24]. In this phase a solid solution of carbon in iron can be visualized as a pyramidal stack of basketballs with golf balls between the spaces in

the pile. In this analogy, the basketballs would be the iron atoms, while the golf balls interspersed between would be the smaller carbon atoms. Thus, the austenite phase capable of containing up to 2% dissolved carbon [25].

The intercritical region is bound by the transformation temperatures A1 and A3. A1 is the lower transformation temperature, where austenite begins to form during heating of the steel. A3 is the upper boundary of the intercritical region and it is the temperature at which the transformation of ferrite to austenite is completed upon heating. These two temperatures can be estimated from the chemical composition of the steel using two equations. The Andrews formula [9] is commonly used to calculate the A1 temperature for steels with less than 0.6 wt%C.

The formula for Ac1 is given as:

$$A1 = 723 - 16.9(wt.\%Ni) + 29.1(wt.\%Si) + 6.38(wt.\%W) - 10.7(wt.\%Mn) + 16.9(wt.\%Cr) + 290(wt.\%As) \quad (2.1)$$

The A3 temperature can be calculated using a formula that was specifically developed for TRIP steels, called the Park formula [9]:

$$A3 = 955 - 350(wt.\%C) - 25(wt.\%Mn) + 51(wt.\%Si) + 106(wt.\%Nb) + 100(wt.\%Ti) + 68(wt.\%Al) - 11(wt.\%Cr) - 33(wt.\%Ni) - 16(wt.\%Cu) + 67(wt.\%Mo) \quad (2.2)$$

The total heating time should be just enough to attain uniform temperature through the section of the part to enable not only the completion of phase transformation, but also to obtain homogeneous austenite. It should not be long to prevent grain growth, oxidation, and decarburization. Therefore the steel must be held at the hardening temperature as short a period of time as possible, generally calculated on the basis of one hour per inch (= 2.54 cm) of wire diameter [26].

Intercritical annealing alone does not sufficiently enrich the austenite with carbon to prevent martensitic transformation during quenching. If the steel were to be quenched directly after the intercritical annealing step, a dual-phase microstructure of ferrite and martensite would be observed. Hence, a second step is needed for further carbon enrichment. There is an optimum hold time in which a maximum volume fraction of R.A can be achieved. An increase in the time leads to more carbon-enrichment of the austenite, but too long of a hold can lead to the precipitation of carbides, which destabilizes the austenite phase [20].

The beneficial changes that occur in microstructure do not take place during the heating process, but during the cooling or quenching from the high temperature to room temperature. Therefore, the cooling rate is a fundamental factor in carrying out of all heat treatments [18]. When the steel is cooled suddenly, the carbon atoms cannot make an orderly escape from the iron lattice. This cause "atomic bedlam" and results in distortion of the lattice, which manifests itself in the form of hardness and/or strength. If cooling is fast enough, martensite is formed, this new structure (an aggregate of iron and cementite) is in the alpha phase [25].

During the microstructural transformation from austenite to martensite, there is a change of the FCC unit cell of gamma (γ) to martensite (M) body-centered tetragonal (BCT) crystal structure, resulting in increase of volume of unit cell. The volume expansion accompanying γ to M transformation is between 2 and 4%, depending on the carbon content the steel. This volume increase causes residual compression and tensile stresses inside the steel. The residual stresses can promote distortions and cracks in the steel, especially on long parts, due to the high cooling gradients developed during the process [27].

Continuous cooling transformation (CCT) diagrams are plots of temperature against log (time) for a given steel alloy having a particular chemical composition. CCT diagrams are used in heat treatments of steels and specially the decomposition of

austenite phase [25]. For a given steel alloy, the CCT diagram includes the critical cooling rate required for producing martensite as demonstrated in the CCT diagram of eutectoid steel shown in Figure 2.2. The critical cooling rate for producing a martensitic microstructure is exactly where the starting of pearlite transformation is just missed [26, 28]. A number of cooling curves on the diagram show how various cooling rates can produce different microstructures. The curve marked "full anneal" represents very slow cooling and usually obtained by cooling specimens in a furnace. This cooling rate normally brings the steel to room temperature in about a day and the final structure is coarse pearlite. The curve marked "normalizing" represents a heat treatment in which specimens are cooled in air (at intermediate rate). In this case, cooling is accomplished in a matter of minutes and the structure obtained is fine pearlite. The curve marked “oil quench” represents a faster cooling rate which may be obtained when a hot specimen is quenched directly in oil. The microstructure in this case is a mixture of pearlite and martensite. Finally, the curve marked "water quench" represents the fastest cooling rate so that no pearlite is able to form and the structure is martensitic [29, 30]. The curve marked “critical cooling rate” represents the minimum cooling rate to miss nose of CCT curve and produce a martensitic structure.

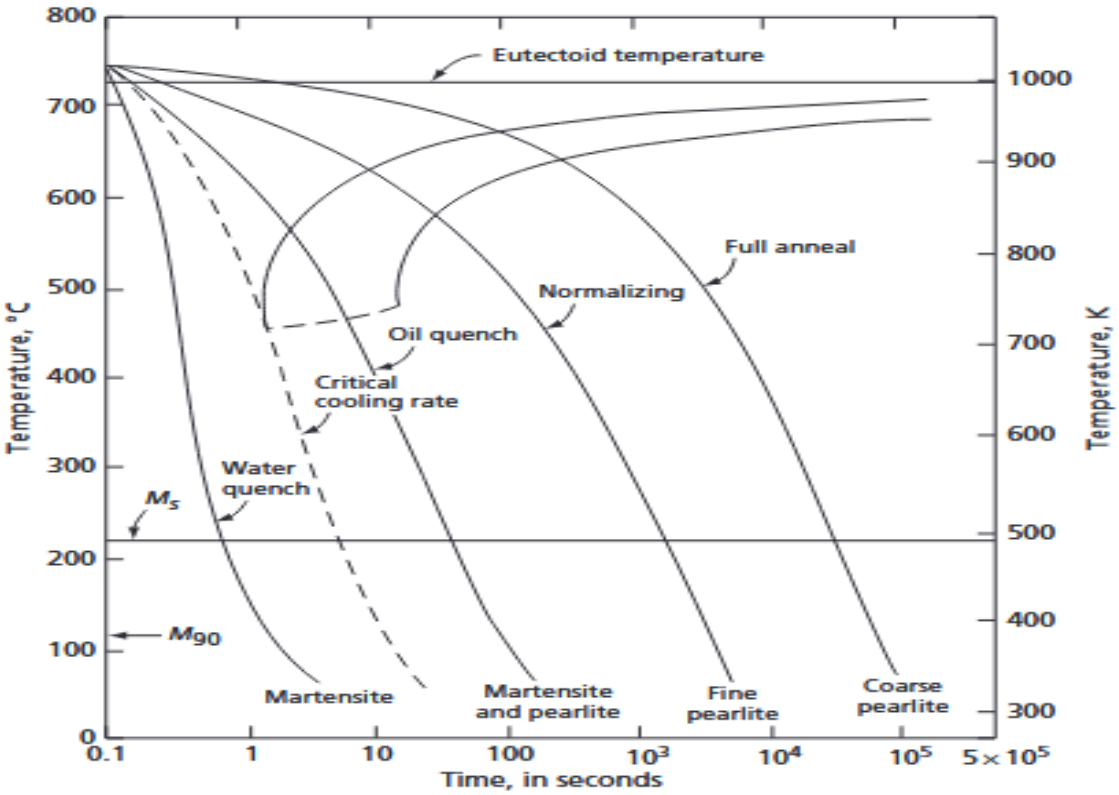

Figure 2.2 CCT Curve of eutectoid steel [29].

The microstructural evolution of martensite in as-quenched and quenched and tempered Fe–0.15C–0.215Si–1.9Mn–0.195Cr wt.% dual phase (DP) steels processed to give four different Ferrite/Martensite ratios was studied by Irina [24]. The samples were heated at 2.7°C/s to six different intercritical annealing temperatures between A1 (746°C) and A3 (845°C), held at temperature for 130 s and then water quenched to 20°C.The microstructures of the as-quenched samples consist of a mixture of martensite and ferrite. The martensite phase is continuous around the ferrite islands. In samples annealed at 810°C and above, the ferrite volume fraction is low (less than

1%) and the microstructure is almost fully martensitic (no retained austenite was detected).
Abdulkareem [7] investigated the effect of cooling rate on retained austenite amount of high strength low alloy steel. Retained austenite effects on microstructure were investigated using scanning electron microscopy (SEM) and optical microscopy and the results show that at low cooling rate the microstructure consist of bainite and/or martensite phase with small amount of retained austenite, while, increasing heating temperature and cooling rate results in microstructure that consist of martensite and retained austenite phases.
QIA et.al.[31] studied thermal stability of R.A. in high-carbon steels during cryogenic and tempering treatments (at liquid nitrogen temperature around − 196°C). The process was started with full austenitisation followed by quenching to ambient temperature in oil for 5 min. Then the specimens were subjected to a cryogenic treatment in liquid nitrogen for different times, from 0.5 to 240 hours. It is shown that the highest fraction of 28.9% R.A. was obtained in as quenched specimen ("0 h") and %R.A. decreased when the holding time increased. However, this decreasing trend was found to be remarkable only at the beginning of 2 h. There is still 8% of RA untransformed even after 240 h treatment.
Akay [32] studied the effect of quenching on physical properties of low carbon steel (0.055% C), the steel was intermediately annealed at 780, 825 and 870ºC for 60 minutes followed by water quenching to obtain different microstructures. The microstructures were composed of martensite (light area) distributed in the ferrite (dark area) matrix (as seen by optical microscope) with small amount of retained austenite (detected only by XRD). The ferrite phase did not experience any structural change after quenching from the austenite plus ferrite region. The volume fraction of martensite increased with growing temperatures.

2.2.2. Quenching Media

The important side effect of quenching is the formation of thermal and transformational stresses that cause changes in size and shape that may result in cracks. Therefore, the technical challenge of quenching is to select the quenchant medium and process that will minimize the various stresses that develop within the part to reduce cracking and distortion while at the same time provide heat transfer rates sufficient to yield the desired as-quenched properties such as hardness [15].
Quenching media is important since it is the effective way of hardening the material. The selection of quenching medium depends on the kind of heat treatment, hardenability of a particular alloy, the section thickness and shape, and the cooling rate needed to achieve desired microstructure [14, 33]. The commonly used quenchants are water, brine, oil and synthetic solutions. Water even though abundant and low cost has a drawback of forming cracks or effecting dimensional changes due to high cooling rates so that oil quench is the common [34]. The reason why oil quenching is so popular is due to its excellent performance results and stability over a broad range of operating conditions. Oil quenching facilitates hardening of steel by controlling heat transfer during quenching, and it enhances wetting of steel during quenching, minimizes the formation of undesirable thermal and transformational gradients, which leads to increased distortion and cracking [35].
Mineral oils have been found to exhibit best cooling capacity for the majority of alloy steels. They are however relatively expensive, toxic and non-biodegradable. Therefore, there has been considerable work in the past on the possibility of replacing mineral oils with aqueous solutions of chemical substances and polymers. More

recently, the use of locally available cooking oils, which are relatively cheap, nontoxic and environmentally friendly has begun to generate attention [36].
For the liquid quenchants like water and oil, cooling generally occurs in three distinct stages as shown in Figure 2.3.
1- Stage A, vapor blanket stage (or film boiling stage),
2- Stage B, nucleate boiling
2- Stage C, convective heat transfer [37].

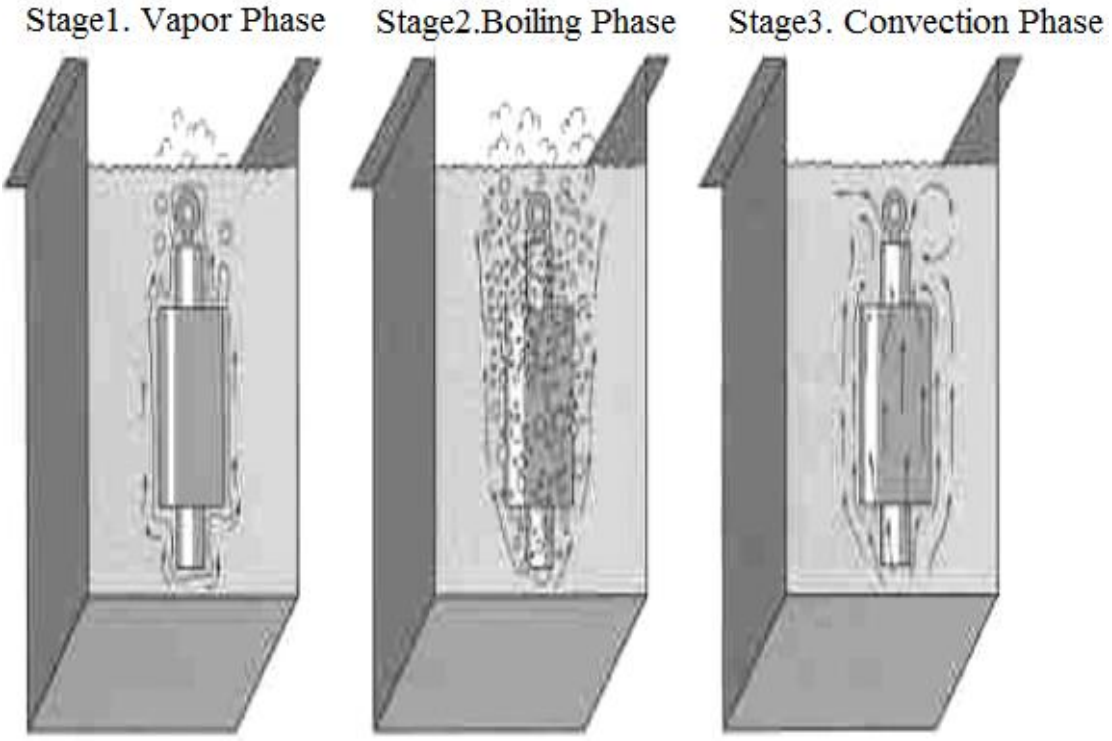

Figure 2.3 Cooling stages in liquid quenchtants [15,35]

Immediately after immersion of the specimen into the oil quenchant, a vapor film (its stability is quenchant dependent) forms around the entire sample surface. Heat transfer from the steel surface into the surrounding fluid is very low because of the high thermal resistance of the vapor film. The surface temperature, at which the vapor film breaks down and wetting occurs, is called the Leidenfrost temperature (TL). An ascending wetting front results in different wetting temperatures along the length of the specimen [38]. The subsequent nucleate boiling stage is the region exhibiting the highest heat transfer rates during immersion cooling. The stable vapor film eventually collapses and cool quenchant comes into contact with the hot metal surface resulting in nucleate boiling and high extraction rates. After the surface temperature is reduced to the boiling temperature of the quenchant, nucleate boiling stops and convective heat transfer starts. Heat transfer during this cooling stage is mainly influenced by free and forced convection and is comparatively low. During quenching, the duration of the vapor phase and the temperature at which the maximum cooling rate occurs have a critical influence on the ability of the steel to fully harden. The rate of cooling in the convection phase is also important since it is generally within this temperature range that martensitic transformation occurs and it can therefore influence residual stress, distortion, and cracking [15, 35].
Ideal quenchant is one that exhibits little or no vapor blanket stage, a rapid nucleated boiling stage, and a slow rate during convective cooling. The high initial cooling rates

allow for the development of full hardness by getting the steel past the 'nose' of the isothermal transformation diagram and then cooling at a slower rate beginning at the time the steel is forming martensite. This allows stress equalization; thus, distortion and cracking are reduced. The first criterion that any quenchant must meet is its ability to approach this ideal quenching mechanism.

When conventional quenching oils are used, the duration of stage A is longer; the cooling rate in stage B is considerably slower; and the duration of stage C is shorter. As such, the "quenching power" of oil is far less drastic than that of water. Water and water solutions exhibit high initial cooling rates. Unfortunately, because of water's low boiling point, this fast cooling persists until the steel is cooled to below 150ºC.

As most steels form martensite by this point, stresses are given little time to equalize. Thus, water is typically limited to simple shapes or low hardenability materials.

Typical oils have a boiling range between 230ºC and 480ºC. This causes the slower convective cooling stage to start sooner enabling the release of transformation stresses. Oil is, therefore, able to quench intricate shapes and high hardenability alloys successfully. As it is heated, oil has a proportional drop in viscosity. This allows the quenchant to move more freely, increasing, in general, the tendency to break the vapor blanket layer. The nucleate boiling stage is not drastically altered by changes in bath temperature. The cooling rate in the convection stage of an oil quench will slow as the bath temperature increases. This is advantageous for obtaining a slower rate of cooling through the austenite to martensite transformation range [35].

Çalik [39] has shown that oil quenching of 1040 and 1060 steels produce an essentially ferrite-martensite dual phase structure with about 4 volume percent of fine particle and thin film retained austenite.

Altaweel et.al. [40] studied the effect of quenching media on the hardenability of 4140 steel. They found that martensite was the dominant phase in the microstructure of the water-quenched sample, whereas bainite was the dominant microstructure found in the compressed air-quenched sample, and only pearlite was observed in the sample that was air cooled.

Odusote et.al. [41] studied the evaluation of mechanical properties of medium carbon steel quenched in water and oil. Samples of medium carbon steel were heated to 900 ^{o}C, 940 ^{o}C and 980 ^{o}C and soaked in these temperatures for 45 minutes. After quenching surface morphologies of the quenched samples were examined using optical microscope, hardness and tensile test. The samples quenched in palm oil displayed better properties compared with that of water quenched samples. This behavior was traced to the fact that the carbon particles in palm oil quenched samples were more uniform and evenly distributed, indicating the formation of more pearlite structure than those quenched in water and in as received samples.

shan et.al. [26] studied the effect of oil quench on the microstructure and the hardness of spring steel. Quench and temper process were used as a major heat treatment method. The resultant microstructures after quenching process are observed as martensite with small amount of retained austenite. They found that more retained austenite is formed in oil quenching than in water quenching.

Abdulkareem et.al. [7] studied the effect of quenching media on the microstructure of high strength low alloy steel. They found that the microstructure of annealed specimen consist of bainite while quenching specimen in air and sand after heating to a certain temperature produces bainite with small particles of retained austenite plus martensite. When quenching process was done in water and oil, the structure was found to be of lath martensite and retained austenite.

Evaluation of palm kernel oil, cotton seed oil and olive oil as quenching media of 0.509 wt%C medium carbon steel was investigated by Dauda1 et.al. [14]. To compare the effectiveness of the oils, the samples were quenched in water and SAE engine oil, which are the commercial quenchants. The machined specimen of the steel was heated at 880 ^{o}C, and then quenched in water, engine oil, palm kernel oil, cottonseed oil and olive oil. The water quenched sample showed martensite structure (dark) with retained austenite (white).The sample quenched in engine oil showed full martensite (dark).The sample quenched in palm kernel oil showed low proportion of martensite structure (dark) in ferritic (white) matrix. The sample quenched in cotton oil showed low proportion of martensite structure (dark) in ferritic (white) matrix. The sample quenched in olive oil showed low martensite structure (white) with retained austenite (dark). They concluded that water quenched specimen has the highest presence of martensite phase with retained austenite. Also evidence of less retained Austenite and martensite was observed more in plain carbon steel specimens quenched in the cotton seed oil, palm kernel oil and olive oil than those quenched in SAE 40 engine oil. The medium carbon steel specimen hardened in these oils showed an increased precipitation of ferrite due to the transformation of retained austenite.

Kadhim [16] studied the effect of quenching media on microstructure and mechanical Properties for medium carbon steel (0.5% C). The steel was austenized at different temperatures followed by rapid quenching in different quenching media, the structure of the steel after quenching from 960 ^{o}C in cold water contains coarse-grained martensite which is hard and brittle. Quenching in water from the same temperature produced structure with fine-grained martensite, while quenched in oil from 960 ^{o}C produced wastroosite (cementite precipitated in ferrite) and martensite structure.

Mohmmed et.al. [22] investigated the effect of quenching media on the microstructure of 0.42%C steel, the steel was quenched from 810^{o}C in water, 10% polymer +90%water, 15%polymer + 85%water, and 20% polymer + 80% water separately. Water quenched sample showed predominantly martensitic structures and retained austenite with various morphologies of cementite. The tempered water quenched sample exhibited mainly larger martensitic structure and retained austenite with smaller amount of cementite. As for samples treated with polymer solution, they exhibited more homogeneous martensitic structures and retained austenite with the disappearance of cementite.

Agurto et.al. [43] studied the effect of using water and mineral oil as quenching media for 1045 steel samples solutionized at 800, 805, 810, 815, and 820 ^{o}C. In case of water quenching all samples showed the typical martensite phase. For the ones quenched in oil, the sample quenched from 800 ^{o}C showed a martensite structure. For the sample quenched from 805^{o}C, a major development of martensite was observed. Likewise, the samples quenched from 810, 815 and 820^{o}C, showed a martensite phase to a lesser extent than samples quenched from 800 and 805^{o}C.

2.2.3. Specimen Shape and Size

The cooling rate of the samples largely depends on the type of quenching medium and specimen shape and size. In quenching process, cooling starts from the surface of the sample, i.e. the heat energy is removed from the surface of the sample, and hence, sample's surface area to volume ratio is a key factor in assessing its heat transfer behavior [40]. When this ratio increases, the associated cooling rate will be higher and consequently a higher hardness in the entire sample can be achieved. [44]. Hence, in a given cooling medium the cooling rate of both the surface and interior decreases as the dimensions of a sample increase and the possibility of exceeding the critical

cooling rate becomes less. The effect of sample size on hardness of quenched steel is tested by measuring hardness traverse of different size steel bars quenched in the same medium. Jominy curve [29]. The effect of specimen size on the hardness of 0.65 percent carbon steel is shown in Figure 2.4. It can be seen that the hardness is greater where the cooling is most rapid near the quenched end.
Shan [26] studied the effect of section thickness on the hardness of the oil quenched process. He found that for a critical bar diameter of about 1.5 inch, the hardness at center of bar is about 50 HRC and at circumference is 57 HRC.

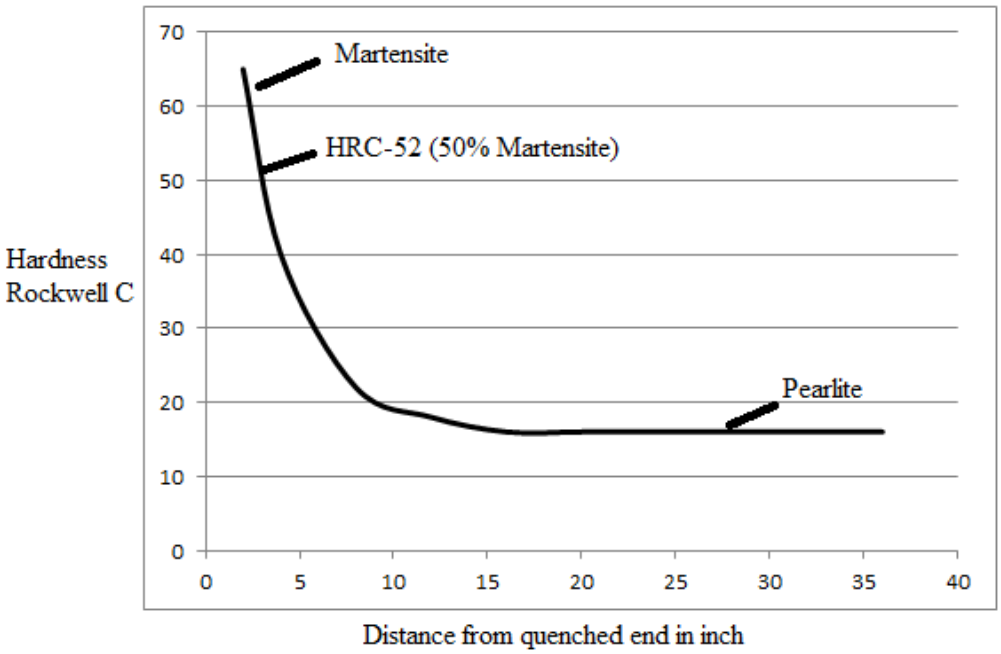

Figure 2.4 Variation of the hardness along a jominy bar [29].

2.3. Retained Austenite

Austenite that does not transform to martensite upon quenching is called retained austenite (R.A). Retained austenite can be found when the steel temperature after quenching does not reach the M_f (martensite finish temperature). Because the M_f temperature is below room temperature for alloys containing more than 0.30% carbon, significant amounts of untransformed, or retained austenite may be present with martensite at room temperature. Retained austenite is a specific crystalline form of iron and steel. R.A usually appears as light-colored areas amongst the dark colored martensite needles [46]. Depending on the composition, austenitizing temperature, quenching rate, final quenching temperature, and stress state, heat-treated steel could contain a significant volume fraction of retained austenite. The role of retained austenite in these microstructures is complex, as it can have both positive and adverse effects on the properties and performance of steel. Too much retained austenite can result in lower elastic limits, reduced hardness, lower high cycle fatigue life, and dimensional instability. Too little retained austenite, however, can result in poor fracture toughness and reduced low cycle fatigue and rolling contact fatigue life [47-49].
The carbon content and the grain size are considered to be the most influential factors of R.A grains. Several factors that affect the R.A. stability will be discussed in the following subsections.

2.3.1. Grain Size

A number of experimental and modeling studies indicate that the stability of austenite is inversely proportional to its grain size. Smaller R.A grains are more resistant to transformation to martensite and are thus more stable for several reasons. In the case where a small austenite grain does transform, it would transform into many small martensite laths since martensite laths are unable to cross grain boundaries or areas with a high concentration of dislocations. Consequently, the interfacial energy component for martensite formation is significantly increased, which in turn, decreases the Ms temperature. Moreover, a high number of nucleation sites would be required for this transformation to occur. On the other hand, R.A grains that are too large will not contribute to the work hardening response because they will transform into martensite upon quenching [6,20].

2.3.2. Grain Shape

Retained austenite can be found in the steel microstructure in one of two morphologies: isolated R.A islands and thin films along prior martensite or bainite lath boundaries. Previous studies have found that R.A thin films do not significantly contribute to most of steels, so the focus has been mainly on isolated R.A islands [20]. In the case of R.A islands, the aspect ratios of these grains affect their stability. Although elongated particles tend to experience higher stresses and stress concentrations, studies have found that retained austenite grains with larger aspect ratios tend to be more stable. Transformation of an elongated austenite grain would require the formation of many small martensite laths to compensate for the morphology of the grain because the laths are unable to cross grain boundaries. This transformation would result in a high interfacial area for the new martensite in comparison to the volume. Thus increasing the interfacial energy component of the energy required for transformation, makes elongated R.A grains more stable [20].

2.3.3. Spatial Distribution of Surrounding Phases

The spatial distribution of the phases around the R.A grains affects the stresses and strains that individual R.A grains experience, and therefore, affects the R.A stability.
The relative hardness of each of the four phases – ferrite, R.A, martensite and bainite are different and thus affect the stress distribution in the microstructure accordingly.
ferrite is the softest phase, followed by bainite, austenite, and finally martensite is the hardest. Under normal circumstances, austenite is considered to be a soft phase; however, R.A. has been found to be harder due to its unusually high carbon content. R.A grain that is surrounded by ferrite grains will transform at relatively low strains because the soft ferrite matrix will yield at low strains and subsequently shed load onto the R.A, leading to earlier R.A transformation. In comparison, R.A grain that is surrounded by bainite will experience less load if it was surrounded by ferrite due to a stress shielding effect, and therefore, transform later in the deformation process. Stress shielding occurs because bainite is stronger than ferrite due to its higher carbon content and higher dislocation density [20].

2.3.4. Carbon Content

The enrichment of carbon is considered to be one of the most important mechanisms for retaining austenite in the steel microstructure. This is because the carbon content affects the thermodynamics of the martensitic transformation which is the strongest austenite stabilizer amongst all the alloying elements in steels. That is, R.A grains with very low levels of carbon (<0.6 wt%C) are susceptible to martensitic

transformation at low levels of strain and R.A. grains with very high levels of carbon (>1.8 wt%C) do not transform at all. Increasing the carbon content of R.A. lowers the Ms temperature, thereby increasing its thermal stability. Therefore, the mechanical driving force required for martensitic transformation increases with a higher carbon content. This means a higher carbon content of R.A corresponds to higher stability [20].

Ouda et.al. [50] studied sintered steel specimens Fe–Mo–C, Fe–Cr–C and Fe–Ni–C-steels with different contents of carbon. The carbon contents chosen were 0.3, 0.5, 0.7, 1.0%. These steels were heat treated at 800 ºC and 900 ºC respectively for 30 minutes and then quenched in water. The retained austenite amount is measured using magnetic and XRD techniques. It was found that higher amounts of retained austenite are recorded at higher carbon content. The reason for this well-known effect is the stabilization of the austenite by carbon.

Zhou et.al. [51] studied the effect of carbon content and dynamic tensile stress on the stability of retained austenite of steel containing 0.6%C and 2.77%C. The specimens were austenized at 880 ºC for 30 mins, and quenched to a salt bath furnace at 150 ºC, left there for 2 minutes and then tempered in salt bath furnace for 30 min at 450 ºC. Finally, the samples were cooled down in water. The results showed that the high carbon film-like austenite was much more stable than the low carbon blocky austenite.

Kokoza et.al [52] studied the mechanical stability of retained austenite in unalloyed C45 and C65 heat-treated steels heated up to 840 ºC and soaked for 30 min then quenched in water. The samples were also tempered at 150 ºC for 120 mins. The retained austenite was measured using XRD technique and the results were 8.7% and 12% R.A for C45 and C65 steels respectively.

2.3.5. Alloying Elements

The main alloying elements in carbon steels are Mn and Si, with possible additions of Al, P, Mo, Nb, V and Ti. Some steels could have deliberate additions of Cu, Cr and Ni which could be present as tramp elements. Genarlly, the lower the Ms temperature, the larger amount of R.A will be stable. Si plays an important role as a ferrite stabilizer and as a suppressor of cementite formation during bainite transformation. Si helps raise the temperature of ferrite formation and assists in more C to be rejected into the remaining austenite, thereby providing its stabilization. Similar to Si, both Al and P also inhibit the formation of cementite, decrease the C activity coefficient and increase the solubility of C in ferrite, and lead to a higher enrichment of C in R.A. [6]. However, Al also has the potentially deleterious effect of making the retained austenite less stable by increasing the Ms temperature to above room temperature [53].

Mn is an austenite stabilizer which reduces the Ms and promotes carbon solution in austenite [54]. Mn has the strongest effect followed by Cr. All alloying elements lower the Ms temperature, except for Co and Al which raise it [29].

Nemecek et.al. [54], used XRD technique to detect the amount of R.A. of two quenched alloyed carbon steels (1st type contains 0.4%C, 0.58%Mn, 2nd type contains 0.2%C, 1.45%Mn). The R.A amounts were 7.2% and 8.3% respectively. These results may explain the effect of Mn on R.A stability.

Vargas et.al. [55] has measured retained austenite and nonmetallic inclusions for trip steel with different amounts of alloying elements (five different steels) by X-ray diffraction and saturation magnetization techniques. The heat treatment consisted of intercritical annealing carried out at 812°C for 30 min, rapid cooling in a salt bath

directly from the annealing temperature down to the bainitic transformation temperature. Multiphase microstructures composed of different contents of ferrite, bainite, martensite, and R.A are found. They found that Steels with higher contents of Si, Al, Mn, and C resulted in higher retained austenite volume fraction.

2.3.6. Austenizing Temperature

It can be recognized that R.A. formation increases as the temperature of austenizing increases for the same quenching media. At high austenizing temperature some (or all) of the carbides dissolve causing an increase in carbon content within the austenite crystal lattice and hence a large increase in R.A fraction [7].

Abdulkareem et.al. [7] have evaluated R.A volume fraction in AISI4340 alloy steel using–XRD and magnetic measurement methods. Their results indicate that R.A formation increases by increase of austenizing temperature as well as by increase of cooling rate. They found that when specimens heated up to 1000˚C then quenched in water, the amount of R.A was 27.2 wt%, and when the specimens heated up to 800 ˚C then quenched in sand, the amount of R.A was lower by 20%.

Yaso et.al. [56] have studied the amount of R.A in quenched high C-high Cr alloy steels. The steel was austenized at different temperatures and quenched in air, the %R.A was 5% for austenizing temperature of 950 ºC and increased to 30% for austenizing temperature of 1100 ºC, %R.A reached approximately 60% for austenizing temperature of 1200 ºC. It can then be understood that R.A becomes more stable with increasing the austenizing temperature. They concluded that as the austenizing temperature increases more carbides dissolve into the austenite matrix resulting in an increase in carbon concentration. This effect leads to greater chemical stability of austenite.

2.3.7. Austenizing Time

Typically, the volume fraction of R.A first increases with holding time and then decreases. During the very early stages of holding, the initial low value of R.A volume fraction with relatively low C content is associated with the beginning of pearlite transformation. With increasing time, the incomplete pearlite transformation progresses further and results in more C being rejected into residual austenite. This makes the R.A more stable on cooling and thus, its volume fraction and C content reach maximum values. At longer holding times, the decomposition of the austenite which is saturated in C into ferrite and carbides takes place and leads to a reduction in the R.A volume fraction and its C content and an increase in the amount of martensite [6].

Pashangeh et.al. [5] explained the effect of austenizing holding time on the stability of R.A. they found that R.A. stability increases with increasing the isothermal holding up to 200 s. The reason for this stability is that with increasing isothermal holding time, more carbon atoms diffuse from the primary supersaturated bainitic crystals into the adjacent prior austenite areas causing higher thermal stability of retained austenite on heating.

Zhao et.al. [8] investigated the volume fraction of retained austenite in TRIP steels by magnetization and XRD measurements. The samples were pre-annealed for 10 min at 900°C and then quenched at rate of 25°C s−1 to 400°C, held at this temperature for 0, 0.5, 1.0, 1.5, 2.0, 3.0, 5.0 and 10.0 minutes, respectively, they have subsequently cooled at approximate rate of 2°C s−1 to room temperature. It was found that about 5.6% and 2.5% of austenite are retained more than in the as-quenched (zero austempering time) samples.

2.3.8. Mechanical Straining

Mechanical stressing has a significant effect on the stability of retained austenite.
It has reported that %R.A inversely proportional to mechanical straining.
Quintin et.al. [57] studied the effect of uni-axial tensile testing on the stability of R.A of TRIP steel. The %R.A as measured by XRD were 7±1% and 4±1% for 15% and 25% straining respectively. The retained austenite values were also calculated at failure to be only 3±1%. It can be concluded that the stability and the volume fraction of retained austenite are greatly affected by the mechanical behavior of TRIP steel.

2.4. Measurements of Retained Austenite

Several techniques were developed to calculate the amount of retained austenite in heat-treated steel. They include metallography, x-ray diffraction (XRD), neutron diffraction, scanning electron microscopy (SEM) and magnetization measurements. Among them, the XRD method is the most commonly used as it is a suitable technique and widely available. The following subsections give more details on some of these characterization methods.

2.4.1. Metallographic Technique

In well-characterized alloy systems, the metallographer can examine the microstructure and compare it to published images to identify phases and constituents. However, in less well-studied systems, phase identification is more challenging [58].

2.4.1.1. Optical Microscopy

Optical microscopy is one of the most commonly used methods in steel microstructure characterization. Metallographic samples are required to be carefully ground and polished to a mirror-like finish followed by chemical etching if necessary. The microstructure is then examined with a light microscope, where the contrast in the image results from the different reflectivity of the different regions of microstructure. The more chemical active regions to the etchant will dissolve faster than the other areas hence reflect the light differently. Optical micrographs can be used to identify/quantify microstructure parameters such as phase type, phase fraction, grain size/distribution, and precipitates. The resolution of an optical microscope is limited by the wavelength of visible light. Therefore, some microstructure features (less than approximately 0.2 micron) are too fine to be observed [59].
Conventional black-and-white and color light metallography techniques have generally been used by numerous researchers in order to reveal retained austenite from other micro-constituents in multiphase low alloy steel microstructures. In general, ease of sample preparation, lack of limitation on exterior geometry of samples are among the key advantages of light metallography techniques [60]. Nevertheless, based on the steel chemical composition and the type of applied heat treatment cycles, detection of various microphases in micro-composite microstructure is quite complex, for example it is hard to distinguish between finely divided retained austenite and martensite. Hence, serious difficulties have been encountered in various cases during the preparation of metallography samples.
Retained austenite is “white-etching” phase (as ferrite, bainite and cementite) that is encountered in steels. Retained austenite is only observed with the light microscope when the carbon content is high, generally > 0.6% [61]. High-alloy steels with carbon contents down to 0.4% can form small amounts of retained austenite which can be

observed only with dark field illumination of thin foils using transmission electron microscope (TEM). In many steels, 10 to 15 percent R.A. is the minimum detectable limit [62]. When amounts are >15%, retained austenite can be seen in the light microscope, but image analysis measurements of retained austenite will be substantially lower than the true level determined by XRD [58,49].
The key to seeing the true microstructure is to choose the etchant that best reveals the phases or constituents in the material. The etching solutions used to reveal steel microstructures are Nital and Picral. Nital attacks ferrite at a rate that varies with the crystal orientation of each grain relative to the plane of polish. Picral is insensitive to crystal orientation. Consequently, Nital reveals the ferrite grain boundaries while Picral does not. However, because Nital is orientation- sensitive, not all of the grain edges are visible. If cementite is present, and this is quite common in sheet steels, it can be hard to see using Nital, as many particles will be in the grain boundaries. However, Picral does not reveal the ferrite grain boundaries, making it easy to observe cementite particles [58].
Klemm's I and Baraha type staining solutions could be helpful to identify retained austenite which can color ferrite strongly. They also color martensite and bainite, but not retained austenite [58]. Table 2.1 lists the different etching solutions used to reveal steel microstructure**.**

Table 2.1. Different etching solutions for steels [58].

Etchant	Composition	Comments	Availability
Nital	99-90 mL ethanol 1-10 mLHNO_3	The most common etchant for steels, reveals ferrite, perlite, Martensite and cementite.	√
Picral	100 mL ethanol Picral, 4 g picric acid	Picral, better than Nital for annealed microstructures. Does not reveal ferrite grain boundaries.	√
Klemm's I	50 mL stock solution 1 g $K_2S_2O_5$ water saturated with $Na_2S_2O_3$	It colors ferrite strongly; also colors Martensite and Bainite, but not carbides or retained austenite.	$Na_2S_2O_3$ is not available
Baraha	85 mL water 15 mL HCl 1 g $K_2S_2O_5$	Colors phases in highly alloyed tool steels and martensitic stainless steels.	$K_2S_2O_5$ is not available
LePera	4% Picral 1% aqueous sodium metabisulfite ($Na_2S_2O_3$)	Etch for duplex stainless steels, it colors ferrite but not austenite.	$Na_2S_2O_3$ is not available

Kučerová et.al. [47] investigated the amount of retained austenite of TRIP and martensitic steels obtained by quenching and partitioning (QP). Color etching by LePera and Klemm applied to TRIP steel tented all phases and structural components

in dark colors, except of retained austenite, which remained white. X-ray diffraction was used to determine the amounts of retained austenite. They found that LePera and Klemm colour etchants can be successfully used for retained austenite revelation.
Nemecek et.al. [54] evaluated retained austenite of 0.24% high strength steel by metallographic methods. Retained austenite was observed with a Nikon Epiphot 200 microscope upon colour etching. They used Nital followed by Na2S2O5. They concluded that it is impossible to detect retained austenite by means of ordinary light microscopy.
Su et.al. [3] compared the difference in determining the austenite amount in SKD 11 tool steel (1.46 C, 12.24 Cr) using the micrographic method as opposed to the X-ray diffraction method. The carbide and prior austenite grain boundaries were observed using Nital etching. Etching of the SKD11 specimen using Beraha's reagent revealed retained austenite, martensite and carbide as white, red and blue in the microstructures, respectively. However, the calculated value of R.A. (11.4%) is lower than that acquired by the X-ray diffraction (16.6%). This leads them to conclude that it is more accurate to evaluate the amount of retained Austenite by X-ray diffraction analysis.
Quintin et.al. [57] tried to determine the R.A.% of 0.2%C steel using metallographic method. The principle of the color etching methods (dry picric acid in ethanol and sodium metabisulfite in distilled water) was used to reveal the microstructure. Ferrite grains appeared in green-blue colour, bainite in brown, and retained austenite (and/or martensite) in white or yellow color. They concluded that only qualitative observation is possible and the quantification of the retained austenite phase required x-ray diffraction method.
Vargas et.al. [55] used LePera method color etching technique to reveal the microstructures of TRIP steels with different alloying contents. The etchant was a mixture of freshly prepared equal portions of 4wt% picral and 2wt% aqueous sodium metabisulfite. The etching time was between 20 and 40 sec, depending on the steel composition. metallographic results for the TRIP steels showed multiphase microstructures composed of ferrite, bainite, martensite, and R.A. The ferrite appeared blue, bainite dark/light brown. However, even when the martensite and retained austenite stand out in white from the rest of the phases, they are not separately identifiable.
Eldis [10] measured the retained austenite content in carburized samples of EX24, EX32, and SAE 4820 by both x-ray diffraction and automated quantitative metallography. The carburized samples were tempered for 1 h at 200 ºC prior to determination of the austenite content. For the metallographic measurements, the specimens were etched in a Nital solution which allowed clear distinction among the three principal microconstituents present that include retained austenite, bulk martensite, and surface martensite. He found that, at lower carbon contents, the morphology of the martensite was predominantly nonlenticular, and detection of the austenite in such a matrix was impossible. Carbon contents in excess of 0.6 %wt percent resulted in a predominantly lenticular martensite matrix, so that retained austenite was readily detectable and good agreement between the x-ray and metallographic measurements was obtained.

2.4.1.2. Electron Microscopy

Electron microscopy can be used to examine the microstructures with much higher resolution resulting from the focused high energy electron beam. The two most common types of electron microscopes are scanning electron microscope (SEM) and

transmission electron microscope (TEM). SEM uses the beam reflection mode and TEM uses the transmission beam mode. Electron microscopes can reach resolutions at the nanometer (nm) scale, making them a powerful technique to characterize the fine details of a steel microstructure, such as martensite/bainite laths, bearlite lamella, small precipitates and dislocation structures. SEM also has great depth of field, which is useful when characterizing non flat surfaces such as fracture surfaces [59].

Most of the SEM and TEM systems are housed in buildings and are relatively expensive. Some portable SEM systems are available now, but small size samples (a few centimeters) are required. The sample size for TEM analysis is normally required to be a 3mm disc which is prepared to 100-150 nm thickness before ion beam thinning or electro-polishing is used to give a region of approximately 30-40 nm thickness that is 'transparent' to the electron beam. The preparation of TEM samples can be challenging and time consuming. Therefore, electron microscopy is a destructive technique for large steel components [59].

Abdulkareem et.al. [7] used image technique by SEM to show the microstructure of quenched steel (%C= 0.42%) and they concluded that SEM results provide more information compared to other microscopic techniques because they take into account the presence of holes as well as the very fine distribution of retained austenite in areas where large amounts of martensite are present.

2.4.2. X- Ray Technique (XRD)

X-Ray Diffraction (XRD) has following advantages over other diffraction methods for characterization of R.A.

i) It is a non-destructive technique,

ii) It is usually used at ambient conditions,

iii) It is a quantitative technique for measurement of phase contents, texture and other structural parameters such as average grain size, strain and crystal defects [63].

High energy electromagnetic x-rays used for x-ray diffraction have wavelength (λ) in the angstrom range comparable to lattice spacing of crystalline elements. The low wavelength allows them to penetrate solids with partial absorption during transmission. When x-rays interact with a sample, a portion of the beam will be scattered by the electrons in the material. A schematic diagram of X-ray diffraction by planes of atoms is given in Figure 2.5.

Bragg's law [9] gives an expression that relates the x-ray wavelength, λ to interplannar spacing, d, and angle of diffraction, θ as:-

$$n\lambda=2d \sin\theta \quad \text{……………………………………………….. (2.3)}$$

Where (n) is the order of order of reflection.

The first Quantitative determination of retained austenite in heat-treated steel was reported by Tamaru and Sekito in quenched and annealed steels [49]. Their method became the most commonly technique used for determining the volume fraction of R.A. Measurements of less than 0.5 percent retained austenite could be detected [49,61].

It should be realized that there are a few drawbacks associated with XRD. XRD is a surface technique, since x-ray radiation can only penetrate to an approximate depth of

2 μm in a steel sample. This means that surface preparation of sample is critical for accurate results [4,5,9]. Surface preparation effects resulting from mechanical stress (by grinding) and surface roughness can result in 3% error for evaluating the amount of retained austenite [3].

Quantitative determination of the amount of retained austenite for steel and carburized steels can be obtained using the x-ray diffraction pattern because austenite phase produces diffraction peaks at different diffraction angle (θ) locations than ferrite and martensite [61]. The intensities of the diffraction peaks are related to the amount of the existing phases, and this is the principal of the quantitative phase analysis by XRD [1,3]. If the crystalline phase or grains of each phase are randomly oriented, the integrated intensity from any diffraction plane (hkl) is proportional to the volume fraction of that phase [65] :

$$I_\alpha/I_\gamma = R_\alpha/R_\gamma \times V_\alpha/V_\gamma \quad \text{.....(2.4)}$$

Where I is the integrated intensity, R is theoretical intensity, and V is volume fraction of phases α , ɣ.

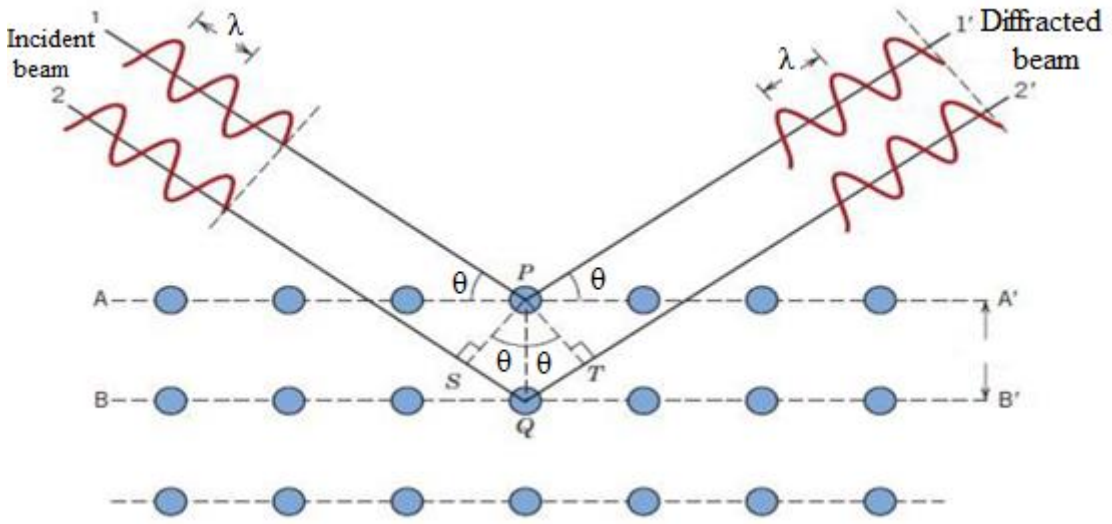

Figure 2.5. A schematic daigram of x-Ray diffraction [59].

Different methods have been developed to use the peak integrated intensity for quantitative analysis. These include Internal Standard Method, External Standard Method, Direct Comparison Method, and others [66].

The Internal Standard Method is the procedure in which, a known quantity of a reference powder is added to the unknown. Any number of constituents in a mixture may be quantified independently. The Internal Standard Method is applied broadly to any mineral or materials systems for which the chemistry is unknown. This may be applied to solid systems, such as alloys, plasma sprayed coatings, or oxide layers [63].

The External Standard Method allows the quantification of one or more components in a system, which may contain an amorphous fraction..

The Direct Comparison Method requires no reference. It is of immense metallurgical interest because it can be applied directly to polycrystalline aggregates. Since its development, it has been used for instance to measure the amount of retained austenite in hardened steels [66]. This method uses separate peaks to determine the amount of austenite. In choosing diffraction lines (peaks) for measurement, one must be sure to avoid overlapping or closely adjacent lines from different phases [63].

Because this method will be used in this work, more details will be given on its use in next section.

2.4.2.1. Determination of R.A Using Direct Comparison Method

In this method, the austenite fraction is determined using the ratio of the austenite and ferrite diffraction peak intensities and the values of theoretical intensities for each phase. According to ASTM E975 standards [65,67,68], the amount of retained austenite in steels can be calculated from the peaks in the X-ray pattern using the following formula:

$$R.A.\% = \frac{\sum(I_\gamma/R_\gamma)}{\sum\{\left(\frac{I\alpha}{R\alpha}\right)+\left(\frac{I_\gamma}{R_\gamma}\right)\}} \times 100. \quad \text{(2.5)}$$

Where: Iγ: is the integrated intensity of a γ – peak.
Iα: is the integrated intensity in of an α – peak.
Rα and Rγ are the theoretical integrated intensity of chosen α and γ peaks respectively.
The theoretical intensity (R) is calculated as:

$$R = \frac{1}{U^2}|F^2|m\frac{1+Cos^2 2\theta}{Sin^2\theta Cos\theta}e^{-2M} \quad \text{(2.6)}$$

Where:
U is the unit cell volume which can be calculated from the lattice parameters of each phase. For austenite (FCC), the lattice spacing (a) can be calculated from te following formula [69].

$$a\ (Å) = 3.555 + 0.0044X \quad \text{(2.7)}$$

For martensite (BCT), the lattice spacing (a) and (c) can be calculated from the following formula:

$$a\ (Å) = 2.867 - 0.013\ X \quad \text{(2.8)}$$

$$c\ (Å) = 2.867 + 0.116X \quad \text{(2.9)}$$

Where X = carbon%, F is structure factor which can be calculated using atomic scattering factor (f) as shown in appendix A) [69] as follows:
For Bcc and BCT (α) structure: F= 2f
For Fcc (γ) structure: F=4f
The term $\frac{1+cos^2 2\theta}{sin^2\theta\ cos^2\theta}$ is the Lorentz polarization factor. (as shown in appendix B) [69].
m is the multiplicity factor, θ is the peak diffraction angle (as shown in appendix C) [69].
e^{-2M} is a temperature factor (as shown in appendix D) [69].
The austenite peaks (111), (200), (220) and the ferrite peaks (110), (200), (211) show up in diffraction patterns containing these phases. In many cases, the (111) austenite and (110) ferrite peaks interfere with each other and are hard to be resolved. So (211), (200) are the typical peaks used for martensite and (220), (200) for austenite.
Su et.al. [3] used several calculated methods of XRD such as choosing two peaks (M_{200}, γ_{200}), three peaks (M_{200}, γ_{200}, γ_{220}) or four peaks (M_{200}, M_{211}, γ_{200}, γ_{220}) for nitrogen quenched JIS SKD11 steel (1.46 C, 12.24 Cr). They compared the results of each method with two standard samples of known R.A%. From the results, they

concluded that the best method among all calculation methods is choosing four peaks (M_{200}, M_{211}, γ_{200}, γ_{220}) provided that the background is carefully removed.
Abudaia [70] used direct comparison method to detect the amount of R.A of carborized steel containing 3% Nickel quenched in oil and deep freeze in liquid nitrogen, Diffraction patterns showed that all hardened specimens consist of martensite and retained austenite. The two phases were readily identified in XRD diffraction patterns. Martensite is characterized by diffraction peaks from α_{200}, α_{211}, and α_{220} planes, while the austenite phase by peaks from γ_{200}, γ_{220}, and γ_{311}. The strongest diffraction peaks of α_{110} and γ_{111} were very close and these lines were avoided in any calculation. Substantial amount of retained austenite is produced in carburized specimens due to the high carbon content and the presence of nickel. The oil quenched specimen showed the highest amount of retained austenite (20.5 %). The retained Austenite content is reduced to 11.2 % after direct deep freezing.

2.4.3. Electrical Resistivity (E.R) Technique

The electrical resistance of a material is a basic material property that defines how well the material will conduct an electric current. The electrical resistivity (Ω-m) is defined by Ohm's law as E = ρj, where E (V/m) is the electrical field and j (A/m2) is the current density. Electrical resistivity can also be defined as the ratio of the potential difference ΔV (V) to the current I (A), across a material which has a cross-sectional area of 1 $m^2$and is 1 m long (ρ = ΔV/I). The reciprocal of resistivity is conductivity, σ (Ω/m).
Electrical resistivity is one of the most characteristic physical properties of materials and is dependent on temperature and crystal defects (such as solute atoms, dislocations and void and very fine discontinuity [71,72,73]. E.R is time and cost effective non-destructive method of producing the shape and location image of an object. It can be used in various applications such as in detecting underground water and cavities, faults, and cracks [74]. Generally, E.R is performed by installing an electrode made of a conductive material.
In metals there are two mechanisms that account for most of the scattering of electrons: the interaction of electrons with chemical impurities and physical imperfections, and the interaction of electrons with thermal vibrations of the atoms of the lattice. If it is assumed that each of these mechanisms is independent of the other, a separate resistivity can be assigned to each. The resistivity arising from scattering by impurity and imperfection is usually referred to as the residual resistivity. The resistivity due to thermal scattering is called intrinsic resistivity[75]. The residual resistivity provides a good indication of a specimen's purity and freedom from strain [76]. It is also found that electrical resistance measurements would be a particularly suitable method for detection of phase transitions as well due to the variations in specific electrical resistivity that is dependent on crystal structure. Electrical resistance measurements also offer the advantage of being applicable to a wide variety of specimen geometries [77,78].
When electrons are conducted through a perfect (defect-free) metal crystal with no thermal effects, there should be no scattering of the electrons and the resistivity is zero. However, 'defects', including impurities, grain boundaries, dislocations from plastic deformation and thermal vibrations, can scatter electrons in a metal. Increasing the number density of defects causes an increase in the electrical resistivity. This is described by Matthiessen's rule in following equation [59,79]:

$$\rho_{tot} = \rho_{temp} + \rho_{phase} + \rho_{solute} + \rho_{defects} \quad \text{.....(2.10)}$$

Where ρ_{tot} is the resistivity of the material, ρ_{temp} is the resistivity from temperature change, ρ_{phase} is the resistivity from second phases (e.g. retained austenite), ρ_{solute} is the resistivity from the substitional solid solution, and $\rho_{defects}$ is the resistivity from dislocations, grain boundaries, etc.

The resistivity of a material is strongly related to its composition and microstructural parameters. These include alloying elements in solid solution phase balance, and precipitates. Different microstructural phases in steels may have different resistivity values. For example, the resistivity of ferrite is about 130 nΩ-m, whereas the resistivity of pearlite is about 180 nΩ-m [59]. A mixture of two phases can be estimated by applying the rule of mixtures using the resistivity of each phase [80].

The resistivity of conductive materials is typically found by sourcing a known current (I), measuring the voltage drop (V) (which is very low for conductors), then calculating the resistivity (ρ) using following equation:

$$\rho = \frac{V \times A}{I \times L} \quad \text{(2.11)}$$

Where A is the cross-sectional area of sample, and L is the distance between voltammeter leads as shown in Figure 2.6 [71]. For conductive materials like metals, the voltage drop is usually in the range of microvolts. So to determine ρ accurately, precise measurement of voltage drop is crucial. Potential error sources include test lead resistance, thermo-electric voltages and the use of voltmeter with insufficient sensitivity. Fortunately, special techniques can reduce the impact of these errors by using a four-point collinear probe method, which eliminates the effect of lead resistance [81].

Four-point probes (FPP) is a tool that is commonly used to measure resistivity values of conductive materials. It is called four-point probes because there are four points that touch on the sample surface. As shown in Figure 2.7, the four points (probes) are aligned in a straight line such that the distance between probes is the same. A constant electric current is streamed along the sample through two outermost probes. If the sample has resistance, there will be a voltage drop when the current flows through it. The voltage drop is measured through two inner probes [82].

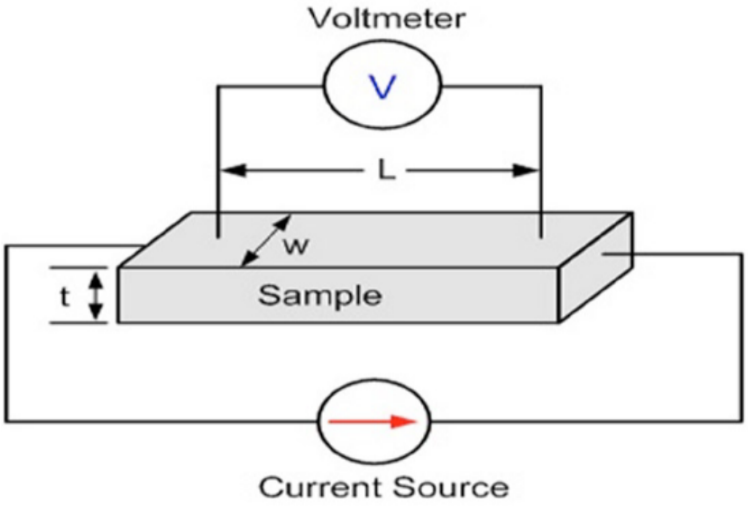

Figure 2.6. Electrical resistivity measurements [71].

The ‘four point probe’ method has proven to be a convenient tool for the measurement of resistivity of small size specimens (of the order of mm). This method is applicable when the distance between the probes is small as compared to the smaller dimension of the sample [83]. To determine the resistivity of bulk samples by this technique it is required that the sample thickness (t) be larger than the spacing between the probes (s).
The resistivity can then be calculated by [82]:

$$\rho = 2\pi s \frac{V}{I} \quad \text{……..……..……..……..} \quad (2.12)$$

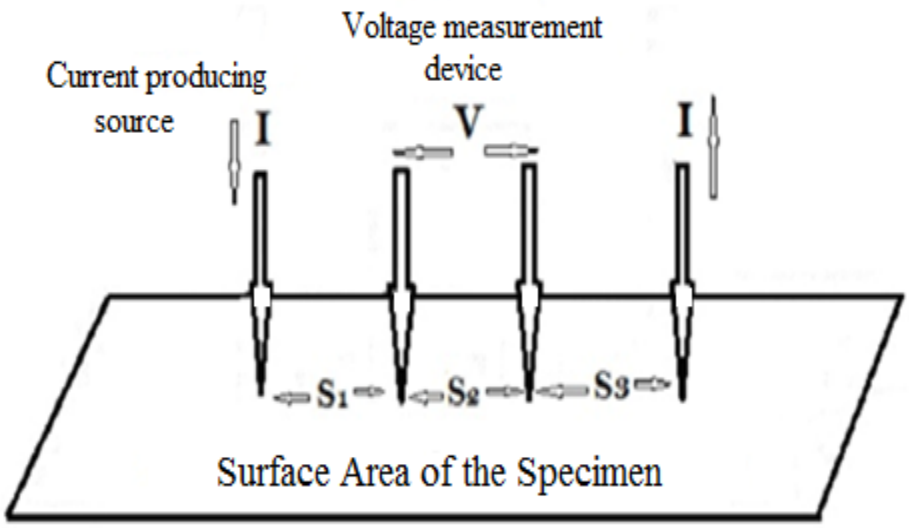

Figure 2.7. Four point prob method [83].

Bahgat et.al. [84] used the E.R. technique to provide an insight into the phase transformation occurring in low carbon and high alloy steels. After continuous measurements of E.R. during heating and quenching from 900 ºC, he noticed a drop in E.R. from 85 to 22 μΩ-cm, when austenite is quenched to form martensite. He concluded that this technique is accurate in the detection of phase transformation in such types of steels.
Mohanty et.al. [85] examined the changes in electrical resistivity accompanying transformation of low and high carbon steel. Samples of such steels were subjected to continuous electrical resistivity measurements for temperatures up to 900ºC during heating and after quenching at a rate 20 ºC/min. They concluded that stabilized retained austenite formed during transformation to martensite is responsible for the anomalous rise in electrical resistivity.
Akay et.al. [32] studied the effect of quenching on physical properties of low carbon steel (0.055C), which was annealed at 780, 825 and 870ºC for 60 minutes then water quenched to obtain different microstructures. The resistivity was measured using a Jandel four point probe (the same type to be used in this project). It was found that resistivity for steel heated to 870 ºC is higher than those heated to 780ºC and 825ºC. This variant is the result of martensite content of the microstructures. Upon quenching of austenized steel, FCC γ transforms to BCT martensite resulting in solute atoms, dislocations, voids, and fine discontinuities to show up in the final structure.

2.4.3.1. Factors Affecting the Electrical Resistivity

It is well known that anything disrupts the periodic potential of the lattice causes an increase in electrical resistivity. Thermal vibrations, dislocations, solute atoms, and other point defects therefore all contribute to electrical resistance.
Here are some of the most important factors that can have an effect on the resistivity of quenched steels.

1- Temperature Effect

When the temperature of a metal increases, thermal energy causes the amplitude of vibration of the atoms in metal to increase. The displacement of atoms from their equilibrium positions, obstruct electrons from their normal movement. Thus the electron mean free path decreases, and electron mobility is reduced causing an increase in resistivity [86].

2- Alloying Elements

An electron moving through metallic conductor under influence of an imposed electrical field would get scattered from any impurity atom. The inelastic scattering of electrons takes place due to the change in the potential field associated with size difference between host atoms and impurity atoms. Thus the presence of foreign atoms will have an effect on the total resistivity [33]. The alloying elements in steel (carbon, silicon …etc) in addition to suppressing carbide formation, form volume fractions of nonmetallic inclusions (NMIs). These NMIs are chemical compounds of metals (e.g., Fe, Mn, Al, and Si) and nonmetals (e.g., O, S, C, H, and N) which increase the distortion of the lattice reflected in high electrical resistivity [55].
Koley et.al. [33] studied the E.R of steel with different alloying elements using a four point probe technique. They found that:

i. Carbon is the most influential element to increase resistivity followed by manganese and silicon.
ii. Steels having low carbon (0.05%) and low silicon (0.02%) show low resistivity (in range of 13 – 14.5 μΩ.cm).
iii. Steels with high carbon (0.5 – 0.8%), moderate silicon (0.1 – 0.2%), and manganese in range of 0.55 to 0.75% show moderate resistivity (in the range of 19 – 22 μΩ.cm).
iv. Steels having low carbon (0.05%) and high silicon (0.8 - 0.9%) and 1.45% manganese show the maximum resistivity (in the range of 28 -32 μΩ.cm).

Vargas et.al. [55] measured the electrical resistivity of TRIP steels with different alloying elements. They found an increase in E.R with increasing alloying content and the inherently accompanying increase in the NMI (nonmetallic inclusions) content. Significant resistivity increases are observed between steels with different NMI contents.

3- Crystal Defects

Defects in crystal structure of metals and alloys can give significant contribution to the low temperature resistivity as shown in Figure 2.8 [86]. In some metals, the defects represent the major contribution to the residual resistivity. The principal point defects are vacancies and interstitials. Vacancies are found primarily in quenched specimens. Other atoms and notably gases may also exist in interstitial positions.

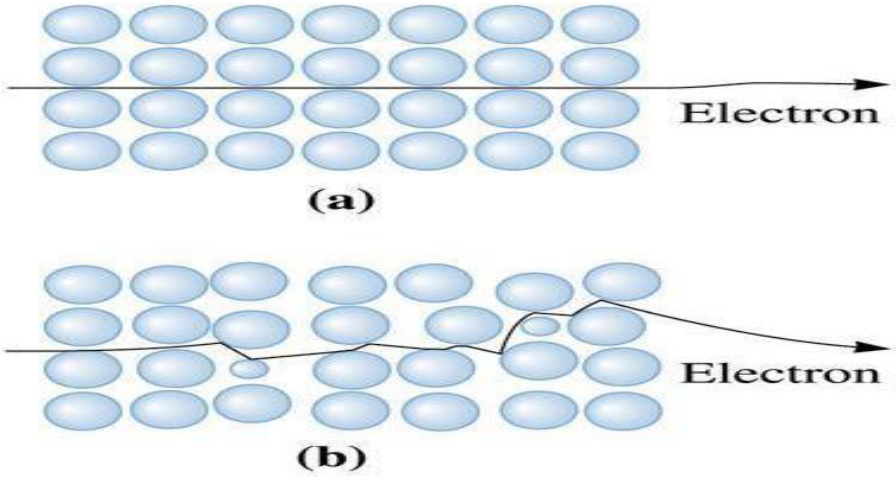

Figure 2.8. Movement of an electron through (a) a perfect crystal, (b) a crystal containing atomic level defects [86].

Dislocations occur naturally in all real metals, and their concentration increases by quenching and by deformation. It is known that measurement of electrical resistivity reflects dislocations which results in residual stresses across the entire cross section [88]. Stacking faults occur in conjunction with dislocations and are most often introduced by quenching.

Masumura et.al. [87] studied the effect of dislocation density and high angle boundary on the electrical resistivity of carbon steels. They reported that the change in the electrical resistivity, ($\Delta\rho_{dis}$), as a function of dislocation density, (N_{dis}), is expressed as follows:

$$\Delta\rho_{dis}\ (m\Omega.mm) = 1.7x10^{-18} \times N_{dis}\ (m^{-2}) \quad \text{.....(2.13)}$$

And the relationship between high-angle grain boundary density, (N_{HAGB}), and the change in the electrical resistivity, ($\Delta\rho_{HAGB}$), is as follows:

$$\Delta\rho_{HAGB}\ (m\Omega.mm) = 1.58 \times 10^{-9} \times N_{HAGB}\ (m^{-2}) \quad \text{.....(2.14)}$$

It is found that N_{dis} and N_{HAGB} depend on carbon content which is shown in Table 2.2.

Table 2.2. Variation of dislocation and high angle grain boundary densities with %C in (2%Mn – 0.5%Si) steel [87].

Carbon%	Dislocation density, N_{dis} [16] $[m^{-2}]$	$\Delta\rho_{dis}$ [mΩmm]	High-angle grain boundary density, N_{HAGB} $[m^{-1}]$	$\Delta\rho_{HAGB}$ [mΩmm]	$\Delta\rho_{dis}+\Delta\rho_{HAGB}$ [mΩmm]
0.1C	0.90×10^{15}	0.00153	1.34×10^{6}	0.00211	0.00364
0.2C	1.11×10^{15}	0.00189	1.16×10^{6}	0.00183	0.00372
0.3C	1.30×10^{15}	0.00221	1.73×10^{6}	0.00274	0.00495
0.4C	1.42×10^{15}	0.00241	2.14×10^{6}	0.00338	0.00579
0.5C	2.00×10^{15}	0.00340	2.89×10^{6}	0.00457	0.00797
0.6C	3.21×10^{15}	0.00546	3.14×10^{6}	0.00497	0.0104

4- Precipitated Phases

The electrical resistivity of steels is influenced by the presence of both impurity atoms and precipitated phases (such as nitrides, sulfides, borides, and oxides). The collision of electrons with such phases results in frictional forces that reduce the electron drift velocity causing an increase in E.R. Generally, different phases in carbon steel have different resistivities. For example, bainite is expected to have lower resistivity than martensite because it has less carbon in its solid solution and lower defect density. On the other hand, bainite has higher dislocation density than pearlite or ferrite. The electrical resistivity at fixed temperature generally decreases in the order from austenite, martensite, bainite and then pearlite as shown in Figure 2.9 [89].

Masumura [87] examined the effect of retained austenite on electrical resistivity in an Fe–2%Mn–0.5%Si–10%Ni–0.3%C alloy. The steel was subjected to austenizing treatment at 1000ºc for 0.5 hours, followed by water quenching to obtain a dual-structure of martensite and retained austenite. Specimens were then cold-rolled by 5%, 10%, and 20% to undergo phase transformation from retained austenite to martensite. The R.A volume fraction in the specimens were approximately 3.3 vol.%, 1.8 vol.%, and 0 vol.% respectively. A decrease in E.R. has been noticed which was attributed to the effect of retained austenite.

Agurto [43] investigated the effect of different quenching media on the electrical resistivity of 1045 steel. Steel samples were heat treated up to 820 ^{o}C and then quenched in water and mineral oil. The E.R values obtained using four-terminal sensing were 16.2, 25.1 and 17.6 μΩ.cm for as-received (non-heat treated), water quenched, and mineral oil quenched samples, respectively. The lower E.R value for oil quenched sample is thought to be due to lower internal stresses produced during the sudden formation of the martensite phase. The presence of the ferrite phase that was observed in oil quenched sample might also contribute to lower E.R value.

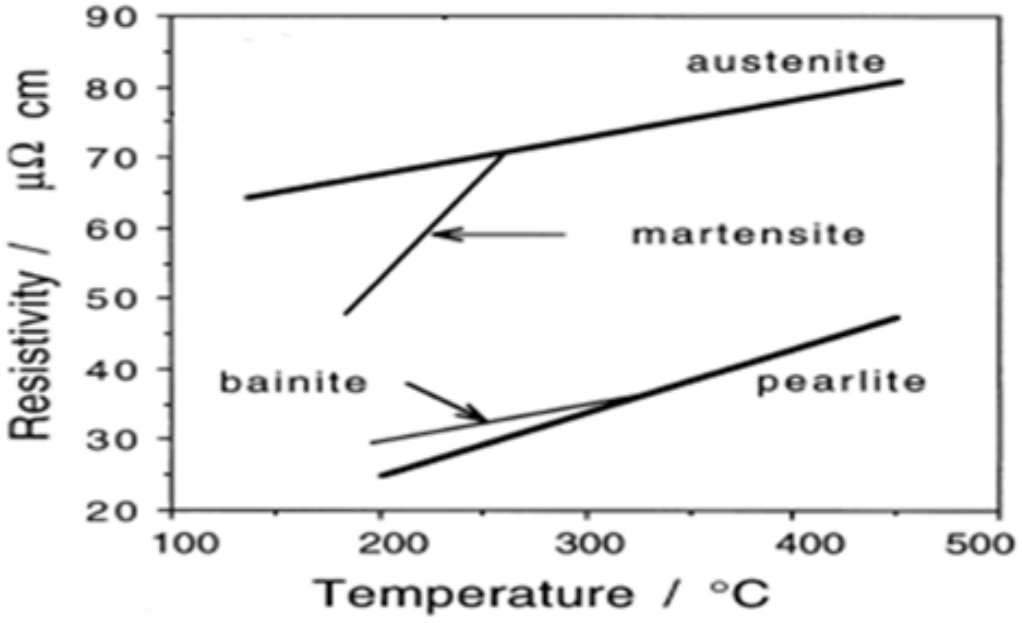

Figure 2.9. Electrical resistivity of different steel phases [89].

Chapter 3
Experimental Methods

This chapter describes the materials and the heat treatment steps used to obtain a specific steel microstructure that consists of martensite phase with different amounts of retained austenite phase. This chapter also elaborates on methods used to determine the % R.A, namely metallography technique, XRD and electrical resistivity methods.

3.1. Materials

The as-received material used in this work is commercial carbon steel used for construction. The samples were received in the form of round discs of 30 mm (sample S1) and 48 mm (sample S2) in diameter and 5 mm in thickness which were obtained from Libyan Iron and Steel Company in Misurata and Technical Research Center in Tripoli respectively as shown in Figure 3.1.

Table 3.1 shows the chemical composition in wt% of these steels. The chemical analysis was done using atomic emission spectroscopy (AES) at Libyan Iron and Steel Company-Misurata-Libya.

It should emphasized that material received from Technical Research Center was supposed to contain more than 0.6%C, but the technical operator gave us by mistake a 0.262%C material. This error was noticed after comparing the chemical analysis originally obtained with material with analysis done in Iron and Steel Company. Unfortunately, this error was detected at stage of final analysis of results. It was then not possible to obtain a material of more than 0.6%C.

Table 3.1. The chemical composition (in %wt) of steels used in this work

Sample Designation	%C	%Si	%Mn	%P	%S	%Cr	%Mo	%Ni
S1	0.371	0.225	1.44	0.019	0.005	0.02	0.001	0.013
S2	0.262	0.233	0.7	0.006	0.019	0.067	0.014	0.09

Sample Designation	%Cu	%Sn	%Al	%Co	%Nb	%Ti	%V
S1	0.022	0.001	0.001	0.004	0.002	-	0.005
S2	0.272	0.016	0.002	0.012	0.002	0.001	0.002

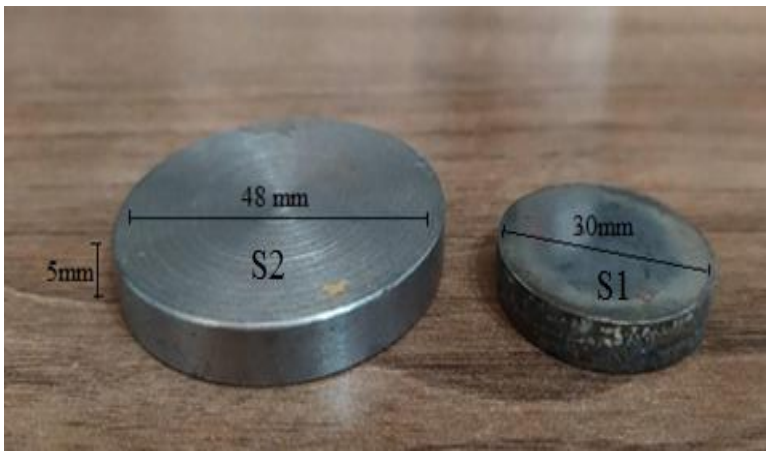

Figure 3.1 As recieved steel samples

Then, the samples were cut into small rectangular plates with dimensions of 5 *5* 10 mm as shown in Figure 3.2. These dimensions were chosen for suitable handling and to ensure uniform rapid cooling and hardening and to prevent any difference in cooling rate in the sample. Samples with theses dimensions enabled us to use them in all experiments in this study.

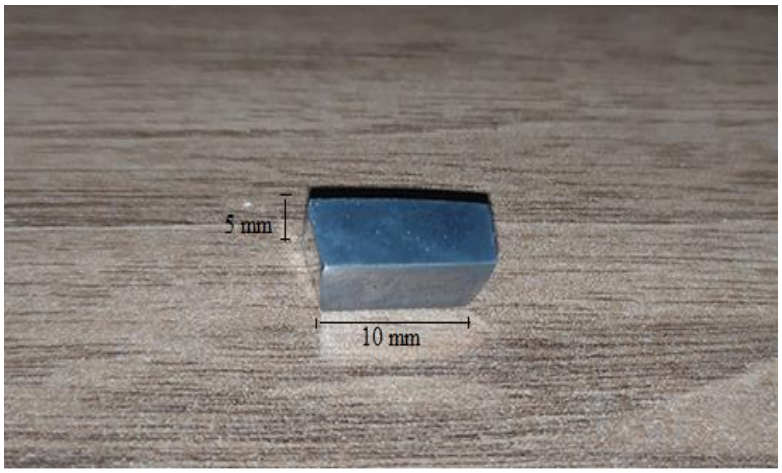

Figure 3.2. Steel sample dimensions after cutting process.

3.2. Heat Treatment Process

Heat treatment process "quenching process" includes heating the steel to certain temperature (950ºC) followed by rapid cooling. The steel samples are placed in a crucible made of ceramic material by using of metallic stands. The crucible containing potassium chloride salt bath was inserted into the Nabertherm electric furnace. This salt bath has been used to ensure uniform heating and to minimize oxidation effect. The electrical furnace used in University of Tripoli Faculty of Engineering at Metallurgical and Materials Engineering Department.

Figure 3.3 shows the steps of the heat treatment where the sample was heated to 950 ºC during 60 minutes. It has been kept at this temperature for 30 min for stabilization of austenitic phase. The sample immediately quenched in the three different quenching media (Tab water, Corn oil and used oil for car engine "RAVANOL 20W50").

Finally the samples were cleaned, dried and prepared for metallographic examination. This experiment was done in both engineering and Medical Collage of University of Tripoli.

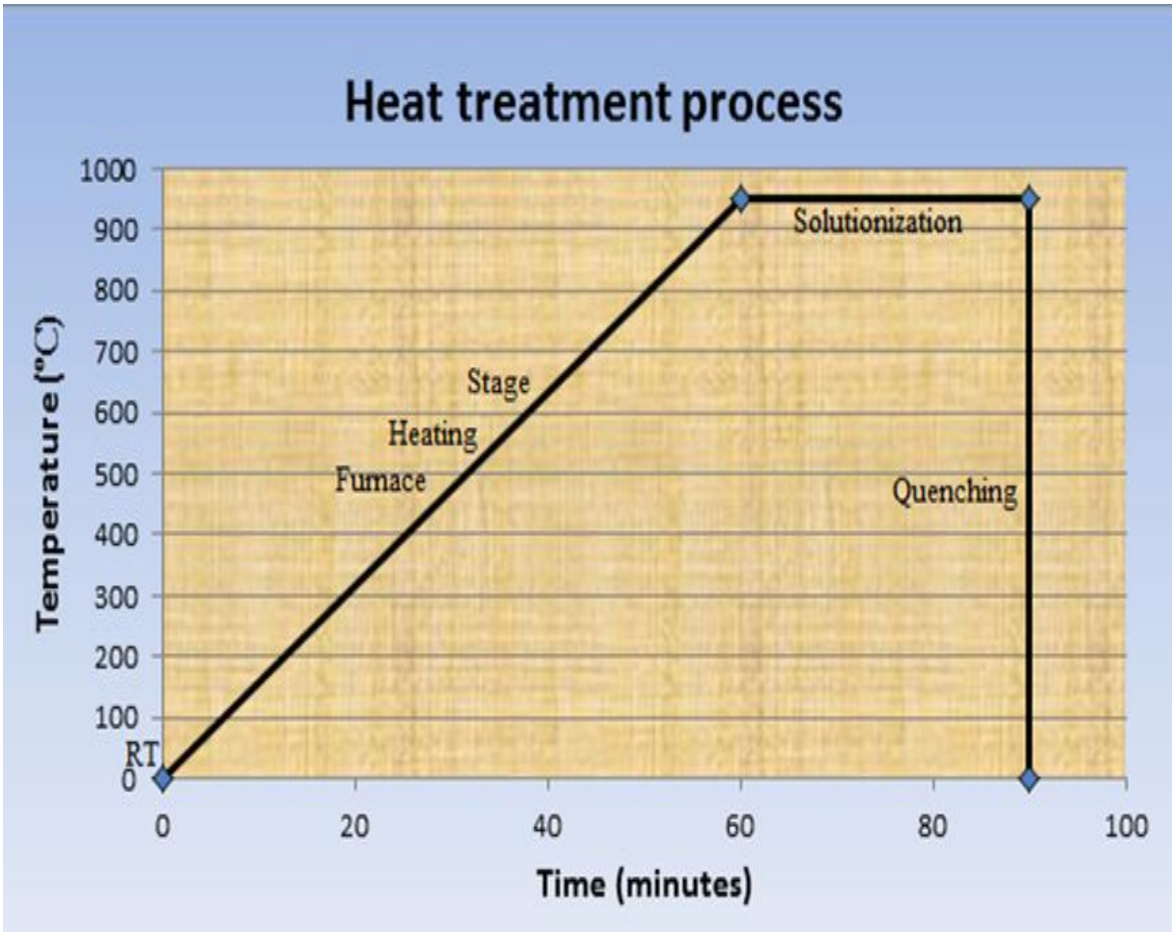

Figure 3.3 The heat treatment process.

3.3. Metallography

Optical microscopy was used to evaluate the types of microstructures formed in the heat treatment and quantize them. This method has been carried out in metallography laboratory of Materials and Metallurgical Department Faculty of Engineering University of Tripoli. Samples were mechanically ground using a rotating and abrasive Silicon carbide peppers of increasing fineness 220, 320, 500, 800 and 1000.
Polishing was carried out on a rotating disc of a synthetic velvet polishing cloth impregnated with 1 ,0.3 and 0.05 micron alumina paste. The specimens were then cleaned and etched for 30 seconds using 2% Nital. Nital can be prepared by addition of nitric acid with alcohol which can be ethanol or methanol [90]. In this work the etching solution was prepared by addition of 0.5 ml nitric acid in 25 ml of methanol. The sample is immediately washed under running water, rinsed with alcohol and then move on to the microscope examination stage.
The optical metallographic examinations were carried out at university of Tripoli "Materials and Metallurigical Engineering Department" using Leica optical microscope at a magnification of 200X. The pictures of microstructures were taken by Amscope camera in the Technical Research Center. The microstructures were differentiated by compared them with the standards established by the American Society for Metals (ASM) [91] .

3.4. X-Ray Diffraction (XRD)

The samples were characterized using X-ray diffraction (XRD), primarily to determine the R.A volume fraction which can be determined from the locations of the diffraction peaks and their integrated intensities.

Sample preparation for XRD measurements focuses on the surface of the sample because the X-rays only penetrate to a depth of 2 μm from the sample surface. Hence, care needs to be taken to ensure that the surface is deformation free. The same metallographic procedure was repeated, and then followed with etching the specimens using 2% Nital for 5sec to remove any deformation imparted by the polishing. procedure [9, 65].

XRD msurements were conducted in Libyan Petroleum Institute using a PW1800 X-ray Diffractometer. Monochromated Cu Kα radiation (λ = 1.5406 A) was used at 40kV and 30mA. The specified 2θ range was from 2° to 90° with a step size of 0.02°. The diffraction patterns for the samples in each quenching media will be shown in the next chapter.

Indexing of martensite and austenite peaks was done using "Crystal Impact" search – match software. Six diffraction peaks were captured in total, three ferrite (α) peaks (110), (200) and (211) and three austenite (γ) peaks (111), (200) and (220).

3.5 Electrical Resistivity

To measure the electrical resistivity of the steel samples (low resistivity materials), the Jandel Four Point Universal Probe has been used which is shown in Figure 3. 4.

It is owned by Libyan Center of Solar Energy Researches. Figure 3.5 shows the experimental setup (operation unit) which consists of probes, samples, constant current generator and digital macrovoltmeter for measuring voltage and current. The samples are put on a holder substrate, while the four probes are arranged linearly at equal distance (1mm) from each other. Upon operation a DC current, I, as measured by current generator is forced between the outer two probes. If the sample has resistance, there will be a voltage drop,V, as measured by macrovoltmeter when the current flows through. This voltage drop is measured by the two inner probes. The average voltage drop is determined using the values of ten measurements for each specimen. The electrical resistivity, ρ, of each samples is then calculated using the expression $\rho = 2\pi s \frac{V}{I}$, where s is the spacing between probs, see equation 2.12. page 24. These electrical resistivity values will be used to determine the %R.A based on Matthiessen's rule as shown in section 2.4.3. which will be discussed in detail in the result and discussion chapter.

Figure 3.4. Jandel device digital screen.

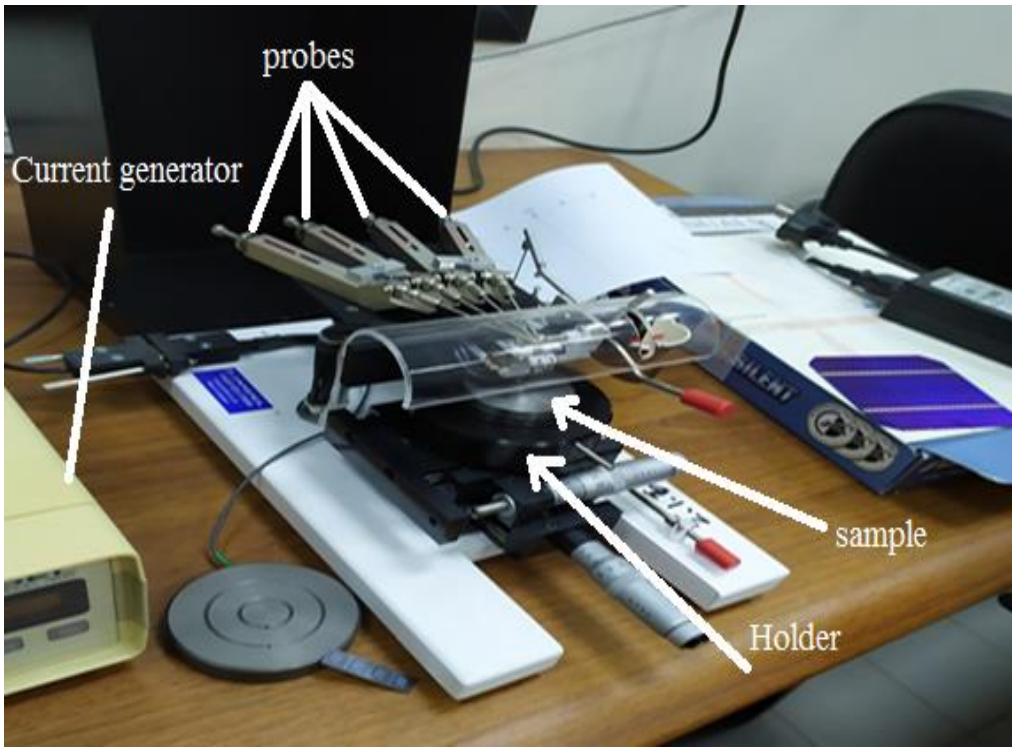

Figure 3.5. Jandel device operation unit.

Chapter 4
Results and discussion

4.1. Introduction

This chapter discusses the experimental results for measuring the % R.A and their significance with reference to previous literature results. The discussion of results is separated into three main sections:

i. The first section 4.2 focuses on the metallographic results and its importance in our work. The microstructures after each quenching process will be shown and the effect of carbon content and the quenching media on the microstructure will be discussed. Because of %C of steel samples, measurement of retained austenite by this technique was not possible.
ii. The second section 4.3 focuses on XRD method for measuring of retained austenite. Based on XRD results, the effectiveness of using electrical resistivity to measure %R.A will be discussed.
iii. The third section 4.4 focuses on the electrical resistivity method and its effectiveness for measuring of retained austenite.

4.2. Measurement of Retained Austenite by Metallography Method

Figures 4.1 and 4.2 show the microstructure of as received S1 and S2 steels respectively. The microstructure of S1 steel (0.37%C) contains ferrite, which is the light etching phase and pearlitic colonies, which etch dark. Based on the chemical composition it should contain 50% ferrite and 50% pearlite. The microstructure of S2 steel (0.262%C) also consists of pearlite in a matrix of ferrite, and by calculation, 65% of ferrite is present.

Figure 4.3 shows the microstructure of water quench of S1 steel etched in Nital for 25 sec which seems clear that consist of martensite (M) shape (lath shape) which is dark and some amount of retained austenite (R.A) (white).

Figure 4.4 shows microstructure of water quench of S2 steel etched in 2% Nital for 30 sec which contains retained austenite (R.A) in small white area (some ferrite could be present) in a matrix of martensite which is dark. The difference in color is due to the quality of the camera.

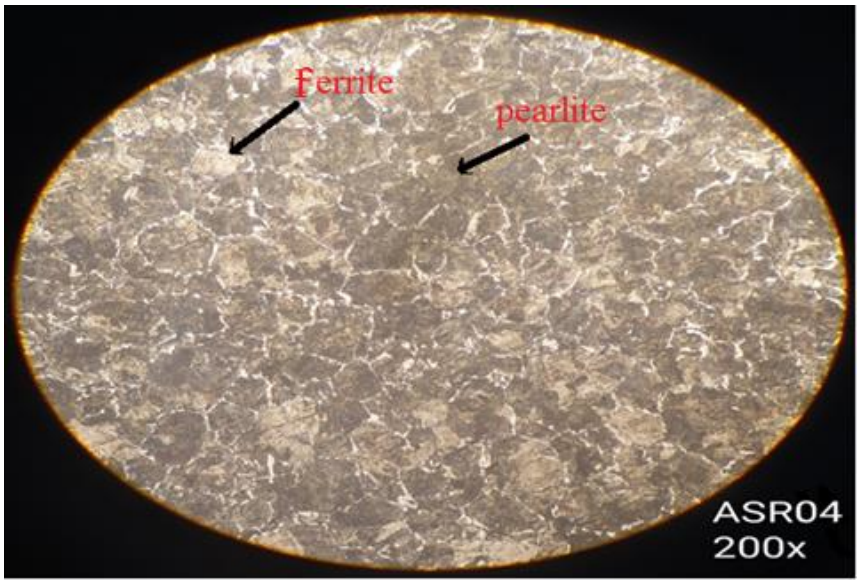

Figure 4.1. Microstructure of as received S1 steel at 200X.

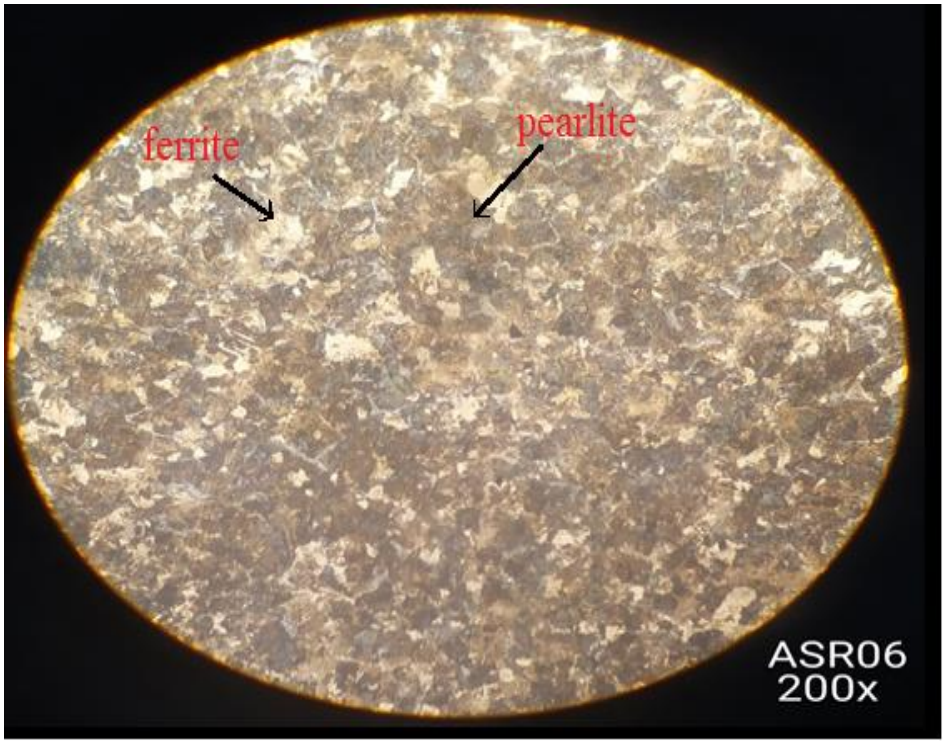

Figure 4.2. Microstructure of as received S2 steel at 200X.

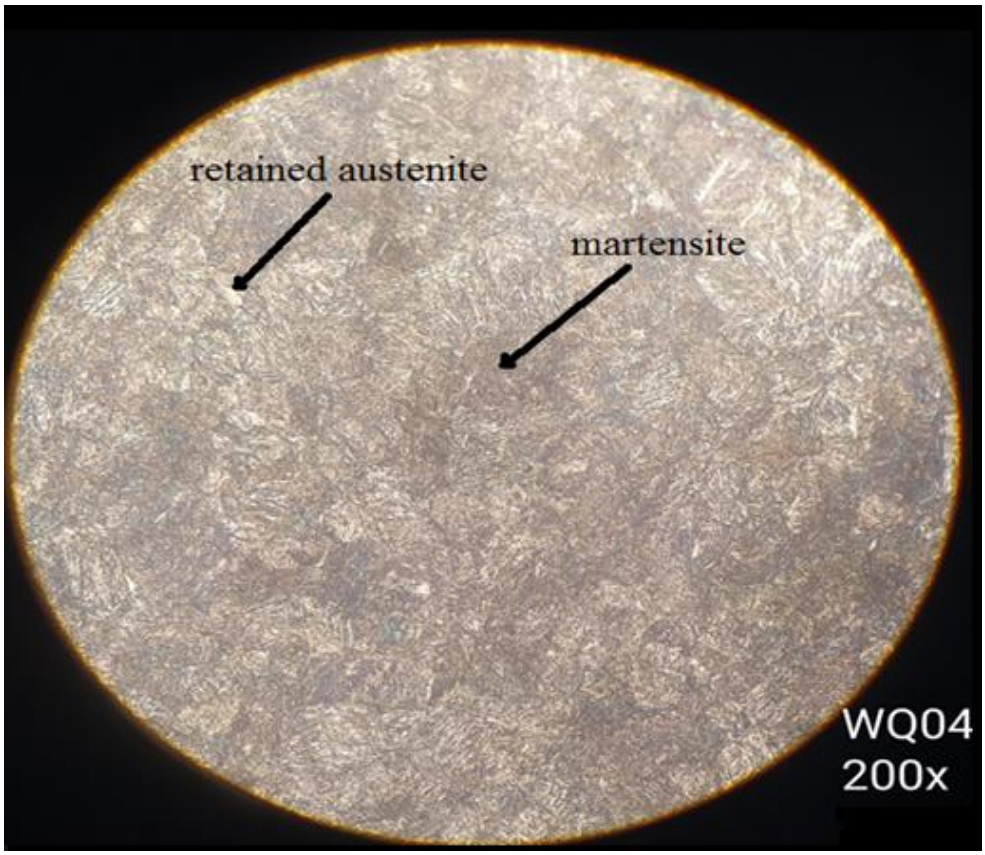

Figure 4.3. Microstructure of water quenched S1 steel at 200X.

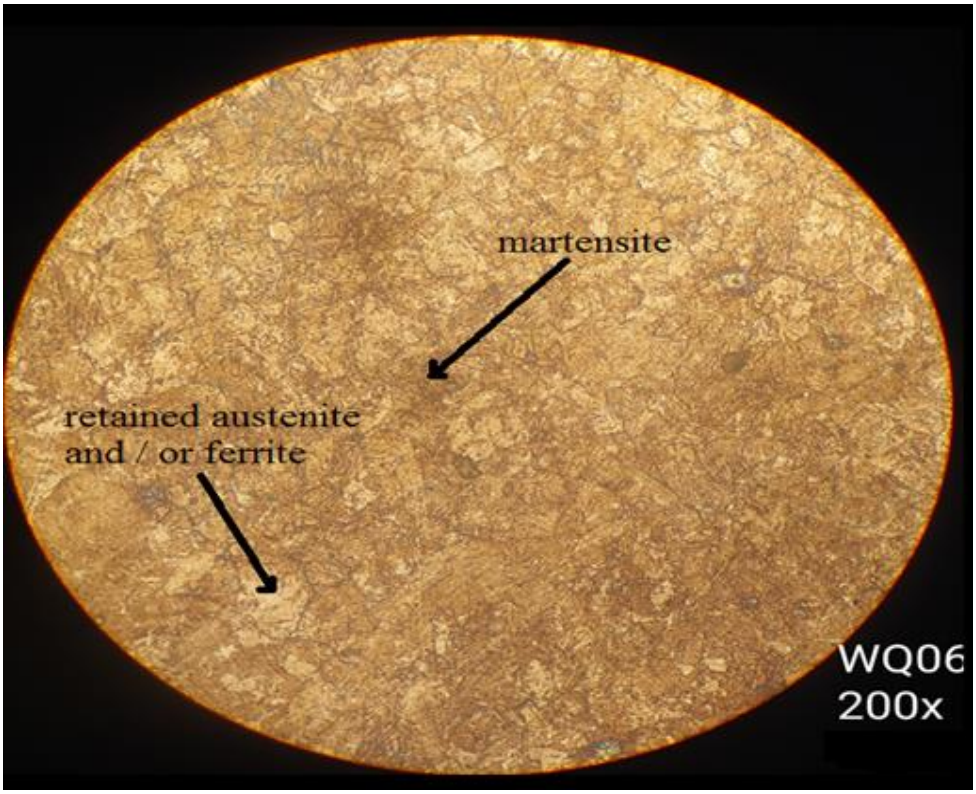

Figure 4.4. Microstructure of water quenched S2 steel at 200X.

Figure 4.5 shows the microstructure of S1 steel quenched in used oil for car engine. This microstructure is mostly martensite phase with thick needle shape and some of retained austenite which are isolated white areas. Figure 4.6 shows the microstructure of S2 steel quenched in the same media. It is expected to consist of small austenite grains in fine needle of martensite matrix.

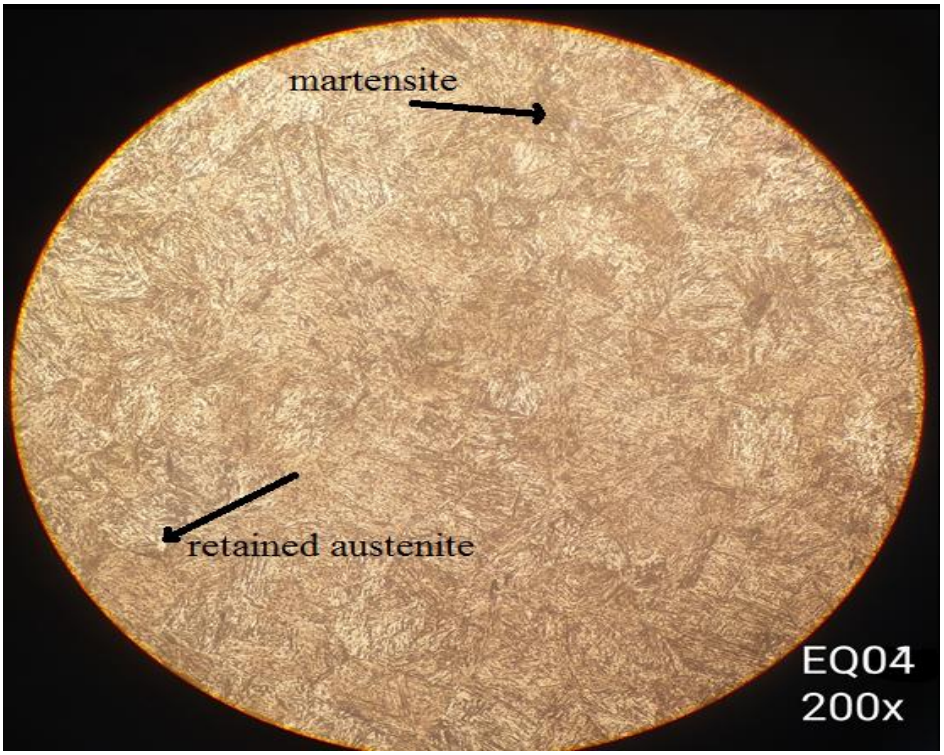

Figure 4.5. Microstructure of used oil for car engine quenched S1 steel at 200X.

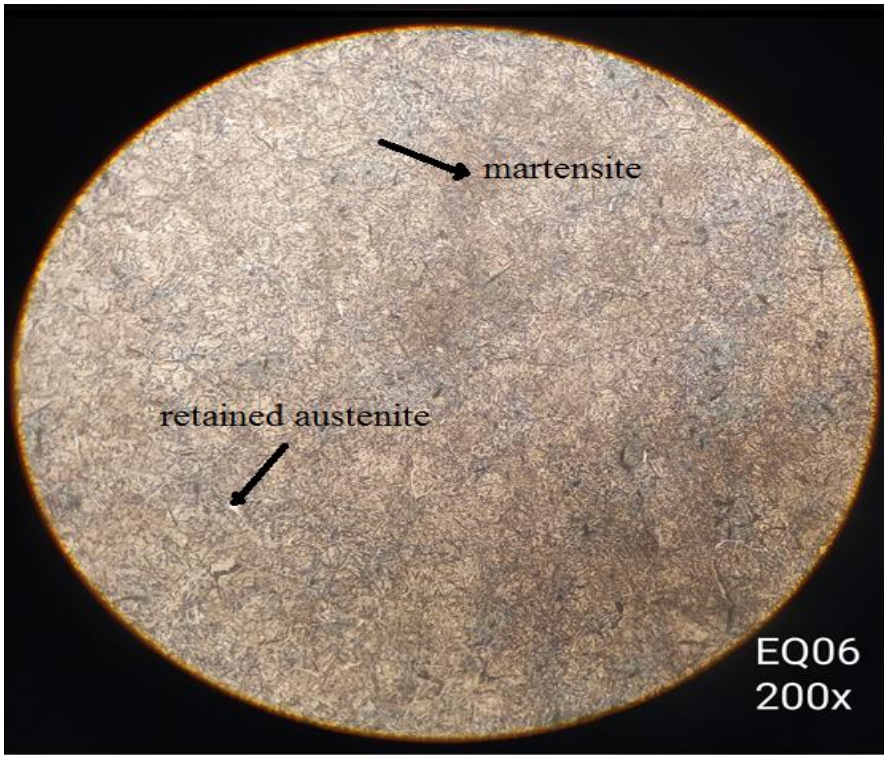

Figure 4.6. Microstructure of used oil for car engine quenched S2 steel at 200X.

Figure 4.7 shows microstructure of S1 steel quenched in corn oil which is mainly martensite (dark), retained austenite (white) and some ferrite is expected to be present due to jacket steam formation. Figure 4.8 shows microstructure of S2 steel quenched in the same media. The microstructure consists of a matrix martensite (mainly dark) and other phases such as ferrite, and small amount of retained austenite which are white phases.

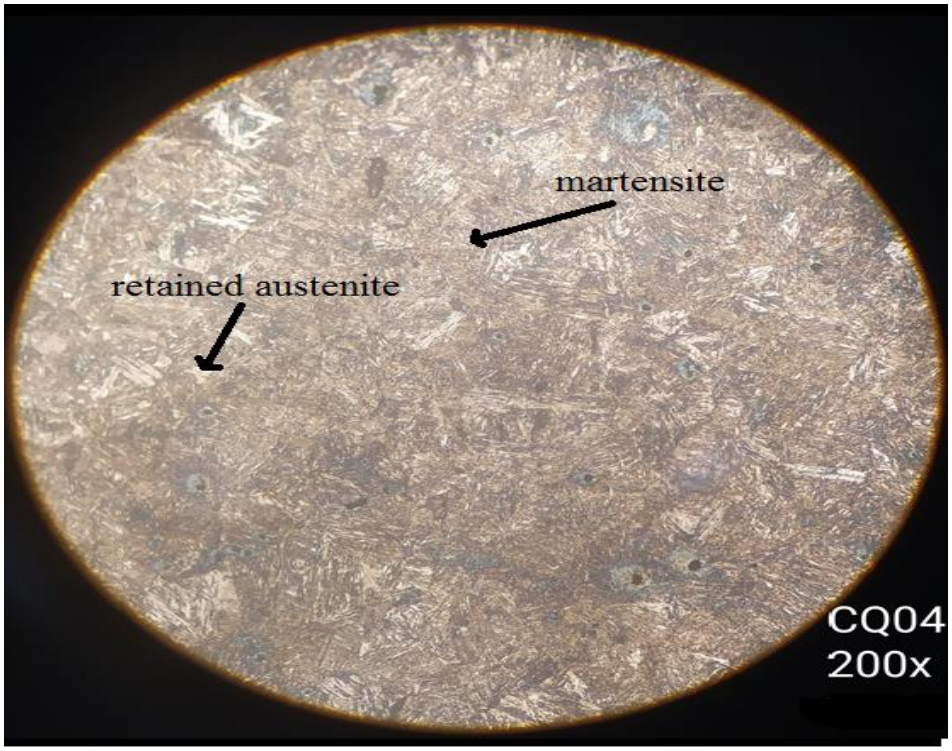

Figure 4.7. Microstructure corn oil quenched S1 steel at 200X.

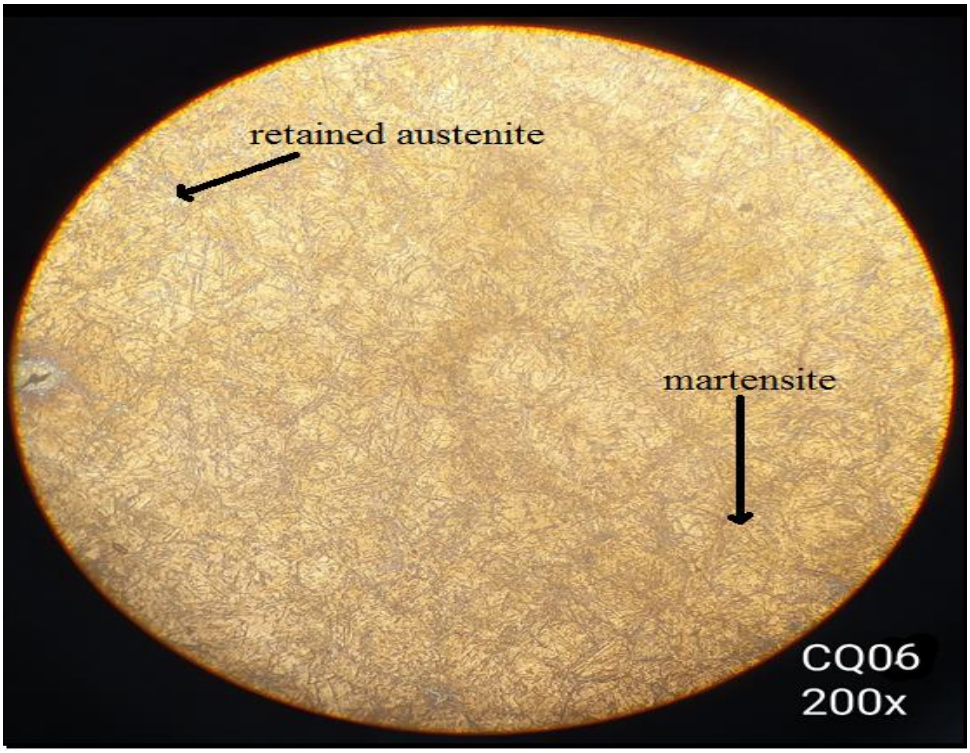

Figure 4.8. Microstructure of Corn oil quenched S2 steel at 200X.

From these figures it can be noticed that S1 steel with higher carbon content has martensitic phase clearer and thicker than S2 steel. That's can be explained as following:

When the steel is cooled suddenly, the carbon atoms cannot make an orderly escape from the iron lattice. This cause "atomic bedlam" and results in distortion of the lattice, this distortion lattice has BCT structure which is the martensite phase, so that as %C increases the distortion of lattice under high cooling will increase resulting in high fraction of martensite [25]. Also the high percent of Mn in S1 steel (1.44%) could have a significant effect. It was found that steels containing manganese have higher hardenability (which is the ability to martensite formation) than steels with low amount of manganese [29].

Also the cooling rate has a significant effect on the microstructure, In general for such steel, at low cooling rate the microstructure consists of bainite phase (gray and black area) with small amount of retained austenite (black area) with small areas of ferrite (gray area) and martensite phases (lath shape), while increasing cooling rate results in microstructure consist of martensite (needle shape) and retained austenite phases (black area), At low cooling rate, martensite appeared as a fine needle while, at rapid cooling rate the needle become thicker. [81].

Unfortunately, quantitative measurements of R.A by metallography are very complex and require a special coloring solution for etching. For example Baraha and LePera solutions which have been shown in Table 2.1. We tried to obtain and prepare these solutions but unfortunately, the process requires special equipments. Also from previous research it was found that for steel with less than 0.6%C, only qualitative observations is possible by metallography technique, but quantification of the retained austenite phase is not possible and requires a X-ray analysis. At lower carbon contents, the morphology of the martensite was predominantly non-lenticular, and detection of the austenite in such a matrix is not easy by metallographic technique [3, 10, 54, 57].

4.3. Measurement of Retained Austenite by X- Ray Diffraction (XRD)

Quantitative phase analysis by the XRD is based on the fact that the intensity of the diffraction peak of a particular phase in a mixture of phases depends on the concentration of that phase [49]. The increase in intensity of the γ peaks corresponds to the increase of the RA volume fraction. In the present analysis six diffraction peaks were captured in total, three Ferrite (α) peaks: (110), (200) and (211) and three austenite (γ) peaks: (111), (200) and (220). % R.A was determined by "Direct comparison method". The integrated intensities of two ferrite (200, 211) peaks and two austenite (200, 220) peaks have been used to decrease errors associated with peak interference according to ASTM E975 standard [92]. Because the (110) peak of martensite may overlap the (111) the austenite peak, it is better not to use them in the calculation of the amount of retained austenite [3,13].

The theoretical intensity (R) has been calculated by equation 2.6 as shown in section 2.4.2.

The results of the theoretical intensities of the S1 and S2 steels are shown in Table 4.1.

Table 4.1. Calculation of theoritical intensity

h k l	2θ	F	m	LP	e−2M	R (S2 steel)	R (S1 steel)
200 α	65	29	6	4.84	0.91	39.56	39.03
200 ɣ	51.4	64.82	6	8.198	0.93	94.91	94.91
220 ɣ	75.7	53.4	12	3.577	0.9	54.4	54.4
211α	82.3	25.60	24	3.117	0.88	76.8	75.87

Figures from 4.9 to 4.14, and Tables from 4.2 to 4.7 shown below represent the x-ray diffraction patterns of all analyzed steels samples using the following abbreviations for respective quenching media:

WQ04 refers to the steel S1 which was quenched in tap water.
WQ06 refers to the steel S2 which was quenched in tap water.
EQ04 refers to the steel S1 which was quenched in engine oil.
EQ06 refers to the steel S2 which was quenched in engine oil.
CQ04 refers to the steel S1 which was quenched in corn oil.
CQ06 refers to the steel S2 which was quenched in corn oil.

Six peaks have been detected using "Crystal Impact" Search – Match Software produced by G. Bergerhoff's research group that established the inorganic crystal structure database in 1983.

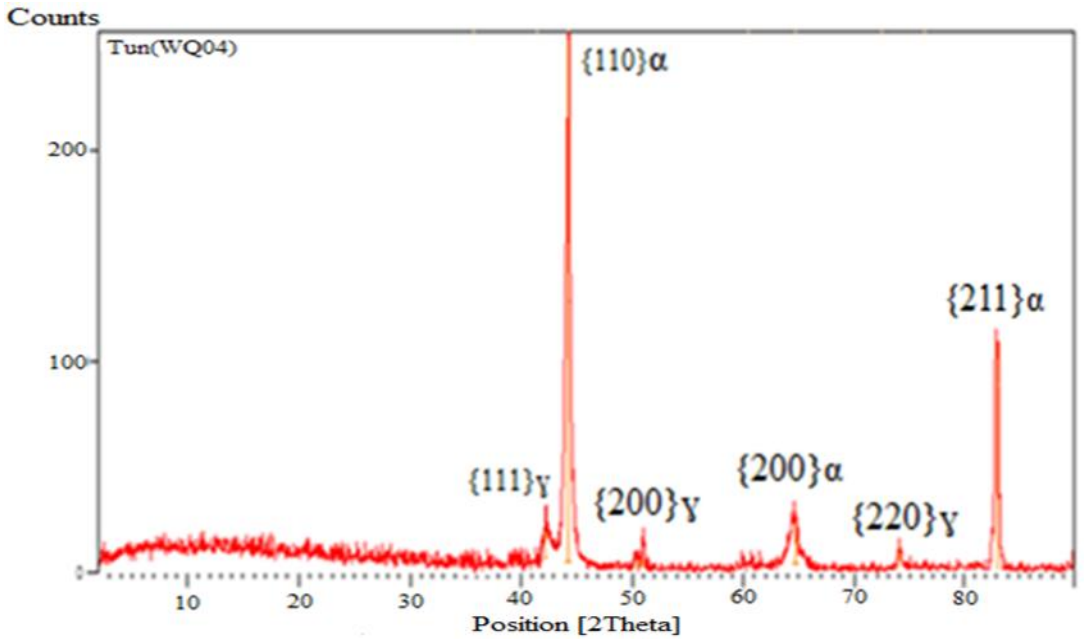

Figure 4.9. XRD pattern of water quenched S1 steel.

Table 4.2. Peak list of water quenched S1 steel.

Position. [2Th.]	Height [counts]	FWHM [2Th.]	d-spacing [Å]	Rel. Int (I/Imax) [%]
42.441230	26.675230	0.656800	2.12750	10.66
45.009850	248.04671	0.354320	2.01414	100
50.823450	19.056121	0.374880	1.79286	7.62
61.356600	3.3596500	0.114311	1.51100	1.34
64.856121	30.254131	0.887040	1.44443	12.10
73.833460	13.339390	0.351640	1.28244	5.33
83.211900	100.86194	0.268008	1.16008	40.33

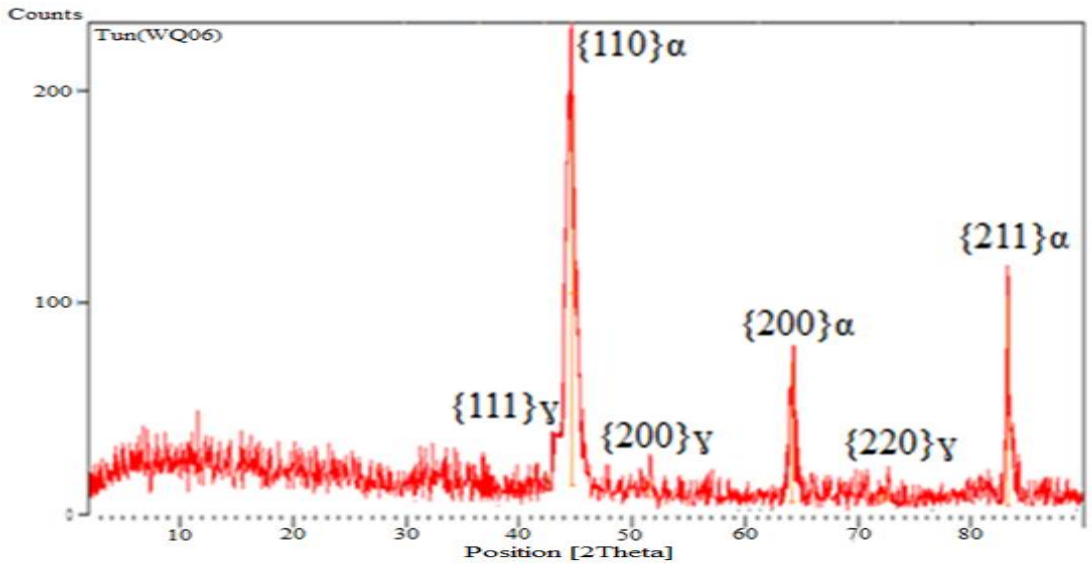

Figure 4.10. XRD pattern of water quenched S2 steel.

Table 4.3. Peak list of water quenched S2 steel.

Position. [2Th.]	Height [counts]	FWHM [2Th.]	d-spacing [Å]	Rel. Int. (I/Imax) [%]
44.777700	221.13740	0.877800	2.02226	100
51.136580	20.397350	0.174640	1.78481	9.22
64.153550	72.521469	0.651455	1.44260	32.79
72.813620	13.500150	0.128602	1.29328	6.55
83.265500	116.67755	0.396600	1.16005	52.76

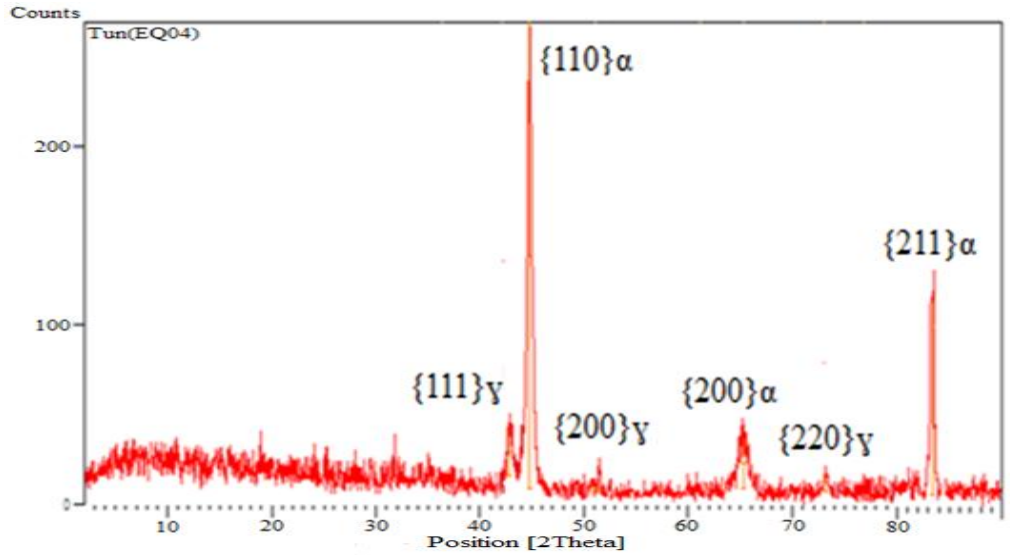

Figure 4.11. XRD pattern of used engine oil quenched S1 steel

Table 4.4. Peak list of used engine oil quenched S1 steel.

Position. [2Th.]	Height [counts]	FWHM [2Th.]	d-spacing [Å]	Rel. Int. (I/Imax) [%]
35.580340	15.898464	0.109760	2.52655	6.06
42.450880	28.879130	0.542320	2.12771	11.02
44.757600	262.01260	0.351040	2.02240	100
51.310520	18.010870	0.304320	1.77918	6.87
65.312670	36.01455	0.788160	1.42538	13.74
73.212740	14.415670	0.311640	1.29481	5.50
83.425800	126.01766	0.226650	1.15944	48.09

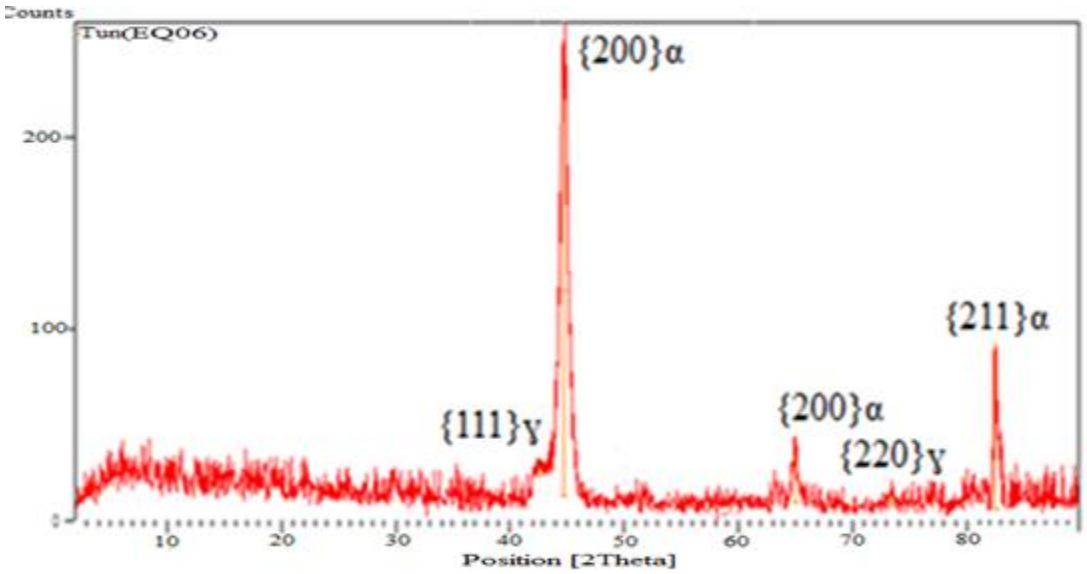

Figure 4.12. XRD pattern of used engine oil quenched S2 steel.

Table 4.5. Peak list of used engine oil quenched S2 steel.

Position. [2Th.]	Height [counts]	FWHM [2Th.]	d-spacing [Å]	Rel. In. (I/Imax) [%]
42.941230	23.845230	0.211800	2.10643	9.89
44.709850	241.04671	0.551320	2.02489	100
65.014520	34.211350	0.472101	1.43169	14.19
73.333460	8.219390	0.151320	1.28965	4.24
82.604335	86.358000	0.324321	1.16711	35.83

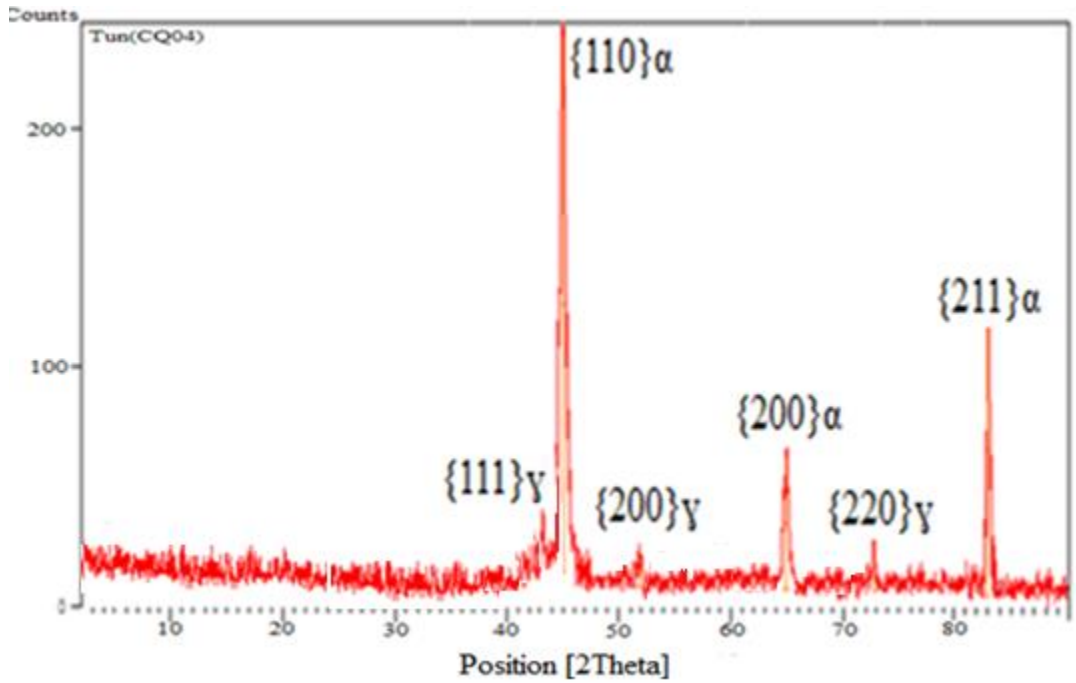

Figure 4.13. XRD pattern of corn oil quenched S1 steel.

Table 4.6 Peak list of corn oil quenched S1 steel.

Position. [2Th.]	Height [counts]	FWHM [2Th.]	d-spacing [Å]	Rel. Int(I/Imax). [%]
36.072310	13.550126	0.170541	2.48710	5.62
43.336770	21.698290	0.484320	2.08111	9.00
45.057860	241.02121	0.402640	2.01351	100
51.952180	18.406380	0.283760	1.75876	7.63
64.982310	59.068000	0.501165	1.43561	24.50
73.350430	21.703210	0.184640	1.29075	9.00
83.134760	124.05031	0.314120	1.16101	51.47

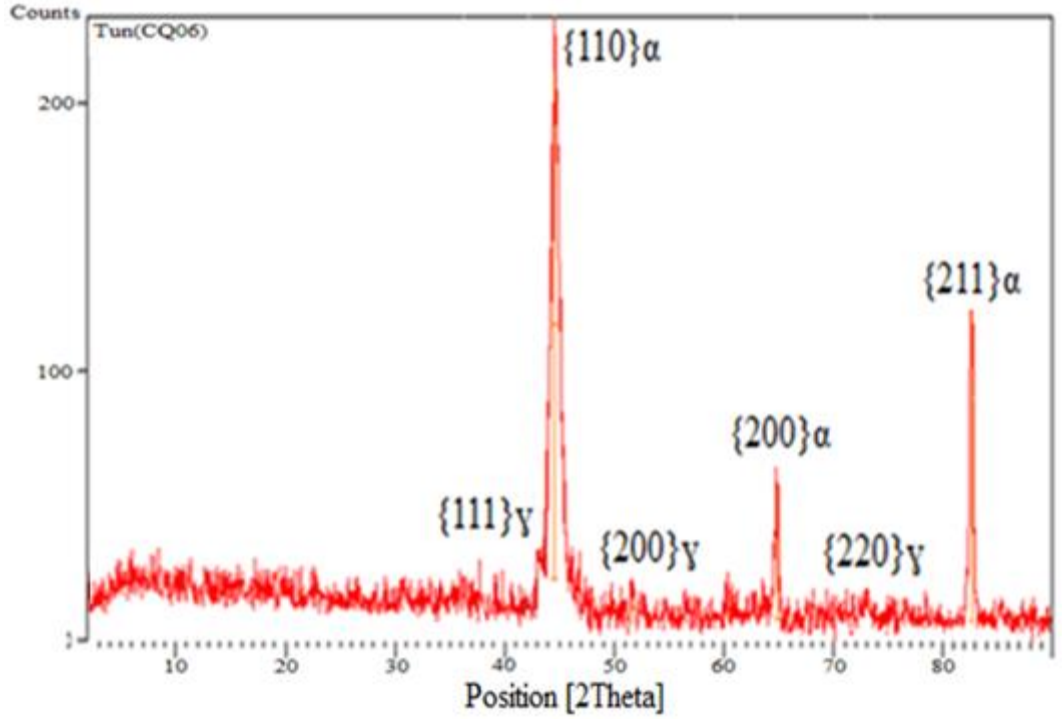

Figure 4.14. XRD pattern of corn oil quenched S2 steel.

Table 4.7. Peak list of corn oil S2 steel.

Position. [2Th.]	Height [counts]	FWHM [2Th.]	d-spacing [Å]	Rel. Int(I/Imax). [%]
44.777700	230.13740	0.944800	2.02404	100
51.436580	12.957350	0.134640	1.77629	5.63
64.853550	52.714690	0.315800	1.43660	22.90
83.807580	108.56732	0.324160	1.15711	47.17

The integrated intensity (I) as defined by the integral area of a peak can be approximated by the area of a triangle with negligible error as shown in Figure 4.15 [74].

Area under the peak = $\frac{1}{2}$ $(2Th2 - 2Th1)$ $\times$ I_{max} ×scan rate ……..(4.4)

Integrated intensity (I) = FWHM × I_{max} × scan rate ...……..(4.5)

Where:
FWHM: is the full width half max of the peak and I_{max} is the maximum intensity of the peak [93]. Fortunately it has been calculated automatically by XRD machine.

Scan rate = $\frac{step\ size}{scan\ step\ time} = \frac{0.02}{0.5} = 0.04$ degree $/sec.$

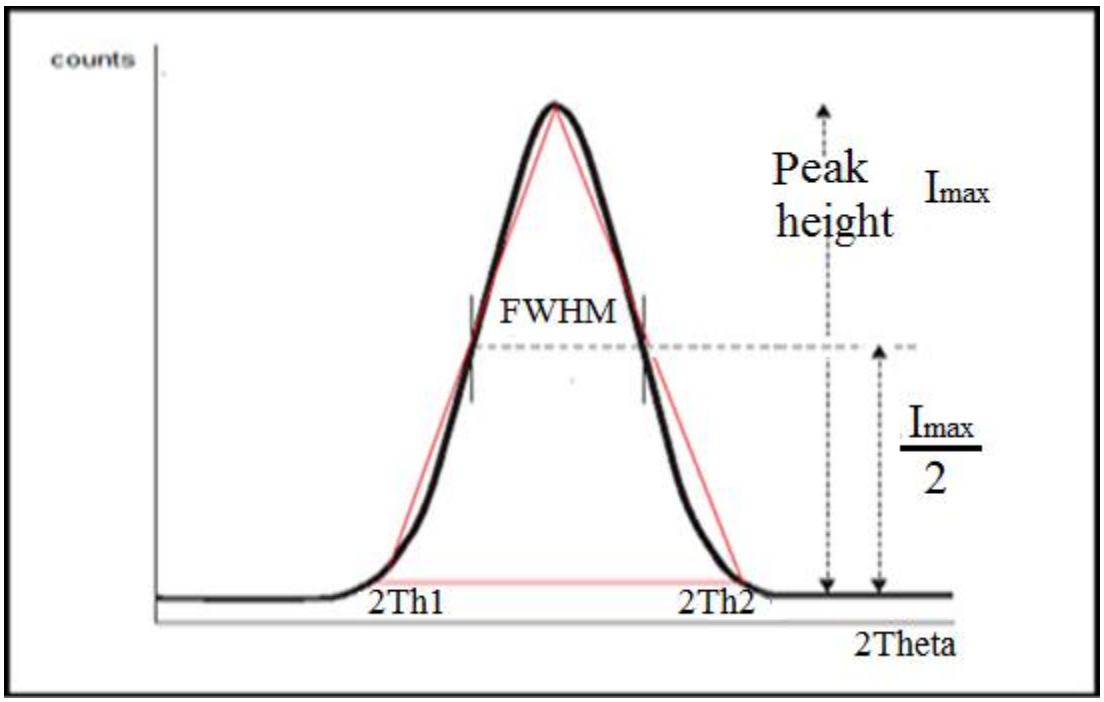

Figure 4.15. Showing full width half max of an XRD peak [74].

Results of calculations of integrated intensities by equation (4.5) are shown in Table 4.8.

Table 4.8. Results of the integrated intensity.

$I_{(220)\gamma}$	$I_{(200)\gamma}$	$I_{(211)\alpha}$	$I_{(200)\alpha}$	Sample label	Condition
0.187	0.285	1.08	1.07	WQ04	Water quench of S1 steel
0.069	0.152	1.85	1.888	WQ06	Water quench of S2 steel
0.18	0.219	1.14	1.13	EQ04	Engine oil quench of S1 steel
0.049	0	1.12	0.646	EQ06	Engine oil quench of S2 steel
0.159	0.208	1.557	1.18	CQ04	Corn oil quench of S1 steel
0	0.069	1.407	0.664	CQ06	Corn oil quench of S2 steel

Applying the data in Table 4.8 gives %R.A (using equation 2.5) which can be seen in Figure 4.16.

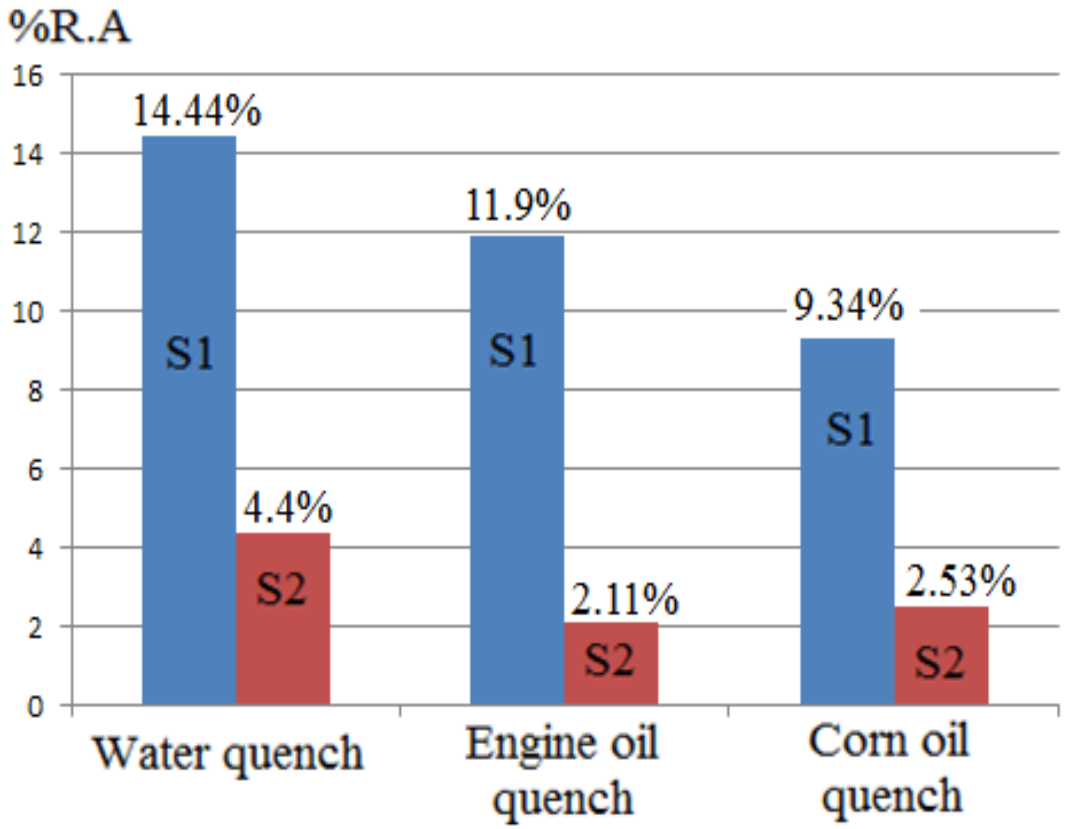

Figure 4.16. Results of %R.A calculated by XRD.

These results will be discussed in terms of the effect of carbon and other alloying elements as well as the effect of quenching media which will be discussed in the following sections.

4.3.1. Effect of carbon and other alloying elements

Based on Table 4.9 of XRD results, it can be noticed that steel S1 (%C=0.37%) has a higher %R.A than steel S2 (%C = 0.262%) for the same quenching media which is in a good agreement with Kokoza et.al [52]. Table 4.10 compares results from present finding with Kokoza et.al results. This effect can be explained as follows:

The increasing in the carbon content of steel lowers the Ms temperature, thereby increasing the thermal stability of austenite phase to a lower temperature. Therefore, the mechanical driving force required for martensitic transformation increases with a higher carbon content, which means higher carbon content corresponds to higher stability of retained austenite [20]. Another element that has a strong effect on retained austenite stability is manganese. Mn is an austenite stabilizer which reduces the Ms and promotes carbon solution in austenite [54] which could also illustrate why steel S1 (%Mn=1.44%) has a higher %R.A than steel S2 (%Mn=0.7%), see Table 3.1.

Table 4.9. Comparison of %R.A between Kokoza results and present results for water quenched steel.

%R.A (Kokoza results)	%R.A (Present results)
8.74 (C45 steel)	4.4 (S2 steel)
12.13 (C65 steel)	14.44 (S1 steel)

4.3.2. Effect of quenching media

Based on Table 4.9 of XRD results it can be noticed that, for the same composition of steel, water quenching gives the highest %R.A followed by used oil for car engine and corn oil quench, i.e. the maximum RA fractions results achieved when water used as quenching media while the minimum ones result from corn oil quenching which is in good agreement with Abdulkareem [7] and contrasted with Shan [26]. Table 4.11 compares results from present finding with Abdulkareem results. Our discussion of this problem is based on the fact that water has the highest cooling rate because there is no formation of a jacket steam which is the most important properties of oil quench (as we mentioned in section 2.2.2). As the cooling rate increased there will be insufficient time for R.A to transform into martensite and RA fractions would be increasing, i.e. that %R.A increases by increasing the cooling rate [7]. Used oil for car engine gives a higher retained austenite fraction than fresh corn oil quenching and the reason for this could be explained as, the used oil has lost its most important properties including viscosity, low viscosity of used oil leads to fast cooling rate which increase %R.A more than in case of fresh corn oil quenching but less than in case of water quenching [22].

Table 4.10. Comparison of %R.A between Abdulkareem results (steel contain 0.42%C) and present results (steel contain 0.37%C) for water and fresh oil quenched steel.

Quenching media	%R.A (Abdulkareem results)	%R.A (present results)
Water	16.4	14.44
Fresh oil	14.3	9.34

4.4. Measurement of Retained Austenite by Electrical Resistivity (E.R)

When electrons are conducted through a perfect metal crystal with no thermal effect, there should be no scattering of the electrons and the resistivity is zero. However, ‘defects’, including impurities, grain boundaries, dislocations from plastic deformation and thermal vibrations, can scatter electrons in metals; increasing the number density of defects causes an increase in the resistivity. From this concept, the electrical resistivity measurements could be useful for retained austenite detection.

After using of Jandel device to measure electrical resistivity of the as received steels S1 and S2, the results were obtained and presented in Tables 4.11 and 4.12. Current range of 45mA was used and the voltage drop was recorded by calculating the average values of ten measurements for each specimen.

Table 4.11. Electrical resistivity measurements of as recieved S1 steel.

Entry	Reading (mV)	Bulk resistivity (mΩ.mm)
1	1.88	0.262364444
2	1.52	0.212124444
3	1.298	0.181143111
4	1.5	0.209333333
5	1.667	0.232639111
6	1.745	0.243524444
7	1.45	0.202355556
8	1.736	0.242268444
9	1.56	0.217706667
10	1.182	0.164954667
avg	1.5538	0.216841422

Table 4.12. Electrical resistivity measurements of as recieved S2 steel.

Entry	Reading (mV)	Bulk resistivity (mΩ.mm)
1	1.2	0.167466667
2	1.051	0.146672889
3	1.08	0.15072
4	1.076	0.150161778
5	1.086	0.151557333
6	1.05	0.146533333
7	0.951	0.132717333
8	1.091	0.152255111
9	1.128	0.157418667
10	1.012	0.141230222
avg	1.0725	0.149673333

The bulk resistivity has been calculated by the equation [82]:

Bulk Resistivity = 2π SV/I ………………………………….….(4.6)

Where S is the probe spacing (0.1cm), V in milli-volts and I in milli-amper. The averages of ten values were taken and the calculated electrical resistivity values in μΩ.cm are shown in Table 4.13.

Table 4.13. Average bulk electrical resistivity of as received S1 and S2 steels.

Sample	E.R (μΩ.cm)
S1	21.68
S2	14.96

For calibration of Jundle four probe electrical resistivity device at room temperature, these values were compared with theoretical values calculated by the equation [33]:

ρ (μΩ.cm) = 9.58 + 5.0273 %C + 5.8212 %Mn + 13.08 %Si + 45.41 %P + 18.5418%S……………………………………………………….………………..(4.7)

The values of theoretical resistivity measurements are 23.6 and 18.2 μΩ.cm for sample S1 and sample S2 respectively which are in good agreement with the experimental measurements as shown in Table 4.14.

Table 4.14. Comparison of electrical resistivity obtained by Jandel device and that calculated by equation 4.7.

Sample	E.R measured by Jandel device (μΩ.cm)	E.R calculated by Equation (4.7) (μΩ.cm)	% Difference
S1	21.68	23.6	8.85
S2	14.96	18.2	21.6

The electrical resistivities have also been measured for steels S1 and S2 after the quenching process using Jundle four probe device and the results are shown in Tables from 4.15 to 4.20.

Table 4.15. Bulk electrical resistivity measurements of water quenched S1 steel (WQ04).

Entry	Reading (mV)	Bulk resistivity (mΩ.mm)
1	2.971	0.414619556
2	2.73	0.380986667
3	2.981	0.416015111
4	2.724	0.380149333
5	2.762	0.385452444
6	3.06	0.42704
7	2.883	0.402338667
8	3.296	0.459975111
9	3.32	0.463324444
10	2.911	0.406246222
avg	2.9638	0.413614756

Table 4.16. Bulk electrical rseistivity measurements of water quench S2 steel (WQ06).

Entry	Reading (mV)	Bulk resistivity (mΩ.mm)
1	2.579	0.359913778
2	2.256	0.314837333
3	1.724	0.240593778
4	2.11	0.294462222
5	2.331	0.325304
6	2.337	0.326141333
7	2.15	0.300044444
8	1.955	0.272831111
9	2.26	0.315395556
10	2.025	0.2826
avg	2.1727	0.303212356

Table 4.17. Bulk electrical resistivity measurements of used engine oil quenched S1 steel (EQ04).

Entry	Reading (mV)	Bulk resistivity (mΩ.mm)
1	3.037	0.423830222
2	3.016	0.420899556
3	3.4	0.474488889
4	2.415	0.337026667
5	2.922	0.407781333
6	2.907	0.405688
7	2.83	0.394942222
8	2.79	0.38936
9	3.25	0.453555556
10	3.04	0.424248889
avg	2.9607	0.413182133

Table 4.18. Bulk electrical resistivity measurements of engine oil quenched of S2 steel (EQ06).

Entry	Reading (mV)	Bulk resistivity (mΩ.mm)
1	1.39	0.193982222
2	2.606	0.363681778
3	1.405	0.196075556
4	1.423	0.198587556
5	1.56	0.217706667
6	2.06	0.287484444
7	1.97	0.274924444
8	1.955	0.272831111
9	2.06	0.287484444
10	2.025	0.2826
avg	1.8454	0.257535822

Table 4.19. Bulk electrical resistivity measurements of corn oil quenched of S1 steel (CQ04).

Entry	Reading (mV)	Bulk resistivity (mΩ.mm)
1	2.204	0.307580444
2	2.728	0.380707556
3	1.821	0.254130667
4	2.06	0.287484444
5	2.265	0.316093333
6	2.045	0.285391111
7	3.158	0.440716444
8	2.162	0.301719111
9	2.412	0.336608
10	2.065	0.288182222
avg	2.292	0.319861333

Table 4.20. Bulk electrical resistivity measurements of corn oil quenched of S2 steel (CQ06).

Entry	Reading (mV)	Bulk resistivity (mΩ.mm)
1	1.812	0.252874667
2	1.73	0.241431111
3	1.69	0.235848889
4	1.503	0.209752
5	1.881	0.262504
6	1.807	0.252176889
7	1.75	0.244222222
8	1.762	0.245896889
9	1.876	0.261806222
10	2.007	0.280088
avg	1.7818	0.248660089

The final results of the electrical resistivity are presented in Table 4.21 that follows using average values of ten measurements.

Table 4.21. Electrical resistivity (E.R) of as recieved, water and oils quenched steels.

Sample	E.R before quenching (μΩ.cm)	E.R of water quench (μΩ.cm)	E.R of used engine oil quench (μΩ.cm)	E.R of corn oil quench (μΩ.cm)
S1	21.68	41.36	41.32	31.98
S2	14.96	30.35	25.75	24.86

These results will be discussed in terms of the effect of impurities, effect of quenching process and effect of retained austenite amount (%R.A).

4.4.1. Effect of impurities

From Table 4.14, it was found that steel S1 has higher electrical resistivity than steel S2. This result could be explained in terms of the effect of impurities (alloying elements). The %C, %Mn and %Si in steel S1 are more than that of steel S2. Presence of these elements leads to both the formation of more non- metallic inclusions and the distortion of the lattice parameters by the introduction of impurity atoms. These two mechanisms can reflect the higher electrical resistivity [55]. A comparison of electrical resistivity for steels S1 and S2 is presented in Figure 4.17.

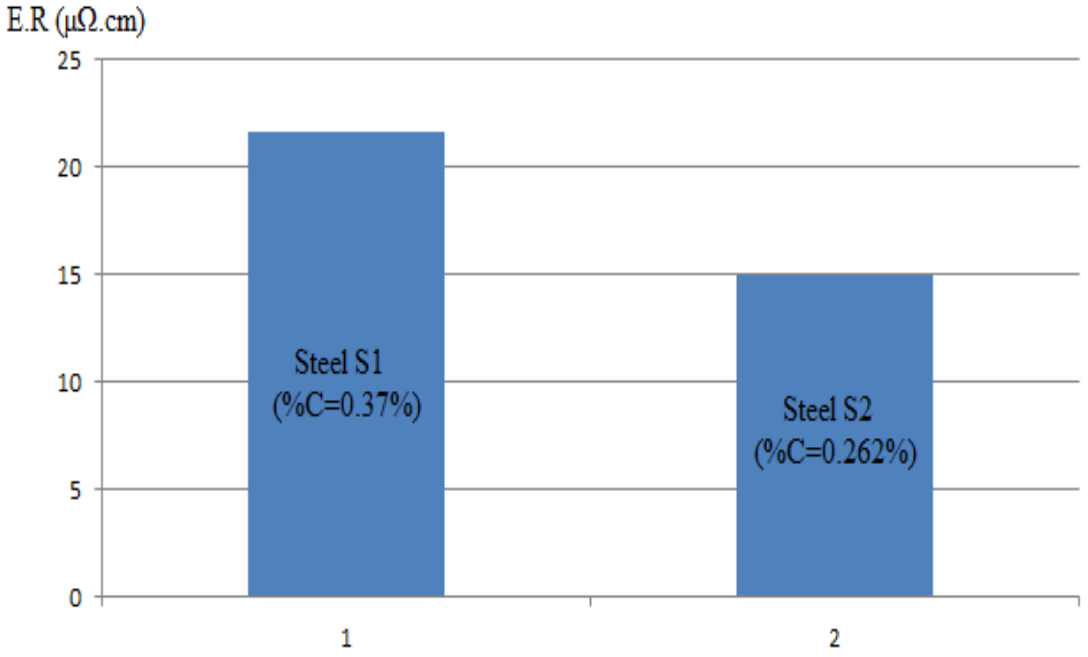

Figure 4.17. Comparison of E.R (µΩ.cm) between S1 and S2 steels.

4.4.2. Effect of Quenching Media

Based on the results in Table 4.21, it is clear that quenching process using water and oils as quenching media raise the value of E.R. Figure 4.18 shows a comparison of electrical resistivity between different heat treatment conditions.

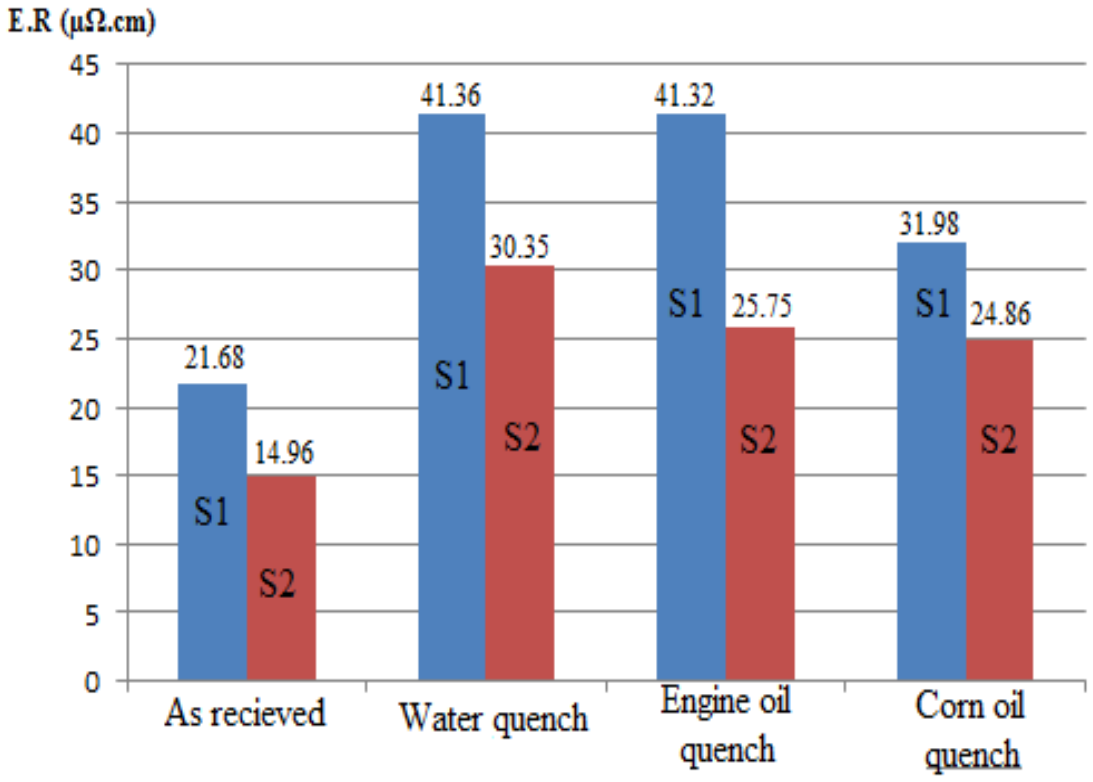

Figure 4.18. Comparison of E.R between different heat treatment condition.

It is well known that water quenching process introduces internal stresses in steels leading to lattice distortion. This distortion gives rise to lattice defects such as dislocations, high angle grain boundaries, and twins. It is also known that the martensitic transformation of steel puts the surface under compression. This is because of the expansion at the surface due to formation of the lower density BCT martensite from FCC austenite [88]. As a consequence of this transformation, the final microstructure can contain more dislocations, voids, and fine discontinuities. This can increase the electrical resistivity of the material. This is in accordance with results that obtained by Agurto et.al [43] that showed martensite was accompanied by an increase in the electrical resistivity.

In corn oil quench there is also an increase of electrical resistivity due to the presence of martensite phase, however, the presence of the ferrite phase was still noticed. This was because unlike water cooling, one of the properties of oil cooling is the formation of a jacket steam, which is called layered boiling. This causes the cooling rate to be relatively slow, decreasing the temperature below Ac3. Likewise, as in the quenching of corn oil, the internal stresses are reduced in comparison with the water quenching. The electrical resistivity did not exceed that of the water-quenched samples. The above explanation does not apply to car engine oil because it has been used for a period of time and has lost its properties. The car engine oil quenched samples have higher electrical resistivity than those quenched in corn oil.

4.4.3. Effect of % Retained Austenite

In this work, measurements of %R.A by E.R method were based on Matthiessen's rule [59] which states that, total resistivity of quenched steel will include resistivity of pure iron, resistivity of impurities which include alloying elements, resistivity of quenching defects (which include dislocations and high angle grain boundaries), and resistivity of 2nd phase which is mostly retained austenite. The above can be represented by following equation:

$$\rho_{tot} = \rho_{(Fe)} + \rho_{(impurities)} + \rho_{(defects)} + \rho_{(2nd\ phase)} \quad \ldots\ldots\ldots\ldots\ldots\ldots\ldots(4.7)$$

The resistivity of pure iron as taken from ASM Metals Handbook volume 1 [94] which is 9.58×10^{-8} Ω.m. ρ_{tot} is the resistivity measured by Jandel four point probe, see Table 4.21. The modulus of resistivity as taken from Radcliffe [89] is 65 $\mu\Omega.cm$. Hence, the resistivity of total austenite phase, $\rho_{2nd\ phase}$, can be computed as follows:

$$\rho_{2nd\ phase}(\mu\Omega.cm) = 65(\mu\Omega.cm) \times C_{\gamma} \quad \ldots\ldots\ldots\ldots\ldots\ldots\ldots\ldots(4.8)$$

Where C_{γ} is the volume fraction of retained austenite.

The resistivity of impurities, $\rho_{(impurities)}$, which represents the contribution of all alloying elements present in steel. According to Table 3.1, the most influential elements that affect the electrical resistivity of steel are C, Mn, Si, P and S, since they are the major elements in the chemical composition. Hence, $\rho_{(impurities)}$, can be measured using the following equation as taken from Koly et.al [33].

$$\rho_{impurities}\ (\mu\Omega.cm) = 5.0273\ \%C + 5.8212\ \%Mn + 13.08\ \%Si + 45.41\ \%P + 18.5418\%S \quad \ldots\ldots\ldots\ldots\ldots\ldots\ldots\ldots\ldots\ldots\ldots\ldots\ldots\ldots\ldots\ldots(4.9)$$

Where the factors indicated in the equation represent the resistivity modulus of indicated elements [33], and % element is the composition in weight percent.
Accorrding to equation 4.9 the resistivity of the main impurities of S1 steel is calculated to be 14.1462 μΩ.cm.
Lastely, the resisitivity contribution of defects, $\rho_{(defects)}$, for any quenched steel is divided in two parts: dislocation and high angle grain boundary. The contribution can be calculated using following two equations as taken from Masumura [87].

$\rho_{(dis)}$ (mΩ.mm) = 1.7×10^{-18} ×Ndis(m^{-2}) ……..……..……(4.10)

$\rho_{(HAGB)}$ (mΩ.mm)=1.58×10^{-9}×NHAGB (m^{-2}) …….....(4.11)

Where, Ndis and NHAGB are the densities of dislocations and high angle grain boundaries in m/ m^3, respectively. The densities depend strongly on carbon percent and these values are shown in Table 2.2. (See the literature review chapter section 2.4.3.1). As an illustration, for the steel samples used in this work, 0.262%C ≈0.3%C, Ndis and NHAGB are 1.3×10^{15} and 1.73 $\times10^{6}$ respectively, and for 0.37% C ≈0.4%C, Ndis and NHAGB are 1.42×10^{15} and 2.14 $\times10^{6}$ respectively. Therefore the resistivity of S1 steel of dislocation and high angle grain boundary using equations 4.10 and 4.11 are found to be 2.414 $\times10^{-3}$ mΩ.mm amd 3.3812 $\times10^{-3}$ mΩ.mm respectively. The sum of which is 0.5795 $\times10^{-3}$ μΩ.cm.
Applying equation 4.7 and 4.8 and substituting the above values, the %R.A of S1 steel can be estimated by the equation:

$$\% \text{ R.A} = \frac{\rho_{tot}-24.29}{65}\times100 \text{……..……..(4.12)}$$

Where $\boldsymbol{\rho_{tot}}$ could be taken from Table 4.21.

By considering the same prementioned approach for S1 steel, the final formula for calculating the %R.A of S2 steel is :

$$\% \text{ R.A} = \frac{\rho_{tot}-19.14}{65}\times100 \text{……..……..(4.13)}$$

Table 4.22 presents a comparison between values obtained by electrical resistivity measurements and values obtained using XRD method.

Table 4.22. Comparison of %R.A measurements between E.R and XRD techniques.

Sample label	Condition	%R.A measured by E.R	%R.A measured by XRD
WQ04	Water quench of steel S1	26.26%	14.44%
WQ06	Water quench of steel S2	17.25%	4.4%
EQ04	Engine oil quench of steel S1	26.20%	11.9%
EQ06	Engine oil quench of steel S2	10.17%	2.11%
CQ04	Corn oil quench of steel S1	11.83%	9.34%
CQ06	Corn oil quench of steel S2	8.80%	2.53%

Based on the results shown in Table 4.22, it can be concluded that %R.A measured by E.R method using Jandel four point probe device have the same trend with %R.A measured by XRD technique. These finding can be further shown in Figures 4.19 and 4.20 for S1steel and S2 steel respectively. Maximum %R.A was obtained using water quenched steels and the lowest %R.A was obtained using corn oil quenched steels in both E.R and XRD methods.

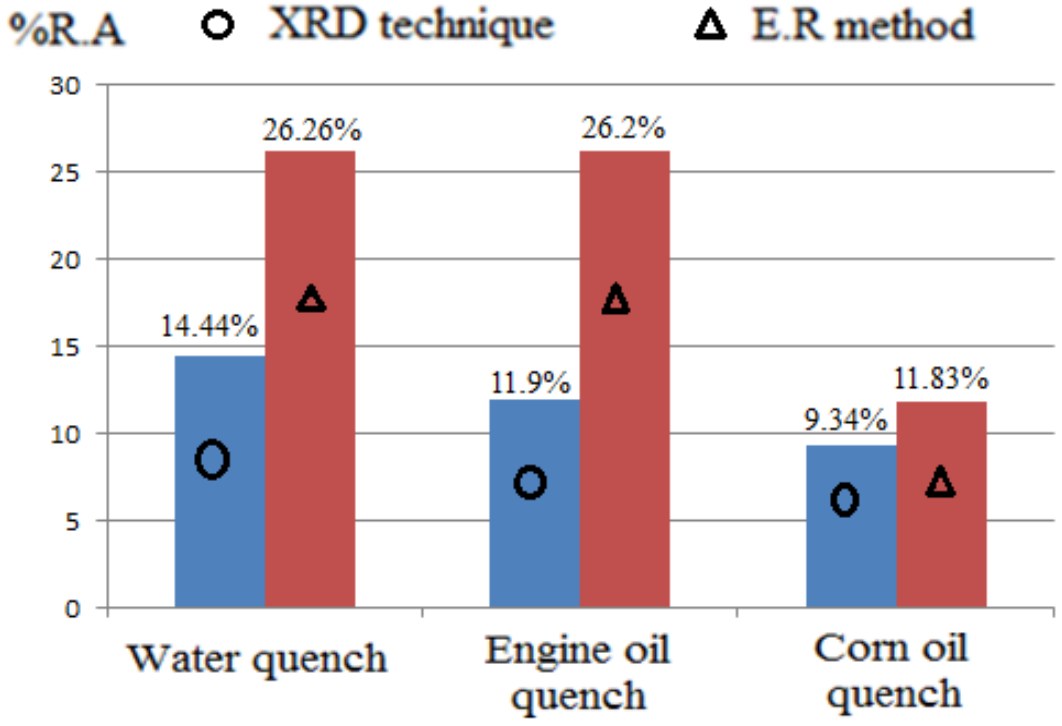

Figure 4.19. Comprison of %R.A (S1 steel) obtained by XRD and E.R methods.

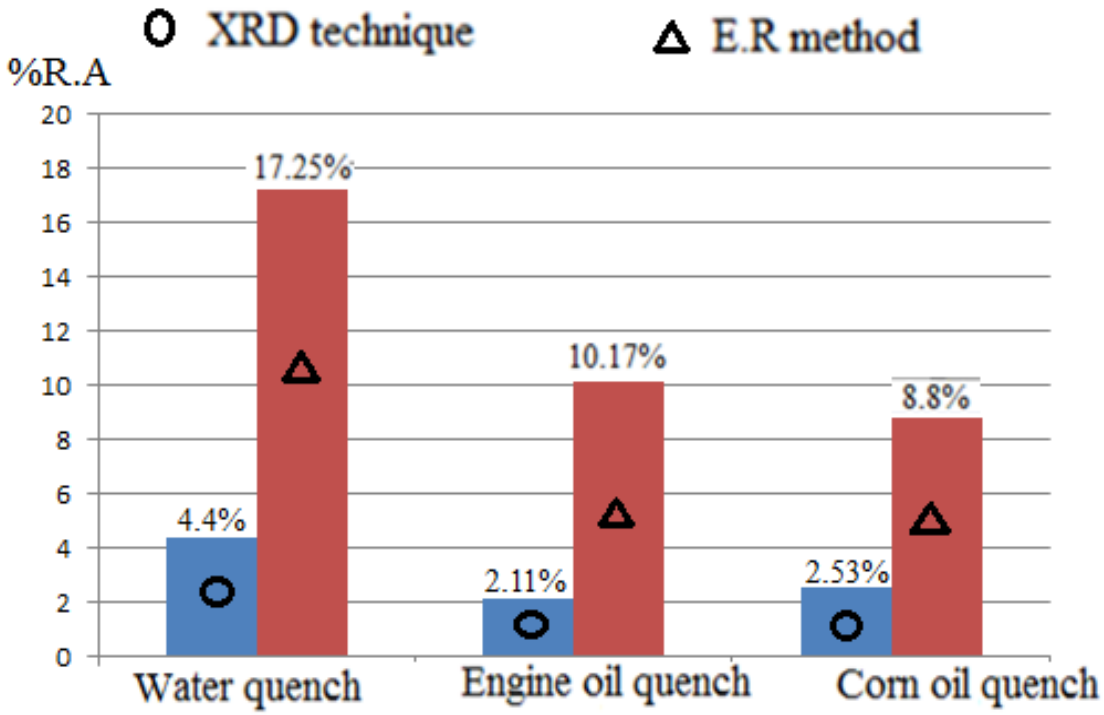

Figure 4.20. Comprison of %R.A (S2 steel) obtained by XRD and E.R methods.

Figure 4.21 shows the relationship between %R.A measured by XRD technique and E.R measured by Jandel four point probe device for S1 and S2 steels. It was found that highest electrical resistivity is obtained for steels contain highest %R.A. This means that retained austenite can be responsible for an increasing in the electrical resistivity of quenched steel which is agreement with Mohanty and Bhagat [85] and contrasted with Msumura[87].

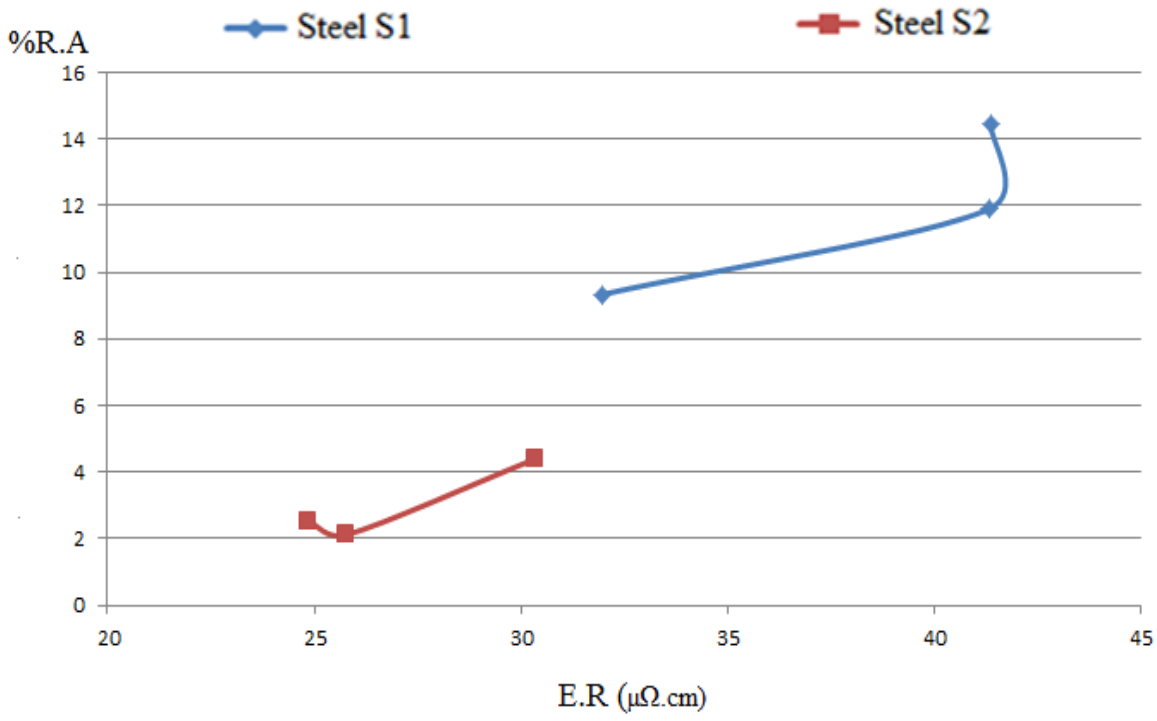

Figure 4.21. Effect of %R.A in electrical resistivity

The effect of retained austenite on electrical resistivity can be explained in terms of austenizing process of the steel. Heating of the steel to 950ºC (within the austenite range) increases the stability of austenite phase. This can have strong effect on the density of vacancies. The density of vacancies in a crystalline metallic material can be exponentially increased with increase temperature up to the level of about 1 over 10,000 atomic positions at temperatures close to the melting point. For this reason when the samples are heated to 950 ºC, the vacancy concentration increases and the solubility of interstitial carbon atoms can increase up to the maximum value resulting in a significant increase in the electrical resistivity [60].

As shown in Figures 4.19 and 4.20, the %R.A as measured by E.R method is always larger than the values measured by XRD. This could be due to the high total resistivity values (ρ_{tot}) in Equation 4.12 which is measured by Jandel four probe device. It should be mentioned that measuring electrical resistivity using Jandel device is a very sensitive process that needs special surface preparation to produce a surface free from any scratches, dust or any isolated stains. Such artifacts can cause an increase in electrical resistivity. Usually surface preparation of this kind requires special laboratories.

Another reason that could affect the results of electrical resistivity is the accuracy and calibration of the Jandel device. Periodic calibration is important to obtain results of a hundred percent accuracy. The device that was used for this research was not used for many years. I had to learn how to calibrate the device. However such margin of errors can definitely have an effect on the retained austenite measurements.

Chapter 5
Conclusions and Recommendation

Conclusions on the factors that affect % retained austenite (carbon %, alloying element, austenizing temperature……etc), and the correlation between the three measurement techniques (metallography, x-ray diffraction and electrical resistivity) are presented in the following points:

A) Conclusion

1. Steels S1 and S2 of different alloying elements showed that a larger amount of retained austenite can be obtained by increasing alloying elements contents (especially carbon and manganese).
2. The amount of retained austenite is thought to be increase with increase of cooling rate.
3. Using of "used oil for car engine " is not useful for oil quenching of steel according to their low cost. It gave almost same results as that for water quenching.
4. Using of metallography technique to quantify the amount of retained austenite is very complicated and unreliable when the amount of carbon less than 0.6%. So that it is preferable to rely on x-ray method to quantify such steels.
5. Electrical resistivity of steel increases by increasing the content of alloying elements such as carbon, silicon and phosphors. It is also increases by increasing the cooling rate of steel where the higher electrical resistivity was obtained using of tab water as quenching media.
6. Retained austenite could be responsible for a noticeable increase in electrical resistivity of quenched steel.
7. Electrical resistivity measurement is not a good technique for quantitative measurements of retained austenite, but it could be helpful for qualitative measurements.

B) Recommendation

1. To better correlate % retained austenite using the three methods, steel samples containing high carbon content with specific alloying elements should be tried.

2. To obtain reliable results for % retained austenite metallugraphically, colouring etchants like Klemm’s I and Baraha type should be used.

References

1. Fair Lane. "Determination of Volume Percent Retained Austenite by X-Ray Diffraction". Cincinnati, OH 45227 (513)561-0883, No. 33 Fall 2006.
2. L. Kučerová, K. Opatová1 and A. Jandová1. "Metallography of AHSS steels with retained austenite". Regional Technological Institute, University of West Bohemia in Pilsen, Univerzitni 8, 30614, Pilsen, Czech Republic.
3. Yang-Yu Su , Liu-Ho Chiu , Tao-Liang Chuang , Chien-Lung Huang , Cheng-Yen Wu and Kuan-Chueh Liao. "Retained austenite amount determination comparison in JIS SKD11 steel using quantitative metallography and X-ray diffraction methods". Advanced Materials Research Vols. 482-484, 2012, pp 1165-1168.
4. W. Hetzner. "X-Ray Determination of Retained Austenite in Steel Using ASTM E975". Microsc Microanal 9(Suppl 2), 2003, pp 710-711.
5. S. Pashangeh , H. Zarchi, S. Banadkouki and M. Somani. "Detection and estimation of retained austenite in a high strength Si- bearing bainite- martensite-retained austenite micro-composite steel after quenching and bainatic holding (Q and B)". journal of metals vol 9, 2019, pp 2-21.
6. Pereloma, Gazder and Timokhina. "Retained austenite: transformation-induced plasticity. In R. Colas & G. E. Totten (Eds.), Encyclopedia of Iron, Steel, and Their Alloys". New York: CRC Press, 2016, pp. 3088-3103.
7. N. Abdulkareem and A. Jabbar, "Effect of Retained Austenite on the Microstructure and Mechanical Properties of AI-SI4340 High Strength Low Alloy Steel (HSLA steel) Using Magnetic Saturation Measurement and X-Ray Diffraction methods". Basrah Journal for Engineering Sciences, vol. 17, no. 2, 2017.
8. L. Zhao, H. van Dijk, E. Bru¨ck, J. Sietsma and S. van der Zwaag. "Magnetic and X-ray diffraction measurements for the determination of retained austenite in TRIP steels". Materials Science and Engineering A313, 2001, pp 145–152.
9. Jasmine. S. "Effect of Microstructure on Retained Austenite Stability and Tensile Behavior in an Aluminum-Alloyed TRIP Steel". Degree of master, Queen's University Kingston, Ontario, Canada, September 2012.
10. T. Eldis. "Correlation of Measurements of Retained Austenite in Carburized Steels by X-Ray Diffraction and Quantitative Metallography". American society for metals. vol 1, no 3, 1980.
11. S. Min, S. Thu and K. Lwin. "Effect of heat treatment on microstructures and mechanical properties of spring steel". Mandaly University, Journal of Metals, Materials and Minerals, Vol.18, No.2, Myanmar, 2008, pp.191-197.
12. H.Zhang, Z.Wei, F. Xie and B. Sun. "Assessment of the Properties of AISI 410 Martensitic Stainless Steel by an Eddy Current Method". Journal of materials, vol 12, 2019.
13. O. Daramola, O. Adewuyi and O. Oladele. "Effects of Heat Treatment on the Mechanical Properties of Rolled Medium Carbon Steel". Journal of Minerals and Materials Characterization and Engineering, Vol. 9, No.8, 2010, pp.693-708.
14. M. Dauda1, L. Kuburi2, D. Obada3 and R. Mustapha. "Effects Of Various Quenching Media On Mechanical Properties Of Annealed 0.509Wt%C – 0.178Wt%Mn Steel". Nigerian Journal of Technology (NIJOTECH) Vol. 34 No. 3, July 2015, pp. 506 – 512.
15. S. Ma. "Characterization of the performance of mineral oil based quenchants using CHTE Quench Probe System". Degree of Master, Worcester Polytechnic Institute, June 27, 2002.

16. Z. Kadhim. "Effect of Quenching Media on Mechanical Properties for Medium Carbon Steel". Int. Journal of Engineering Research and Application, Vol. 6, Issue 8, August 2016, pp.26-34.
17. J. Davis. "Metals Handbook Desk Edition". Second Edition, p 153-173.
18. V. Sreeja, P. Dinesh and S. Patil. "Study of Mechanical Properties of Steel Quenched in a Blend of Biodegradable Oils with Quench Accelerators". IJLTEMAS, Volume V, Issue V, May 2016, pp 20-24.
19. Z. Kadhim and M. Abdulrazzaq. "Effect of Tempering Temperatures on Mechanical Properties for Medium Carbon Steel". International Journal of Research in Engineering and Science (IJRES), Volume 5, Issue 8, August. 2017, PP. 87-93.
20. 2. L. Kučerová, K. Opatová and A. Jandová. "Metallography of AHSS steels with retained austenite". Regional Technological Institute, University of West Bohemia in Pilsen, Univerzitni 8, 30614, Pilsen, Czech Republic.
21. B. Qasim, T. Khidir, A. Hameed and A. Abduljabbar. "Influennce Of Heat Tretment On The Asorbed Energy Of Carbon Steel Alloys Using Oil Quenching And Water Quenching". Journal of Mechanical Engineering Research and Developments (JMERD), 2018, pp.43-46.
22. J. Mohmmed and Z. Hashimy. "Effect of Different Quenching Media on Microstructure. Hardness, and Wear Behavior of Steel Used in Petroleum Industries". Journal of Petroleum Research & Studies, 2017, pp.198-207.
23. V. Rudnev and G. Fett. "Principles of Induction Hardening and Inspection". Induction Heating and Heat Treatment", vol 4c, 2014, pp.58-66.
24. Irina, C. Philip, G. Mohamed, V. Nathalie, R. Abdelkrim and M. Antoine. "Distribution of Carbon in Martensite During Quenching and Tempering of Dual Phase Steels and Consequences for Damage Properties". ISIJ International, Vol. 53, No. 7, 2013, pp. 1215–1223.
25. J. Dossett. "Practical Heat Treating. united state of America". Second Edition, 2006.
26. M. Shan, S. Thu and K. Thi. "Effect of Heat Treatment on Microstructures and Mechanical Properties of Spring Steel". Journal of Metals, Materials and Minerals, Vol.18 No.2, 2008, pp.191-197.
27. E.Vieira, L. Biehl, J. Medeiros, V. Costa and R. Macedo. "Evaluation of the characteristics of an AISI 1045 steel quenched in different concentration of polymer solutions of polyvinylpyrrolidone". Nature research, 2021.
28. W. Fonda, A.Vandermeer, and G. Spanos. "Continuous Cooling Transformation (CCT) Diagrams for Advanced Navy Welding Consumables". Naval research laboratory,1998.
29. R. Abbaschain, L. Abbaschain and R. Reed-Hill. "Physical metallurigy principles". USA, fourth edition, 2009.
30. T. Digges and J. Samuel. "Heat Treatment and Properties of Iron and Steel", National Bureau of Standards Monograph 18, 1960.
31. X. Qiao, L. Han, W. Zhang and G. Jianfeng. "Thermal Stability of Retained Austenite in High-carbon Steels during Cryogenic and Tempering Treatments". ISIJ International, Vol. 56, No. 1, 2016, pp. 140–147.
32. S. Akay, M. Yazici and A. Avinc. "The Effect of Heat Treatments on Physical Properties of a Low Carbon Steel". The Publishing House of the Romanian academy, Volume 10, Number 2009, pp. 1-5.
33. D. Koly, T. Ray and C. Soumya. "Prediction of electrical resistivity of steel using artificial neural network". Iron making and steel making, 2017, pp 2-8.

34. K. Salman. "Effect of Quenching Media on Mechanical Properties of Medium Carbon Steel 1030". Journal of University of Babylon, Engineering Sciences, Vol.(26), No.(2): 2018, pp.214-222.
35. D. Herring. "Oil Quenching Part One: How to Interpret Cooling Curves". Industrial Heating, August 2007.
36. M. Ndaliman. "An Assessment of Mechanical Properties of Medium Carbon Steel under Different Quenching Media". AU J.T. Vol.10, Number 2, 2006، pp 1-4.
37. G.Totten, H. Tensi and K. Lainer. "Performance of Vegetable Oils as a Cooling Medium in Comparison to a Standard Mineral Oil". Journal of Materials Engineering and Performance, Volume 8(4), August 1999, pp.409-416.
38. N. Jones. "Managing Used Oil". Lubes 'n' Greases, Vol 2, No. 6, 1996, p 20-21.
39. A. Çalik. "Effect of cooling rate on hardness and microstructure of AISI 1020, AISI 1040 and AISI 1060 Steels". International Journal of Physical Sciences, Vol. 4 (9), September, 2009, pp. 514-518.
40. A. Altaweel and M. Tolouei-Rad. "Effect Of Quenching Media, Specemen Size and Shape On The Hardenability Of AISI 4140 Steel". Emirates Journal for Engineering Research, Vol 19 (2), 2014, pp.33-39.
41. J. Odusote, T. Ajiboye and A. Rabiu. "Evaluation of Mechanical Properties of Medium Carbon Steel Quenched in Water and Oil". Journal of Minerals and Materials Characterization and Engineering, Vol 11, 2012, pp.859-862.
42. M. Dauda, L. Kuburi, D. Obada and R. Mustapha. "Effect of various quenching media on mechanical properties of annealed 0.509Wt%C – 0.178Wt%Mn Steel". Nigerian Journal of Technology (NIJOTECH), Vol. 34 No. 3, July 2015, pp. 506 – 512.
43. M. Agurto, E. Atencio, F. Navarro and J. Ramos. "Metallographic Analysis and Electrical Resistivity of the 1045 Steel after being Heat-treated". Journal of Metals, Materials and Minerals, Vol.27 No.1, 2017, pp.53-58.
44. W. Smith and J. Hashemi. "Foundations of materials science and engineering". Mcgraw-Hill Publishing, 2006.
45. Jomlny. "Hardenabillty of alloy steels". Am. Soc. Metals, 1939, pp. 75.
46. D. Herring. "A Discussion of Retained Austenite". The Heat Treat Doctor, 2005, pp.14-16.
47. L. Kučerová, K. Opatová and A. Jandová. "Metallography of AHSS steels with retained austenite". Microscopy and imaging science, pp.455-463.
48. M. Piešováa, A. Czána, M. Šajgalíka, T. Czánováa and R. Čepb. "Experimental quantification of the austenitic phase in steels using the Average peak method of x-ray diffractometry". Procedia Engineering, Vol 192 , 2017, pp.689 – 694.
49. S. Magner, R. De Angelis, W. Weins and J. Makinson. "A Historical Review Of Retained Austenite And Its Measurements By X-Ray Diffraction". International Centre for Diffraction Data, Vol 45, 2002, pp.92-97.
50. K. Ouda, H. Danninger and C. Gierl-Mayer. "Magnetic measurement of retained austenite in sintered steels – benefits and limitations". Powder metallurgy, 2018, pp.1-11.
51. W. Zhou, T. Hou , C. Zhang, L. Zhong and K. Wu. "Effect of Carbon Content in Retained Austenite on the Dynamic Tensile Behavior of Nanostructured Bainitic Steel". Journal of metals, Vol 8, 2018, pp.2-11.
52. A. Kokosza and J. Pacyna. "Mechanical Stability of Retained Austenite In Unalloyed Structural Steels Of Various Carbon Content". Archives of metallurgy and materials, Vol 55, issue 4, 2010, pp. 1001-1006.

53. J. Mahieu. J. Maki, B. De Cooman and S. Claessens. "Phase transformation and mechanical properties of Si-free CMnAl transformation- induced plasticity-aided steel". Metall. Mater. Trans; 33A, 2002.
54. S. Nemecek, Z. Novy, J.Uhlir, J. Janovec and M. Kusy. "Evaluation of Retained Austenite In High Strenght Steel". Czech Republic, 2016.
55. V. Vargas, I. Mejía, V. Baltazar-Hernández, and C. Maldonado. "Effect of retained austenite and nonmetallic inclusions on the thermal/electrical properties and resistance spot welding nuggets of Si-containing TRIP steels". International Journal of Minerals, Metallurgy and Materials Volume 26, Number 1, January 2019, pp. 52.
56. M. Yaso, S. Hayashi, S. Morito, T. Ohba, K. Kubota and K. Murakami. "Characteristics of Retained Austenite in Quenched High C-High Cr Alloy Steels". Materials Transactions, Vol. 50, No. 2, 2009, pp. 275 – 279.
57. A. Poulon-Quintin, J. Vogt, V. Shivanyuk and J. Foct. "Characterisation and understanding of TRIP steels". J. Phys. IV France, Vol 118, 2004, pp. 355–368.
58. G. Vander Voort. "Hints for Imaging Phases In Steels". Advanced Materials & Process, feb 2005, pp.32-37.
59. L. Zhou. Non-Destructive Characterization of Steel Microstructures Using Electromagnatic Sensors". Degree of doctor of physiology, The University of Birmingham (UK), Dec 2014.
60. S. Pashangeh, H. Zarchi, S. Banadkouki and M. Somani. "Detection and Estimation of Retained Austenite in a High Strength Si-Bearing Bainite-Martensite- Retained Austenite Micro-Composite Steel after Quenching and Bainitic Holding (Q&B)". Journal of metals, vol 9, 2019, pp.2-21.
61. E. Klimek. "Metallographic method for measuring retained austenite". Metals engineering quarterly, Vol 15, numer 1, Feb 1975.
62. G.Vander Voort and L. Buehler. "Laboratory Safety in Metallography". Metallography and Microstructures, Vol 9, ASM Handbook, ASM International, 2004, pp. 1081–1090.
63. F. Khokhar. "Quantitative analysis of multi-phase systems - steels with mixture of ferrite and austenite". Degree of master, Department of Physics and Measurement Technology Linköping University, Sweden.
64. W. callister. "Materials science and engineering", 7th ed, 2008.
65. ASTM. "Standard Practice for X-Ray Determination of Retained Austenite in Steel wit Near Random Crystallographic Orientation". American society for testing and materials, Designation: E975 – 13.
66. J. Ridenfeldt. "Stainless steel Metal Matrix Composite". 1988.
67. C. Babbage." Material Property Data for Quench Simulations". WILEY-VCH Verlag GmbH and Co. KGa, Weinheim, 2010, pp.702-715.
68. L. Zhang, D. Gong, Y. Li, X. Wang, X. Ren and E. Wang. "Effect of Quenching Conditions on the Microstructure and Mechanical Properties of 51CrV4 Spring Steel". Journal of metals, Vol 8, 2018, pp2-16.
69. B.D Cullity. "Elements of x-ray diffraction". 2nd Edition. Indiana, 1977.
70. F.B. Abudaia. "On The Stabilization of Retained Austenite". Journal of Engineering Research, Issue (5), March 2006, pp.48-58.
71. M. Tupta. "Techniques for Measuring the Electrical Resistivity of Bulk Materials". keithley, November 18, 2010, pp. 2-56.
72. P. Browen and D. Mack. "Electrical Resistivity and Microstructural Changes Accompanying the Isothermal Decomposition of Austenite in Eutectoid Steel". Metallurgical Transaction,Vol 4, Nov 1973, pp.2639 – 2643.

73. G. Hersir. "Resistivity Surveying and electromagnetic Method". Santa Tecla and Ahuachapán, El Salvador, March 14 - 22, 2015.
74. R. Putiska, M. Nikolaj, I. Dost´ and D. Kusnir. "Determination of cavities using electrical resistivity tomography". Contributions to Geophysics and Geodesy, Vol. 42/2, 2012, pp.201–211.
75. C. Park, J. Jeong, H. Park and K. Kim. "Experimental Study on Electrode Method for Electrical Resistivity Survey to Detect Cavities under Road Pavements". Sustainability, Vol 9, 2017.
76. J. G. Hust and P. J. Ciarratano. "Thermal Conductivity and Electrical Resistivity Standard Reference Materials". Washigton, june 1975.
77. P. Kirbiš, I. Anžel, and M. Brunčko. "Application of in-situ Electrical Resistance Measurements to the Study of Phase Transformations in Ferrous Alloys". Fizika Metallov i Metallovedenie, Russia, Vol. 117, No. 11, 2016, pp. 1130–1139.
78. J. Nejezchlebova , H. Seiner , P. Sedlak , M. Landa , J. Smilauerova , E. Aeby-Gautier ,B. Denand ,M. Dehmas and B. Appolaire. "On the complementarity between resistivity measurement and ultrasonic measurement for in-situ characterization of phase transitions in Ti-alloys". Journal of Alloys and Compounds, Vol 762, 2018, pp.868-872.
79. U. Bohnenkamp and R. Sandstrom. "Evaluation of the electrical resistivity of steels". Steel research, Vol 71, No. 10, 2000, pp.410-416.
80. S. Chaudhuri, R. Mahanti, C. Sivaramakrishnan and M. Singh. "Physical properties of some thermomechanically processed microalloyed steels". Materials & Design, 2002, pp.489-96.
81. M. Tupta. "Measuring the resistivity of bulk materials". Desighn and products, Jun 2011, pp.21-24.
82. R. Waremra and P. Betaubun. "Analysis of Electrical Properties Using the four point Probe Method". E3S Web of Conferences, Vol 73, 2018.
83. Y. Singh. "Electrical Resistivity Measurements: A Rerview". International Journal of Modern Physics: Conference Series,Vol. 22, 2013, pp.745–756.
84. A. N. Bahgat and O. N. Mohanty. "Electrical resistivity studies in low carbon and HSLA – 100 steels". Material science and technology, Vol 19, Mar 2003, pp.343-346.
85. O.N. Mohanty and A. N. Bhagat. "Electrical resistivity and phase transformation of steel. Mat-wiss. U. werkstofftech, Vol 34, 2003, pp. 96-101.
86. P. S. Neelakanta. "Handbook of electronic materials. Boca raton , Florida, 1995, pp. 215-216.
87. T. Msumura, T. Taniguchi, S. Uranaka, I. Hirashima, T. Tsuchiyama, N. Maruyama, H. Shirahata and R. Uemori. "Estimation of Solute Carbon Concentration by Electrical Resistivity Measurement in Martensitic Steel, ISIJ International, Vol. 61, No. 5, 2021, pp.1708–1715.
88. S.V.Lomte, C. L.Gogte and D.R.Peshwe. "On Electrical Resistivity Of AISI D2 Steel During Various Stages of Cryogeni Tretment". Advances in Cryogenic Engineering, AIP Conf. Proc. Vol 1434, 2012, pp.1183-1189.
89. S. V. Radcliffe and E. C. Rollason: Z Iron Steellnst, 1959, vol. 191, p. 56.
90. Apsc-mtrl.sited.olt.ubc.ca."Safe Preparation of Nital (nitric acide-a;coho; so;ution", June 2013.
91. R.F.Mehl. "Atlas of microstructure of industrial alloys". 8th edition, USA, 1972.
92. Stressteach.com, "Retained austenite measurments". Nov 2021.

93. F. Girgsdies. "Peak Profile Analysis in X-ray Powder Diffraction". Department of Inorganic Chemistry, Fritz-Haber-Institut der MPG, Berlin, Germany.
94. ASM. "Conductivity and Resistivity Values for Iron & Alloys". ASM Metals Handbook--Volume 1, Tenth Edition, MAR2002.

Appendix A

Atomic scattering factor

Table A.1 Atomic scattering factors].

$\frac{\sin\theta}{\lambda}$ (A^{-1})	0.0	0.1	0.2	0.3	0.4	0.5	0.6	0.7	0.8	0.9	1.0	1.1	1.2
Fe	26	23.1	18.9	15.6	13.3	11.6	10.2	8 9	7.9	7.0	6.3	5.7	5.2
Co	27	24.1	19.8	16.4	14.0	12.1	10.7	9.3	8.3	7.3	6.7	6.0	5.5
Ni	28	25.0	20.7	17.2	14.6	12.7	11.2	9.8	8.7	7 7	7.0	6.3	5.8
Cu	29	25.9	21.6	17.9	15.2	13.3	11.7	10.2	9.1	8.1	7.3	6.6	6.0
Zn	30	26.8	22.4	18.6	15.8	13.9	12.2	10.7	9.6	8.5	7.6	6.9	6.3
Ga	31	27.8	23.3	19.3	16.5	14.5	12.7	11.2	10.0	8.9	7.9	7.3	6.7
Ge	32	28.8	24.1	20.0	17.1	15.0	13.2	11.6	10.4	9.3	8.3	7.6	7.0
As	33	29.7	25.0	20.8	17.7	15.6	13.8	12.1	10.8	9.7	8.7	7.9	7.3
Se	34	30.6	25.8	21.5	18.3	16.1	14.3	12.6	11 2	10.0	9.0	8.2	7.5
Br	35	31.6	26.6	22.3	18.9	16.7	14.8	13.1	11.7	10.4	9.4	8.6	7.8
Kr	36	32.5	27.4	23.0	19.5	17.3	15.3	13.6	12.1	10.8	9.8	8.9	8.1
Rb	36	33.6	28.7	24.6	21 4	18.9	16.7	14.6	12.8	11.2	9.9	8.9	
Rb	37	33.5	28.2	23.8	20.2	17.9	15.9	14.1	12.5	11.2	10.2	9.2	8.4
Sr	38	34.4	29.0	24.5	20.8	18.4	16.4	14.6	12.9	11.6	10.5	9.5	8.7
Y	39	35.4	29.9	25.3	21.5	19.0	17.0	15.1	13.4	12.0	10.9	9.9	9.0
Zr	40	36.3	30.8	26.0	22.1	19.7	17.5	15.6	13.8	12.4	11.2	10.2	9.3
Nb	41	37.3	31.7	26.8	22.8	20.2	18.1	16.0	14.3	12.8	11.6	10.6	9.7
Mo	42	38.2	32.6	27.6	23.5	20.8	18.6	16.5	14.8	13.2	12.0	10.9	10.0
Tc	43	39.1	33.4	28.3	24.1	21.3	19.1	17.0	15.2	13.6	12.3	11.3	10.3
Ru	44	40.0	34.3	29.1	24.7	21.9	19.6	17.5	15.6	14.1	12.7	11.6	10.6
Rh	45	41.0	35.1	29.9	25.4	22.5	20.2	18.0	16.1	14.5	13.1	12.0	11.0
Pd	46	41.9	36.0	30.7	26.2	23.1	20 8	18.5	16.6	14.9	13.6	12.3	11.3
Ag	47	42.8	36.9	31.5	26.9	23.8	21.3	19.0	17.1	15.3	14.0	12.7	11.7
Cd	48	43.7	37.7	32.2	27.5	24.4	21.8	19.6	17.6	15.7	14.3	13.0	12.0
In	49	44.7	38.6	33.0	28.1	25.0	22.4	20.1	18.0	16.2	14.7	13.4	12.3
Sn	50	45.7	39.5	33.8	28.7	25.6	22.9	20 6	18.5	16.6	15.1	13.7	12 7
Sb	51	46.7	40.4	34.6	29.5	26.3	23.5	21.1	19.0	17.0	15.5	14.1	13.0
Te	52	47.7	41.3	35.4	30.3	26.9	24.0	21.7	19.5	17.5	16.0	14.5	13.3
I	53	48.6	42.1	36.1	31.0	27.5	24.6	22.2	20.0	17.9	16.4	14.8	13.6
Xe	54	49.6	43.0	36.8	31.6	28.0	25.2	22.7	20.4	18.4	16.7	15.2	13.9
Cs	55	50.7	43.8	37.6	32.4	28.7	25.8	23.2	20.8	18.8	17.0	15.6	14.5
Ba	56	51.7	44.7	38.4	33.1	29.3	26.4	23.7	21.3	19.2	17.4	16.0	14.7
La	57	52.6	45.6	39.3	33.8	29.8	26.9	24.3	21.9	19.7	17.9	16.4	15.0
Ce	58	53.6	46.5	40.1	34.5	30.4	27.4	24.8	22.4	20.2	18.4	16.6	15.3
Pr	59	54.5	47.4	40.9	35.2	31.1	28.0	25.4	22.9	20.6	18.8	17.1	15.7
Nd	60	55.4	48.3	41.6	35.9	31.8	28.6	25.9	23.4	21.1	19.2	17.5	16.1
Pm	61	56.4	49.1	42.4	36.6	32.4	29.2	26.4	23.9	21.5	19.6	17.9	16.4
Sm	62	57.3	50.0	43.2	37.3	32.9	29.8	26.9	24.4	22.0	20.0	18.3	16.8
Eu	63	58.3	50.9	44.0	38.1	33.5	30.4	27.5	24.9	22.4	20.4	18.7	17.1
Gd	64	59.3	51.7	44.8	38.8	34.1	31.0	28.1	25.4	22.9	20.8	19.1	17.5
Tb	65	60.2	52.6	45.7	39.6	34.7	31.6	28.6	25.9	23.4	21.2	19.5	17.9
Dy	66	61.1	53.6	46.5	40.4	35.4	32.2	29.2	26.3	23.9	21.6	19.9	18.3
Ho	67	62.1	54.5	47.3	41.1	36.1	32.7	29.7	26.8	24.3	22.0	20.3	18.6
Er	68	63.0	55.3	48.1	41.7	36.7	33.3	30.2	27.3	24.7	22.4	20.7	18.9
Tm	69	64.0	56.2	48.9	42.4	37.4	33.9	30.8	27.9	25.2	22.9	21.0	19.3

Appendix B

Lorentz – polarization factor ($\frac{1+\mathrm{Cos}^2 2\theta}{\mathrm{Sin}^2\theta\mathrm{Cos}\theta}$)

Table B.2 Lorentz – polarization factors.

θ°	.0	.1	.2	.3	.4	.5	.6	.7	.8	.9
2	1639	1486	1354	1239	1138	1048	968.9	898.3	835.1	778.4
3	727.2	680.9	638.8	600.5	565.6	533.6	504.3	477.3	452.3	429.3
4	408.0	388.2	369.9	352.7	336.8	321.9	308.0	294.9	282.6	271.1
5	260.3	250.1	240.5	231.4	222.9	214.7	207.1	199.8	192.9	186.3
6	180.1	174.2	168.5	163.1	158.0	153.1	148.4	144.0	139.7	135.6
7	131.7	128.0	124.4	120.9	117.6	114.4	111.4	108.5	105.6	102.9
8	100.3	97.80	95.37	93.03	90.78	88.60	86.51	84.48	82.52	80.63
9	78.79	77.02	75.31	73.66	72.05	70.49	68.99	67.53	66.12	64.74
10	63.41	62.12	60.87	59.65	58.46	57.32	56.20	55.11	54.06	53.03
11	52.04	51.06	50.12	49.19	48.30	47.43	46.58	45.75	44.94	44.16
12	43.39	42.64	41.91	41.20	40.50	39.82	39.16	38.51	37.88	37.27
13	36.67	36.08	35.50	34.94	34.39	33.85	33.33	32.81	32.31	31.82
14	31.34	30.87	30.41	29.96	29.51	29.08	28.66	28.24	27.83	27.44
15	27.05	26.66	26.29	25.92	25.56	25.21	24.86	24.52	24.19	23.86
16	23.54	23.23	22.92	22.61	22.32	22.02	21.74	21.46	21.18	20.91
17	20.64	20.38	20.12	19.87	19.62	19.38	19.14	18.90	18.67	18.44
18	18.22	18.00	17.78	17.57	17.36	17.15	16.95	16.75	16.56	16.36
19	16.17	15.99	15.80	15.62	15.45	15.27	15.10	14.93	14.76	14.60
20	14.44	14.28	14.12	13.97	13.81	13.66	13.52	13.37	13.23	13.09
21	12.95	12.81	12.68	12.54	12.41	12.28	12.15	12.03	11.91	11.78
22	11.66	11.54	11.43	11.31	11.20	11.09	10.98	10.87	10.76	10.65
23	10.55	10.45	10.35	10.24	10.15	10.05	9.951	9.857	9.763	9.671
24	9.579	9.489	9.400	9.313	9.226	9.141	9.057	8.973	8.891	8.810
25	8.730	8.651	8.573	8.496	8.420	8.345	8.271	8.198	8.126	8.054
26	7.984	7.915	7.846	7.778	7.711	7.645	7.580	7.515	7.452	7.389
27	7.327	7.266	7.205	7.145	7.086	7.027	6.969	6.912	6.856	6.800
28	6.745	6.692	6.637	6.584	6.532	6.480	6.429	6.379	6.329	6.279
29	6.230	6.183	6.135	6.088	6.042	5.995	5.950	5.905	5.861	5.817
30	5.774	5.731	5.688	5.647	5.605	5.564	5.524	5.484	5.445	5.406
31	5.367	5.329	5.292	5.254	5.218	5.181	5.145	5.110	5.075	5.040
32	5.006	4.972	4.939	4.906	4.873	4.841	4.809	4.777	4.746	4.715
33	4.685	4.655	4.625	4.595	4.566	4.538	4.509	4.481	4.453	4.426
34	4.399	4.372	4.346	4.320	4.294	4.268	4.243	4.218	4.193	4.169
35	4.145	4.121	4.097	4.074	4.052	4.029	4.006	3.984	3.962	3.941
36	3.919	3.898	3.877	3.857	3.836	3.816	3.797	3.777	3.758	3.739
37	3.720	3.701	3.683	3.665	3.647	3.629	3.612	3.594	3.577	3.561
38	3.544	3.527	3.513	3.497	3.481	3.465	3.449	3.434	3.419	3.404
39	3.389	3.375	3.361	3.347	3.333	3.320	3.306	3.293	3.280	3.268
40	3.255	3.242	3.230	3.218	3.206	3.194	3.183	3.171	3.160	3.149
41	3.138	3.127	3.117	3.106	3.096	3.086	3.076	3.067	3.057	3.048
42	3.038	3.029	3.020	3.012	3.003	2.994	2.986	2.978	2.970	2.962
43	2.954	2.946	2.939	2.932	2.925	2.918	2.911	2.904	2.897	2.891
44	2.884	2.878	2.872	2.866	2.860	2.855	2.849	2.844	2.838	2.833

Table B.2 Lorentz – polarization factors.

θ°	.0	.1	.2	.3	.4	.5	.6	.7	.8	.9
45	2.828	2.824	2.819	2.814	2.810	2.805	2.801	2.797	2.793	2.789
46	2.785	2.782	2.778	2.775	2.772	2.769	2.766	2.763	2.760	2.757
47	2.755	2.752	2.750	2.748	2.746	2.744	2.742	2.740	2.738	2.737
48	2.736	2.735	2.733	2.732	2.731	2.730	2.730	2.729	2.729	2.728
49	2.728	2.728	2.728	2.728	2.728	2.728	2.729	2.729	2.730	2.730
50	2.731	2.732	2.733	2.734	2.735	2.737	2.738	2.740	2.741	2.743
51	2.745	2.747	2.749	2.751	2.753	2.755	2.758	2.760	2.763	2.766
52	2.769	2.772	2.775	2.778	2.782	2.785	2.788	2.792	2.795	2.799
53	2.803	2.807	2.811	2.815	2.820	2.824	2.828	2.833	2.838	2.843
54	2.848	2.853	2.858	2.863	2.868	2.874	2.879	2.885	2.890	2.896
55	2.902	2.908	2.914	2.921	2.927	2.933	2.940	2.946	2.953	2.960
56	2.967	2.974	2.981	2.988	2.996	3.004	3.011	3.019	3.026	3.034
57	3.042	3.050	3.059	3.067	3.075	3.084	3.092	3.101	3.110	3.119
58	3.128	3.137	3.147	3.156	3.166	3.175	3.185	3.195	3.205	3.215
59	3.225	3.235	3.246	3.256	3.267	3.278	3.289	3.300	3.311	3.322
60	3.333	3.345	3.356	3.368	3.380	3.392	3.404	3.416	3.429	3.441
61	3.454	3.466	3.479	3.492	3.505	3.518	3.532	3.545	3.559	3.573
62	3.587	3.601	3.615	3.629	3.643	3.658	3.673	3.688	3.703	3.718
63	3.733	3.749	3.764	3.780	3.796	3.812	3.828	3.844	3.861	3.878
64	3.894	3.911	3.928	3.946	3.963	3.980	3.998	4.016	4.034	4.052
65	4.071	4.090	4.108	4.127	4.147	4.166	4.185	4.205	4.225	4.245
66	4.265	4.285	4.306	4.327	4.348	4.369	4.390	4.412	4.434	4.456
67	4.478	4.500	4.523	4.546	4.569	4.592	4.616	4.640	4.664	4.688
68	4.712	4.737	4.762	4.787	4.812	4.838	4.864	4.890	4.916	4.943
69	4.970	4.997	5.024	5.052	5.080	5.109	5.137	5.166	5.195	5.224
70	5.254	5.284	5.315	5.345	5.376	5.408	5.440	5.471	5.504	5.536
71	5.569	5.602	5.636	5.670	5.705	5.740	5.775	5.810	5.846	5.883
72	5.919	5.956	5.994	6.032	6.071	6.109	6.149	6.189	6.229	6.270
73	6.311	6.352	6.394	6.437	6.480	6.524	6.568	6.613	6.658	6.703
74	6.750	6.797	6.844	6.892	6.941	6.991	7.041	7.091	7.142	7.194
75	7.247	7.300	7.354	7.409	7.465	7.521	7.578	7.636	7.694	7.753
76	7.813	7.874	7.936	7.999	8.063	8.128	8.193	8.259	8.327	8.395
77	8.465	8.536	8.607	8.680	8.754	8.829	8.905	8.982	9.061	9.142
78	9.223	9.305	9.389	9.474	9.561	9.649	9.739	9.831	9.924	10.02
79	10.12	10.21	10.31	10.41	10.52	10.62	10.73	10.84	10.95	11.06
80	11.18	11.30	11.42	11.54	11.67	11.80	11.93	12.06	12.20	12.34
81	12.48	12.63	12.78	12.93	13.08	13.24	13.40	13.57	13.74	13.92
82	14.10	14.28	14.47	14.66	14.86	15.07	15.28	15.49	15.71	15.94
83	16.17	16.41	16.66	16.91	17.17	17.44	17.72	18.01	18.31	18.61
84	18.93	19.25	19.59	19.94	20.30	20.68	21.07	21.47	21.89	22.32
85	22.77	23.24	23.73	24.24	24.78	25.34	25.92	26.52	27.16	27.83
86	28.53	29.27	30.04	30.86	31.73	32.64	33.60	34.63	35.72	36.88
87	38.11	39.43	40.84	42.36	44.00	45.76	47.68	49.76	52.02	54.50

Appendix C
Multiplicity factor

Table C.1 Multiplicity factor

Cubic:	hkl	hhl	$0kl$	$0kk$	hhh	$00l$	
	48*	24	24*	12	8	6	
Hexagonal and Rhombohedral:	$hk\cdot l$	$hh\cdot l$	$0k\cdot l$	$hk\cdot 0$	$hh\cdot 0$	$0k\cdot 0$	$00\cdot l$
	24*	12*	12*	12*	6	6	2
Tetragonal:	hkl	hhl	$0kl$	$hk0$	$hh0$	$0k0$	$00l$
	16*	8	8	8*	4	4	2
Orthorhombic:	hkl	$0kl$	$h0l$	$hk0$	$h00$	$0k0$	$00l$
	8	4	4	4	2	2	2
Monoclinic:	hkl	$h0l$	$0k0$				
	4	2	2				
Triclinic:	hkl						
	2						

Appendix D
Temperature factor

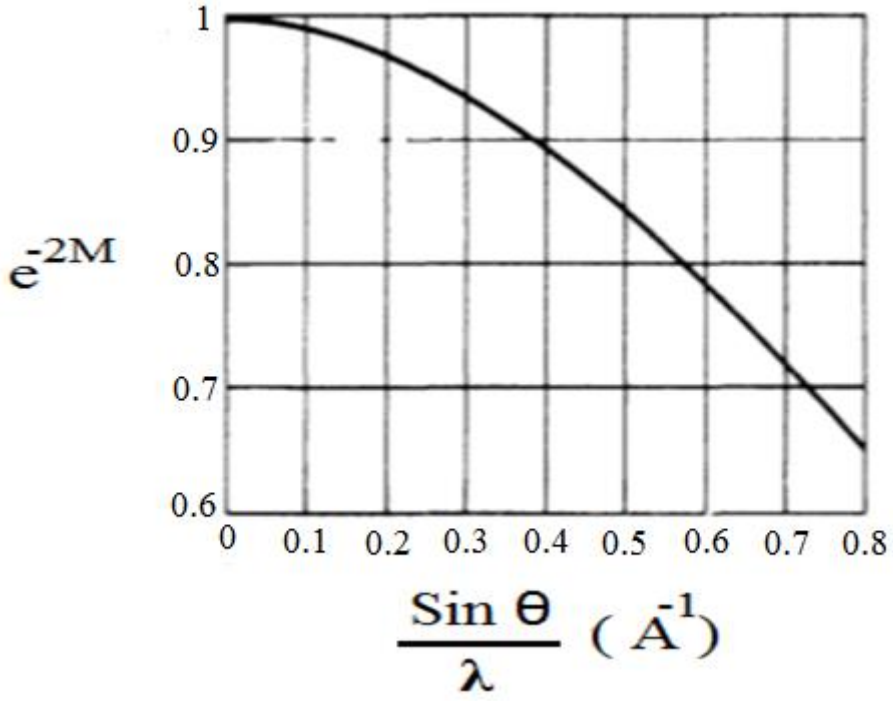

Figure D.1 Temperature factor of iron at 20 ºC as function of (sin θ / λ).